INFORMATION TO USERS

This manuscript has been reproduced from the microfilm master. UMI films the text directly from the original or copy submitted. Thus, some thesis and dissertation copies are in typewriter face, while others may be from any type of computer printer.

The quality of this reproduction is dependent upon the quality of the copy submitted. Broken or indistinct print, colored or poor quality illustrations and photographs, print bleedthrough, substandard margins, and improper alignment can adversely affect reproduction.

In the unlikely event that the author did not send UMI a complete manuscript and there are missing pages, these will be noted. Also, if unauthorized copyright material had to be removed, a note will indicate the deletion.

Oversize materials (e.g., maps, drawings, charts) are reproduced by sectioning the original, beginning at the upper left-hand corner and continuing from left to right in equal sections with small overlaps. Each original is also photographed in one exposure and is included in reduced form at the back of the book.

Photographs included in the original manuscript have been reproduced xerographically in this copy. Higher quality 6" x 9" black and white photographic prints are available for any photographs or illustrations appearing in this copy for an additional charge. Contact UMI directly to order.

UMI

A Bell & Howell Information Company
300 North Zeeb Road, Ann Arbor MI 48106-1346 USA
313/761-4700 800/521-0600

Experimental and Theoretical Studies on Vasculature and Heat Transfer in the Rat Spinotrapezius Muscle

by
Ji Song

A dissertation submitted to the Graduate Faculty in Engineering in partially fulfillment of the requirements for the degree of Doctor of Philosophy, The City University of New York

1998

This manuscript has been read and accepted for the Graduate Faculty in Engineering in satisfaction of the dissertation requirement for degree of Doctor of Philosophy.

Sept. 8, 1998
Date

Professor Lisa X. Xu
Chair of Examining Committee

Sept. 9, 1998
Date

Professor Mumtaz K. Kassir
Executive Officer

Professor Lisa X. Xu

Professor Sheldon Weinbaum

Professor Daniel E. Lemons

Professor Latif M. Jiji

Professor Neil T. Wright

Supervisory Committee

The City University of New York

Abstract

Experimental and Theoretical Studies on Vasculature and Heat Transfer in the Rat Spinotrapezius Muscle

by

Ji Song

Advisers: Professor Lisa X. Xu

Professor Sheldon Weinbaum

Professor Daniel E. Lemons

In this dissertation both experimental and theoretical studies were conducted to investigate microvascular heat exchange of thermally significant countercurrent artery-vein pairs in an exteriorized rat spinotrapezius tissue preparation. The vascular architecture of the spinotrapezius was first quantified. The blood flow in the artery of the countercurrent vessel pairs was then measured in normal and pharmacologically vasoconstricted and vasodilated states. The results were then used to evaluate the enhancement in the effective thermal conductivity (k_{eff}) due to blood perfusion according to the Weinbaum-Jiji theory. The scaling relations for the vascular architecture and blood flow were also explored. These relations were later used to extrapolate the blood flow in vessels greater than 130 μm diameter, where it was difficult to make direct optical

measurements of blood flow velocity. Furthermore, the axial thermal equilibration between the countercurrent vessel pair and its surrounding tissue was studied in the spinotrapezius. The thermal disturbance caused by the vasodilated first-order vessel pair and its background tissue temperature field were measured and compared with theoretical predictions. Finally, the Weinbaum-Jiji k_{eff} theory for heat exchange between the paired vessels and their surrounding tissue was also examined. k_{eff} was estimated by the Weinbaum-Jiji theory and compared with the experimentally derived tissue thermal conductivity by approximating the tissue as a fin. The results of the current study indicate that countercurrent blood flow can produce a dramatic increase in tissue thermal conduction in the vasodilated state, and the Weinbaum-Jiji k_{eff} theory can be used to describe heat exchange of the countercurrent vessel pairs of the rat spinotrapezius muscle that are less than 200 μm in diameter.

Chapter 1 gives a brief background of blood-tissue heat exchange in the microcirculation and the basic concepts for scaling relations in biological systems. The effect of perfusion rate on blood-tissue heat exchange due is presented in Chapter 2. Chapter 3 describes the vascular scaling relations in the spinotrapezius muscle. The thermal equilibration between countercurrent vessel pairs and their surrounding tissue in spinotrapezius is investigated in Chapter 4. Finally, in Chapter 5 the conclusions have been drawn from the present study.

Directions for future research are suggested.

To the memory of my father, Zhongmo Song

Acknowledgments

I wish to express my deepest gratitude and appreciation to my advisors, Professor Lisa X. Xu, Professor Sheldon Weinbaum and Professor Daniel E. Lemons for their constant support, encouragement, patience and guidance which made it possible for me to enter the frontier of this promising and challenging field of research.

Also, my thanks go to Professor Latif M. Jiji for his fruitful discussions and to Dr. Liang Zhu, as well as my fellow graduate student Mr. Peter Butler for their friendship and assistance during all these years. I am grateful to Dean Gerard G. Lowen for handling administrative details in such a warm and friendly manner. My gratitude is also to my friends who shared my joys and pains throughout the course of this work: Binmei Fu, Jinnan Chen, Yaqi Huang, Yongyi Yin, Jianjun Feng, Xiaping Hu, Liyun Wang, Dajun Zhang and Yulong Wu.

Finally, I wish to thank my husband, Qiming Li, for his forbearance and encouragement, and my daughter, Angela Li, for providing a strong motivation to keep going on.

This thesis is dedicated to my mother, my brother and my step-farther.

This research was supported by NSF grant CTS-9523082 and PSC-CUNY grant 991959.

Table of Contents

List of Symbols

a	Biot number, $h \cdot (H^{\bullet}/2)/k_t$
Bi	specific heat of blood
c_b	vessel diameter, $2a$
d	dimensionless half width of tissue, $D^{\bullet}/a$
D	dimensional half width of tissue
$D^{\bullet}$	Green's function
G	thermal convective coefficient
h	dimensionless equivalent tissue thickness, $H^{\bullet}/a$
H	dimensional total thickness of tissue
$H^{\bullet}$	dimensional tissue thickness above the countercurrent vessel pair
$H_1^{\bullet}$	dimensional supporting glass slide thickness
$H_g^{\bullet}$	dimensional tissue thickness
$H_t^{\bullet}$	tissue thermal conductivity in vasodilation
k	blood thermal conductivity
k_b	effective thermal conductivity
k_{eff}	intrinsic tissue thermal conductivity, 0.5 W/m °C
k_t	tissue thermal conductivity excluding the effect of the glass slide
$k^{\bullet}$	thermal conductivity
l	countercurrent vessel center to center spacing

Le	characteristic thermal equilibration length, $\pi a Pe/2\sigma$
L_i	length of countercurrent vessel pair for vessel generation i
L^*	tissue strip length
n_i	number density per unit cross-sectional area of vessel pair for vessel generation i
Pe	blood flow Peclet number, $\rho_b c_b d u/k_b$
Re	Reynold number, $4\rho_b Q/\pi\mu d$
Q	volumetric blood flow rate
T	temperature
T_{exp}	temperature obtained from infrared image and averaged in x direction
T_{ave}	temperature obtained from fin model
T_∞	environment temperature
u	average blood flow velocity
V	centerline red cell velocity
w	tissue weight
W	rat weight

Greek Symbols

μ	blood viscosity
ρ_b	density of blood

σ	conduction shape factor
τ	shear stress
ε	ratio of characteristic thermal equilibration length to vessel length

Subscript

a	artery or arteriole
b	blood
eff	effective
g	glass
i	vessel generation
t	tissue
v	vein or venule

List of Tables

List of Figures

Chapter 1. Introduction

For more than a century, researchers have studied heat transfer phenomena in living tissues. The convective effect of blood flow has long been recognized. However, we still have an incomplete understanding of this effect. The complex nature of vasculature and the vasoregulation that occurs in biological systems have made it difficult to describe the convective effect of blood flow in mathematical terms. Prior to 1948, research in bioheat transfer was largely performed to describe heat transfer between the body and its surroundings, and the associated quantitative analysis mostly used an overall effective conductivity to account for the blood flow effect.

The Pennes Bioheat Equation. The first quantitative relationship that described heat transfer in human tissue was proposed by Pennes (1948). His pioneering study included both experimental and theoretical approaches. In his experiments, skin temperature distributions along the axis of the upper limb, as well as around the circumference of the forearm and in a transverse line through the forearm were examined. In addition, the effect on proximal forearm and hand skin temperature of circulatory occlusion for 30 to 40 minutes either the distal forearm or the upper arm was quantified. Using these experimental results, Pennes presented his quantitative analysis of heat transfer in the human forearm

to describe the effect of blood flow on tissue heat transfer. In deriving his equation, Pennes assumed that the heat transferred from blood to tissue is equivalent to a heat source or sink term given as $\omega\rho_b c_b(T_a-T_v)$, where ω is the volumetric rate of blood perfusion per unit volume of tissue, and T_a-T_v is the arterial-venous temperature difference. Since T_v is unknown, it is approximated by the local tissue temperature, T_t. Also, T_a is approximated by the body core temperature, T_{a0}, by assuming that heat exchange between blood and tissue primarily takes place in capillary beds. Therefore, the Pennes equation has the following general form:

$$\rho c_p \frac{\partial T_t}{\partial t} = k\nabla^2 T_t + \omega\rho_b c_b(T_{a0}-T_t) + q_m \qquad (1.1)$$

The perfusion term expression, $\omega\rho_b c_b(T_{a0}-T_t)$, assumes that when blood enters the capillary beds, it undergoes complete thermal equilibration with the surrounding tissue and enters the venous circulation at the tissue temperature. All pre- and post-capillary heat exchange between blood and tissue has been neglected.

Although the fundamental approximations underlying the perfusion term have been the focus of attention since its inception, the Pennes equation has been broadly accepted as the well-known bioheat transfer equation. For many years it was widely believed that the primary thermal equilibration between blood and

tissue, occurred in capillaries, as described by the Pennes equation, because of their large total area for heat exchange. Reasonable agreement between the theory and experimental results have been obtained over the years (Pennes 1948, Roemer *et al.* 1989), although the initial approximations were never confirmed.

Alternatives to the Pennes Equation. Beginning in the 1970's, a number of researchers began to question the underlying assumptions of the Pennes' equation and developed more rigorous analyses of the blood-tissue thermal equilibration.

Wulff (1974) proposed one of the earliest alternatives to the Pennes bioheat equation. He argued that three different aspects of the Pennes theory were in error. Considering the thermal equilibration of blood in the microcirculation, Wulff derived the Pennes equation in its original form before any assumptions were made. He found that the local and global control volumes were both used in the Pennes derivation, which was physically inconsistent. Also, the equation actually contained three different unknown temperatures: T_t, T_a and T_v in the microcirculation, which meant two more equations should be added. One of the major criticisms by Wulff was the omission of the blood flow direction, and he found the errors introduced by this omission were on the same order as the effect of blood flow itself. Wulff therefore concluded that the effect of blood flow could be properly modeled only if spacial variations in the local

blood velocity were known.

Klinger (1974, 1976) presented an analytical model of heat diffusion with convection. The primary motivation of this model was to explain the results of some thermal clearance experiments in perfused biological tissues. Klinger argued that the convection inside a tissue should be modeled based upon its *in vivo* vascular anatomy. Using a conduction tensor k_{eff}, Klinger introduced the concept of an enhancement of tissue thermal conductivity due to the presence of flowing blood in a tissue. By applying the Green's function solution, Klinger quantified the importance of vessel number density, blood perfusion rate, and vessel architecture on this enhancement. Klinger's work emphasized the importance of the geometry and flow direction of the microcirculation, which was not considered in the Pennes equation.

Chen and Holmes (1980) introduced the concept of thermal equilibration length of blood vessel in their analysis to examine the blood-tissue thermal equilibration process. They demonstrated that the thermal equilibration between blood and tissue mostly takes place from the small arteries to the small arterioles between 500 and 50 μm in diameter. It was concluded that due to the precapillary thermal equilibration in the microcirculation the main assumption of the Pennes's bioheat equation was questionable. In the Chen and Holmes model, an effective thermal conductivity was also defined to quantify the

enhancement of tissue thermal conductivity by the convection transport associated with blood flow. However, the effect of countercurrent heat transfer between the closely spaced artery and vein was not considered.

Development of Countercurrent Heat Exchange. The thermal significance of countercurrent flow in the closely spaced artery and vein was first observed over a hundred years ago. This structure has been observed in many parts of the circulatory system, including rete in the limbs of many animals. The deep arteries and veins that supply blood to and drain blood from the extremities of many animals are also countercurrently arranged. Such arrangement plays an important role in reducing heat loss from the limb to the environment. As warm arterial blood flows towards distal parts, it exchanges heat with cooler venous blood flowing in the opposite direction, which causes a reduction in the arterial and mean tissue temperature in the limb and a reduction in heat loss. The experimental study by Bazett *et al.* (1948) was one of the first to explore the role of countercurrent heat exchange in bioheat transfer. Their study showed that temperatures in the major axial arteries and veins of the human limb are influenced by the environmental temperature and it was suggested that heat exchange between these vessels has a heat conservation function.

Scholander and Krog (1957) developed a theoretical heat transfer model to study heat transfer between the paired artery and vein, where they assumed

that the axial temperature profiles in both the artery and vein were linear with a constant temperature difference along the vessel axes. This "perfect" countercurrent heat exchange assumption implied that all heat leaving the arterial blood entered the cool venous blood with no heat exchange with the surrounding. Two thin-walled copper tubes were used to simulate an artery-vein pair and verify their heat transfer model. Their later experiment in the rete of the sloth extremities showed that when arteries and veins were in close contact the efficient heat exchange between these vessels reduced the heat loss. These experiments demonstrated the importance of countercurrent heat exchange in bioheat transfer.

Mitchell and Myers (1968) questioned both the perfect countercurrent heat exchange assumption in Scholander and Krog's theoretical model and the use of copper tubes in their experimental simulation, since neither existed *in vivo*. Mitchell and Myers mathematically modeled the countercurrent heat exchange in a more general manner than that presented by Scholander and Krog. In their whole limb model, the artery and vein were treated as a one-dimensional countercurrent heat exchanger with constant vessel radius. This model demonstrated that any finite amount of countercurrent heat exchange will reduce heat loss from the extremity to its surroundings. The "heat transfer unit" was introduced to characterize countercurrent exchangers. The numerical values of this parameter was estimated for the human extremity, sloth rete, and porpoise

fin. The theoretical predictions for the temperature were compared with the experimental data collected from the human arm by Bazett *et al.* (1948). It was concluded that there was little countercurrent heat exchange between the major artery and vein that supply the human arm. Mitchell and Myers' research represented a starting point for more sophisticated mathematical models of countercurrent heat exchange in the circulation.

Keller and Seiler (1971) presented a one-dimensional model of peripheral heat transfer that included the effect of countercurrent heat exchange as well as conduction, bulk convection with perfusion bleed-off, and metabolic heat production. By combining these various heat transfer modes, they presented one of the earliest mathematical models of bioheat transfer in the microcirculation that considered the coupled heat transfer between the tissue, artery, and vein which were treated as separate compartments. This approach became the standard procedure in later formulations that used more geometrically complex vascular related bioheat transfer models. Unlike the model proposed by Mitchell and Myers (1968) in which the countercurrent heat exchange was considered in an entire extremity, Keller and Seiler hypothesized that a countercurrent heat exchange mechanism would be important in the peripheral circulation near the body surface where the smaller arteries and veins were often positioned next to each other. By considering this countercurrent heat exchange in the local

peripherical regions coupled with conduction and bulk bleed-off convection, they developed a model in the nonisothermal subcutaneous layer of tissue to assess the relative importance of each effect under various conditions. Several dimmensionless parameters were used in their model to characterize heat transfer in tissue accounting for the effect of large vessel interaction with the tissue. Keller and Seiler also proposed an expression for an effective thermal conductivity in tissue, and demonstrated that the effect of vasoconstriction on the effective conductivity was small at low perfusion rates. At high perfusion rates, the effect of added vasodilation on the effective conductivity was also limited.

Chato (1980) examined heat transfer between tissue and blood vessels in three different arrangements: a single vessel surrounded by tissue cylinder, a countercurrent pair of vessels surrounded by infinite tissue medium, and a single vessel close to an isothermal surface such as the skin. Chato introduced the concept of the heat transfer effectiveness and evaluated its value for the three vascular configurations. He concluded that between the large vessels and the microcirculation there exists a vascular region where the blood contained in the vessels has a different temperature from its surrounding tissue, and it becomes increasingly thermal equilibrated with the tissue as the microcirculation is approached. Chato also investigated the thermal equilibration between countercurrent vessels in an infinite medium with a linear decrease in blood flow

due to capillary bleed-off. It was demonstrated that the effect of perfusion bleed-off is to increase the heat transfer between the blood vessels.

Development of the Weinbaum-Jiji Bioheat Transfer Equation. Weinbaum and Jiji (1979) studied heat transfer in the peripheral circulation. By accounting for the complex geometry of the countercurrent artery-vein network, a two-phase theory was developed to model the effect of the circulation on tissue heat transfer associated with the vascular architecture. In 1984, Weinbaum *et al.* (1984) presented a more thorough investigation of the peripheral tissue. In their study, vascular casts of the rabbit thigh were examined to determine the detailed vascular geometry as a function of the tissue depth. Three different vascular structures were identified: deep tissue layer, intermediate tissue layer, and cutaneous layer. Based on the vasculature, a quantitative three layer microvascular model for the peripheral tissue heat exchange was proposed. In addition, the detailed temperature fluctuations in the microvasculature were measured using high spatial resolution thermocouple probes to confirm the conceptual assumptions made in the model. The three-layer model predicted that all thermally significant vessels in skeletal muscle were larger than 50 μm in diameter. Nearly all vessels of these dimensions were observed as closely spaced countercurrent pairs in the skeletal muscle. It was, therefore, concluded that the heat transfer due to capillary blood perfusion could be negligible, and the primary

mechanism for the blood-tissue heat exchange was the incomplete countercurrent exchange in the thermally significant vessels. Based on these results, a three-dimensional bioheat transfer equation was subsequently developed (Weinbaum and Jiji 1985) from their initial three coupled heat transfer equations for the artery, vein and tissue, respectively. By approximating for nearly equilibrium conditions that $T_t \cong (T_a+T_v)/2$, $(q_a-q_v) \ll q_a$ or q_v, they derived a more compact equation for the tissue temperature:

$$\frac{\pi^2 k_b^2}{4k_t\sigma} n a^2 Pe^2 l_j \frac{dl_i}{dx_i}\frac{dT_t}{dx_j} = \frac{d}{dx_i}\left((k_{ij})_{eff}\frac{dT_t}{dx_j}\right) + q_m \qquad (1.2)$$

where $(k_{ij})_{eff} = k_t\left(\delta_{ij} + \sum_i \frac{\pi^2}{4\sigma k_t^2} n_t a^2 k_b^2 Pe^2 l_i l_j\right)$. The second term in the parenthesis is the enhancement in $(k_{ij})_{eff}$ due to the incomplete countercurrent heat exchange. In this newly derived equation, Weinbaum and Jiji combined the convective effect of countercurrent vessel pairs and capillary bleed-off from these vessels with the traditional conduction term and showed that the overall effect could be represented by an effective thermal conductivity, $(k_{ij})_{eff}$. Thus, the tissue thermal conductivity was for the first time related to the local microvascular geometry and blood flow in this expression.

Like the Pennes equation, the Weinbaum-Jiji equation has its own limitations. The fundamental assumptions that $T_t \cong (T_a+T_v)/2$ and $(q_a-q_v) \ll q_a$ or q_v used in deriving the Weinbaum-Jiji equation are equivalent to the requirement

that the gradient of the mean tissue temperature is approximated by the mean blood temperature gradient in the countercurrent artery-vein pair. This relationship is valid only when ε, the ratio of the vessel thermal equilibration length to the characteristic length of the macroscopic temperature (Le/L) is much smaller than 1. Physically, it requires that the heat exchange between the paired artery and vein should not significantly depart from perfect countercurrent exchange. Based on the model proposed by Baish *et al.*(1986), Charny *et al.* (1990) have compared the solutions of a more rigorous three-equation model with those of the one-dimensional Weinbaum-Jiji equation and the Pennes equation in the peripheral tissue. They concluded that the later two formulations are appropriate in different tissue regions. The Pennes equation is valid for vessels > 500 μm in diameter, where there is little countercurrent equilibration of the arterial blood due to the high blood flow rate. However, for 50 to 200 μm diameter vessels countercurrent convective heat exchange becomes increasingly important and the Weinbaum-Jiji equation provides more accurate predictions. The recent study by Zhu *et al.* (1996) in the feeding countercurrent artery-vein pair of the rat cremaster muscle preparation showed that the Weinbaum-Jiji equation is valid when $(d/2)\cdot Pe<3$ mm, where Pe is the blood flow Peclet number based on the vessel radius, d.

Various theoretical and experimental studies have been recently performed

to elucidate how and where vascular heat transfer occurs and to determine whether the Pennes or the Weinbaum-Jiji bioheat transfer model is more appropriate. This research has involved several aspects: (i) Essential confirmation of the starting point for the use of the Weinbaum-Jiji equation. In 1987, Lemons *et al.* (1987) measured the temperature disturbances in the vicinity of the paired vessels from 50 to 500 μm in diameter. It was found that the blood temperature differences in the primary heat exchange vessels were only 0.1 to 0.2 °C for vessels of 100 μm diameter or larger, whereas for vessels less than 100 μm diameter there was no measurable temperature difference. This suggested that the primary vessels involved in thermal equilibration are equal to or larger than 100 μm diameter. (ii) Studies in the peripheral tissue. The Weinbaum-Jiji equation was also applied in the peripheral tissue to study the thermal behavior of the tissue (Song *et al.* 1987). (iii) Studies in the whole limb. Previous experimental results of whole limb heat transfer, such as the Pennes experiment, motivated a series of theoretical studies to examine the heat exchange between two vessels embedded in a tissue cylinder (Song *et al.* 1988, Zhu *et al.* 1992, Wu *et al.* 1993). These theoretical models were compared with the Pennes' experiment for the temperature profiles in the human arm. (iv) Macroscopic clearance method. Crezee and Lagendijk (1990) inserted a small plastic tube into the tissue of a bovine kidney and measured the temperature field in a plane perpendicular to the

tube when heated water was circulated through the tube and the kidney cortex perfused at different rates. They also used thermocouples to map the temperature distribution in the tissue of isolated perfused bovine tongues at various perfusion rates (Crezee *et al.* 1991). The temperature measurements were found to agree better with predictions of the Weinbaum-Jiji model than those of the Pennes equation. Roemer *et al.* (1989) measured the steady state temperature profiles in the canine thighs heated by ultrasound. A comparison of the measurements was made with both models, and the results were in a better agreement with the Pennes equation. Several more recent studies have used the self-heated thermistor technique to measure the heat exchange due to perfusion in the renal cortex of isolated canine and pig kidneys perfused with saline (Anderson and Valvano 1994, Valvano *et al.* 1994, Xu *et al.* 1991). In these studies the expression for the effective thermal conductivity derived in the Weinbaum-Jiji bioheat equation was applied to the vascular anatomy of the cortex, and thus to relate the value of k_{eff} to the local blood flow. However, it was difficult to apply the theory to these organs because of the complexity of the vascular architecture and the fact that, unlike the skeletal muscle tissue, the arteries and veins in the renal cortex do not occur primarily as countercurrent pairs. (v) Heat transfer in microvascular circulation. While there have been many theoretical studies on the microvascular countercurrent heat exchange, there were relatively few

experimental investigations of local blood-tissue heat transfer in the microvasculature. Recently, efforts have been made to relate local microvascular geometry and flow to tissue temperature measurements in two-dimensional tissue preparations. Zhu *et al.* (1995, 1996) performed experiments on the exteriorized rat cremaster muscle to measure the blood flow velocity, the vessel diameter and thermal equilibration length. They initially tried to quantify the two-dimensional vasculature in the rat cremaster muscle, and to show the blood flow velocity and vessel diameter responses of the 1A to 4A vessels (75 to 10 μm diameter) to the temperature of tissue bath. No significant enhancement in k_{eff} was observed in this vessel range. In their later experiment, high resolution infrared thermography was used to obtain the first measurements of the axial thermal equilibration in a microvessel pair. Measurements were performed on a vasodilated 1A feeding artery-vein pair in the rat cremaster muscle. In this experiment, the local blood flow Peclet number was changed from 1 to 14 by the vasodilator (Na nitroprusside). It was clearly indicated that increasing blood flow rate produced a higher inlet temperature at the proximal boundary and thus an elevation of the temperature of the entire preparation. The uncertainties associated with the rat cremaster muscle experiment were that some vessels were unavoidably cut during the microsurgery, and the *in vivo* temperature of the muscle is lower than the core temperature which may result in a relatively low blood flow in the vessels. (vi)

Modification of the blood perfusion term. In their most recent paper, a new simplified perfusion source term has been derived by Weinbaum *et al.* (1997) to describe the effect of blood perfusion on local tissue heat transfer. Using Myrhage and Eriksson's (1984) description of a muscle tissue cylinder surrounding secondary vessels (s vessels) as the basic heat transfer unit, the blood perfusion term was developed to describe the countercurrent thermal equilibration in this unit. The model started from analyzing countercurrent heat exchange mechanism in an idealized anatomical structure. The analysis resulted in a blood perfusion term, which can be expressed as $\omega\rho_b c_b \xi(T_{ab0}-T_t)$, in the tissue energy equation. This expression is similar to the Pennes perfusion term except that there is a correction coefficient ξ and T_{ab0} is the local arterial blood supply temperature in the s vessel tissue cylinder. ξ was found to be between 0.6 to 0.7 for most muscle tissues. The major break through of this study is that it demonstrates the relationship between the Weinbaum-Jiji and the Pennes models.

Despite all these advances, a thorough understanding of blood-tissue heat transfer requires some further development of an experimental approach which permits measurement of the vascular structure, blood flow and temperature profiles in a typical muscle tissue so that one can directly correlate the *in vivo* physiological parameters with the local tissue heat transfer. Moreover, a comparison between the theoretical analysis and the experimental results needs

to be performed to examine the validity of the Weinbaum-Jiji bioheat transfer model in the muscle. These combined experimental and theoretical approaches are the main goals of this dissertation, which have been accomplished in the following three primary areas: (i) Development of a combined theoretical and experimental approach to study the change of vascular blood flow and the resultant enhancement in the effective tissue thermal conductivity due to vasoregulation. This approach was used to reveal the importance of blood flow in blood-tissue heat transfer and to show the feasibility of the experimental study for analyzing the thermal equilibration in the microcirculation. (ii) Examination of the vascular blood flow in the rat spinotrapezius muscle and the scaling relations that can be applied to the same organ in animals of the same species but of different weights. These allometric scaling relations provide an opportunity to predict blood flow in the microvessels where it is difficult to make direct measurements. (iii) Study on the thermal equilibration between the countercurrently paired microvessels and their surrounding tissue in an exteriorized rat spinotrapezius muscle using high resolution infrared thermography. A theoretical model for heat transfer in two-dimensional tissue preparations (Zhu *et al.* 1996) was modified and employed to analyze the experimental measurements. This approach was used to investigate heat transfer in microvessels where the countercurrent blood flow was high enough to result in

an observable enhancement in k_{eff} and to experimentally verify the validity of the Weinbaum-Jiji theory.

The main body of this dissertation consists of three major chapters, devoted to each of the three aforementioned areas, respectively. Briefly, in the experiments described in Chapter 2, the rat spinotrapezius muscle has been used to examine the vascular geometry, blood flow and tissue heat transfer. As a two-dimensional tissue preparation, the spinotrapezius is an ideal preparation for the experiments. Two-dimensional tissue preparations, such as rabbit ear, frog mesentery, hamster cheek pouch, rat cremaster and spinotrapezius, offer the advantages of near transparency and uniform thickness. The blood flow in several successive generations of vessels can be measured in the preparations, and the blood perfusion can be pharmacologically controlled to produce the corresponding changes in k_{eff}. In the rat spinotrapezius, the first-order major feeding blood vessels (1A) are countercurrent artery-vein pairs. The second-order (2A) and third-order vessels (3A) are also countercurrent pairs and the separation of the paired vessels occurs only after the 3A vessels. Depending on the rat age and size, the 1A feeding vessels vary from 50 to 200 μm in diameter, where it is believed that the primary blood-tissue heat exchange occurs. The preparation is flat enough to allow accurate vascular and thermal images to be taken. Moreover, vasoconstrictors and vasodilators can be added in the tissue bath to change blood

flow through the entire preparation. Therefore, the muscle is quite suitable for the study of vascular dynamics and the tissue thermal response to vasoactive agents.

In the research presented in Chapter 3, the optical Doppler velocimetry was used to measure the vascular blood flow in the rat spinotrapezius. The allometric scaling relation between the blood flow rate and vessel size has been investigated in rats of greatly different weight, as well as that of blood flow rate and the muscle weight. These observed relationships were later used to predict the vascular blood flow where it was difficult to make direct measurements using optical methods due to the high blood flow rate and the thickness of the tissue and vessel wall. Previous investigators have shown that qualitative morphological and functional characteristics of biological organs can be described by the power law equations relating a particular variable to body size. Allometric scaling relations have been used for analyzing the form, structure, composition, and function in animals of different sizes. Power functions have either been theoretically derived from dimensional analysis and similarity principles (Günther 1972, Heusner 1984, Koops and Grossman 1993, West *et al.* 1997) or empirically obtained from the observed data (Adolph 1949, Pilbeam and Gould 1974, Schmidt-Nielsen 1975, Calder III 1981). A practical application of the allometric scaling is the extrapolation of animal toxicity data to man (Vocci and Farber

1988, Ings 1990, Travis 1991). Based on the assumption that extrapolation of biological data from animals to humans is valid, laboratory animals have been used as models for human toxicity studies. This is a typical interspecies application of the allometric scaling relations. However, if species-specific differences are considered, the intraspecies scaling is expected to be more reliable. Based on this consideration, the scaling relations for blood flow rate in spinotrapezius were studied in Chapter 3 for later applications.

Chapter 4 presents a high-resolution infrared technique to study heat exchange at the microvascular level. High-resolution, two-dimensional thermal measurements can not be achieved at the microvascular level with either thermocouples or self-heated thermistor probes. In contrast, high-resolution infrared thermography has been proven to be effective in measuring the detailed tissue surface temperature above the microvessels in two-dimensional tissue preparations. To study the thermal disturbances of the microvessels in the exteriorized rat spinotrapezius muscle, a theoretical model for two-dimensional tissue preparations (Zhu *et al.* 1996) has been modified and employed to analyze the tissue temperature measurements. The Weinbaum-Jiji theory was also used to estimate the value of k_{eff}, which was compared to the measured tissue thermal conductivity value calculated by using a fin approximation for the muscle tissue. A close agreement was found between the average values, though a paired *t*-test

showed that the Weinbaum-Jiji predicted k_{eff} value is significantly higher than the measured one.

Chapter 2. Enhancement in the Effective Thermal Conductivity in Rat Spinotrapezius Due to Blood Perfusion

The study described in this chapter was undertaken to gain a better understanding of the countercurrent heat exchange of thermally significant blood vessels in skeletal muscles by measuring the vascular structure and flow in an exteriorized rat spinotrapezius muscle and by estimating the enhancement in the effective thermal conductivity of the muscle. Detailed anatomic measurements of the number density and length of countercurrent vessel pairs between 45 and 165 μm diameter were obtained. Moreover, diameter and blood flow in the 1A to 3A vessels were measured for the muscle in which pharmacological vasoactive agents were introduced allowing one to vary the local blood flow Peclet number ($Pe=\rho_b c_b\, d\, u/k_b$) from 1 to 18 in the major feeding artery. These combined measurements have been used to estimate the range of possible enhancement in the effective thermal conductivity of the tissue. The newly derived conduction shape factor in Zhu and Weinbaum (1995) for countercurrent vessels in two-dimensional tissue preparations was used in this analysis. Our experimental data indicated that the value of this conduction shape factor is about one-third to two-thirds of the value for the paired countercurrent vessels of the same size and spacing in an infinite medium. The experiment also revealed that the Weinbaum-

Jiji expression for k_{eff} was valid for the spinotrapezius muscle when the largest vessels were less than 195 μm diameter. A 5-fold increase in k_{eff} was predicted for 195 μm diameter vessels. Blood perfusion due to vasoregulation was also shown to have a dramatic effect on k_{eff}. A tissue which exhibits only small increases in k_{eff} due to countercurrent convection in its vasoconstricted state can exhibit a more than 5-fold increase in k_{eff} in its vasodilated state.

2.1 Introduction

In the recent studies by Zhu *et al.* (1995,1996), a two-dimensional tissue preparation, the rat cremaster muscle, was used for the first time to examine the countercurrent thermal equilibration in the microvasculature and to estimate the possible enhancement in thermal conductivity that arises from the incomplete countercurrent thermal equilibration occurring in the 1A to 4A vessels of this tissue. Because of the tissue and measurement limitations, the paired blood flow velocity and diameter measurements were performed only for vessels up to 75 μm diameter (Zhu *et al.* 1995). However, the theoretical predictions of the Weinbaum-Jiji equation revealed that a significant enhancement in k_{eff} should occur for vessels >70 μm diameter and that the Weinbaum-Jiji expression for k_{eff} should be valid for vessels up to approximately 200 μm diameter. In this study, a new two-dimensional tissue preparation which is much more suitable for

exploring these concepts, the rat spinotrapezius muscle is used. This tissue is also probably more representative of the skeletal muscle than the rat cremaster. Doppler velocity measurements have been obtained for vessels up to 130 μm diameter and the vascular geometry of 1A vessel pairs were examined. These data were used to estimate the enhancement in the effective thermal conductivity, the ratio of thermal equilibration to vessel length, ε, and the magnitude of the important convective parameter $(d/2)\cdot Pe$ in the 1A, 2A, and 3A vessel generations.

A number of different bioheat transfer models have been developed (Chen and Holmes 1980, Pennes 1948, Weinbaum *et al.* 1984) to describe the mechanism of blood-tissue energy exchange. In 1984, it was shown by Weinbaum *et al.* that nearly all thermally significant vessels in the skeletal muscle appeared as closely spaced countercurrent pairs, and the primary mechanism by which the microvascular blood flow altered the blood tissue heat transfer was the incomplete countercurrent exchange in the thermally significant microvessels (Weinbaum *et al.* 1984). Based on this model, a new bioheat transfer equation was derived (Weinbaum and Jiji 1985). In the Weinbaum-Jiji bioheat equation the convective effect of countercurrent pairs and capillary bleed-off from these vessels were combined with the traditional conduction term and represented by an effective thermal conductivity k_{eff} to account for the enhancement of heat transfer due to the thermally significant vessels. The expression for k_{eff} was related

to the local vascular geometry and blood flow. This approach differed from the traditional Pennes bioheat equation (Pennes 1948) in which the effect of blood perfusion was modeled as an isotropic heat source. The Pennes equation neglected all pre-arteriole and post-venule heat transfer between blood and tissue. Subsequent asymptotic analysis (Weinbaum and Jiji 1989) and numerical calculations (Charny *et al.* 1990, Wissler 1987a, Wissler 1987b) showed that the Weinbaum-Jiji equation also has its limitations. In particular, it requires that ε, the ratio of the vessel thermal equilibration length to either the vessel's actual length or the characteristic length of the macroscopic tissue temperature gradient, be less than 0.2. If this requirement was satisfied, the axial gradient of the average artery and vein temperatures would closely follow the local gradient of the local tissue temperature. The Weinbaum-Jiji equation has been applied to the peripheral tissue (Song *et al.* 1987) as well as the deeper muscle tissue layer in the limb where the criterion for its validity was clearly violated (Charny *et al.* 1990, Zhu *et al.* 1992).

Many investigators have performed *in vivo* and *in vitro* experiments to examine the validity of the physical and physiological assumptions upon which various bioheat transfer models have been developed (Anderson and Valvano 1994, Charny *et al.* 1990, Crezee and Lagendijk 1990, Lemons *et al.* 1987, Weinbaum *et al.* 1984, Xu *et al.* 1991, Zhu *et al.* 1995, Zhu *et al.* 1996). The

original experiment by Weinbaum *et al.* (1984) presented the vascular structure and the first temperature measurements in the vicinity of thermally significant vessels of the rabbit thigh to show the existence and importance of countercurrent heat exchange. Subsequently, experiments by Lemons *et al.* (1987) showed that the microvascular artery-vein temperature differences in the primary heat exchange vessels were only 0.1 to 0.2 °C for vessels 100 μm diameter or larger, whereas for vessels less than 100 μm diameter there was no measurable temperature difference. It was concluded that thermal equilibration in the branching countercurrent vascular network of the rabbit limb occurred in the vessels of at least one order of magnitude larger than capillaries as first predicted by Chen and Holmes (1980).

To test the foregoing ideas, Zhu *et al.* (1995, 1996) have made velocity, diameter and thermal equilibration measurements on an exteriorized rat cremaster muscle, the muscle surrounding the testes. This organ has a normal *in vivo* temperature of approximately 34 °C, which is 4 or 5 °C lower than the rat's normal rectal temperature of 38 to 39 °C. Due to its special function, this muscle can be strongly affected by age. Another difficulty in using the rat cremaster is that some of the vessels have to be cut during the microsurgery and this affects the blood pressure distribution. Data were obtained for the 1A to 4A vessels which ranged from 10 to 75 μm in diameter. Unfortunately, as noted earlier, no

significant enhancement in k_{eff} occurred in the range of vessels studied in Zhu's experiment (1995). It was also not realized at the time that the full range of perfusion values had not been elicited since the baseline values were close to those of the maximally vasodilated state. However, a significant enhancement in k_{eff} was predicted to occur for vessels larger than 70 μm diameter and a 2.5-fold increase in k_{eff} was predicted for 200 μm diameter vessels using extrapolated velocity and diameter measurements obtained for the rat cremaster muscle in (House and Lipowsky 1987).

In this study, an experimental approach was designed to evaluate the enhancement in k_{eff} that is associated with the vasoregulatory *in situ* response of a two-dimensional tissue preparation that is much more characteristic of the skeletal muscle in general, the exteriorized rat spinotrapezius muscle. This preparation also has the advantage that the main feeding vessels and nerves can be kept intact during the microsurgery and all major generations of the feeding vessels are paired. Another important advantage of using this muscle is that its largest 1A vessels in the 150 gm mature rats approach 200 μm diameter, the predicted upper limit of validity of the Weinbaum-Jiji theory.

In our experiment, anatomic measurements were obtained for the number density and length of countercurrent vessel pairs between 45 and 165 μm in diameter. The response of the vessels was explored over the full vasoregulatory

range from maximum vasoconstriction to maximum vasodilation. The blood flow velocity in vessels that were in the 25 to 130 μm diameter range was measured using an optical Doppler velocimeter. The upper limit in the vessel diameter for velocity measurements was due to the limitations of the optical Doppler velocimeter to accurately measure the red cell velocity in larger vessels. These measurements of the vascular anatomy and blood flow were then used to evaluate the enhancement in the effective thermal conductivity using the theory developed by Weinbaum and Jiji (1985). This study, to the best of my knowledge, provides the first experimental evidence of a significant increase in the enhancement in the effective thermal conductivity due to blood flow in the larger countercurrent vessels of the microvasculature and the potential of vasoregulatory adjustments to change this conductivity.

An important factor in evaluating the enhancement in k_{eff} is the conduction shape factor, σ. The original form of the shape factor used in Weinbaum and Jiji (1985) is for paired vessels in an infinite medium. In (Zhu and Weinbaum 1995), a new expression for conduction shape factor was derived for a countercurrent vessel pair in a two-dimensional tissue preparation. In the present study, this expression for conduction shape factor has been evaluated using detailed measurements of the vessel-tissue geometry and flow rates obtained in the 1A to 3A vessels of the rat spinotrapezius muscle.

One of the requirements necessary to apply Weinbaum-Jiji theory is that the axial thermal equilibration length be much smaller compared to the actual length of the vessel or the characteristic length of the tissue temperature gradient. As noted earlier this is usually expressed by the criterion $\varepsilon<0.2$. In (Zhu *et al.* 1996) a more rigorous theoretical criterion was established for two-dimensional tissue preparations. It was shown that the value of $(d/2)\cdot Pe$ could be used to predict when either conduction or countercurrent convection would be the dominant mode of axial thermal equilibration. The theoretical prediction indicated that when $(d/2)\cdot Pe<1$ mm tissue conduction would be the dominant mode of heat transfer whereas if $(d/2)\cdot Pe>3$ mm countercurrent convection would dominate. These accurate predictions were compared with a simpler one-dimensional model of the Weinbaum-Jiji equation and the latter was shown to provide a reasonable agreement with the more accurate model provided $(d/2)\cdot Pe<3$ mm. Both criteria, $\varepsilon<0.2$ and $(d/2)\cdot Pe<3$ mm, were used in the present study to predict the limits of validity of the Weinbaum-Jiji theory in the rat spinotrapezius muscle.

2.2 Methods

2.2.1 Spinotrapezius Muscle

The spinotrapezius is a paired muscle, which extends longitudinally along

the backbone in the thoracic and upper lumbar region. Its major first- to third-order arteries are normally paired with countercurrent veins, but the fourth branching generation of arteries supplies an extensive meshwork of interconnecting or arcading arterioles. Connections from these arcade arteries to the capillaries are provided by transverse arteries, which branch off the arcades at regular intervals yielding uniform tissue perfusion. Figure 1 shows a photomontage of a typical rat spinotrapezius muscle obtained in our experiments. The main artery feeding the spinotrapezius muscle is defined as the first-order artery (1A). Successive branches from the 1A are denoted as the second-order arteries (2A), and so forth up to 3A. Although the general vascular structure in the spinotrapezius has been described by previous researchers (Englson *et al.* 1985, Gray 1973), the number density, diameter, and the length of the countercurrent paired feeding vessels, which are the essential vascular parameters for evaluating k_{eff}, have not been quantitatively analyzed. In this research, a more detailed morphological study of these parameters is performed for the first time.

2.2.2 Experimental Conditions and Setup

Male Sprague-Dawley rats were used in this experimental study. Rats were anesthetized with an intraperitoneal injection of sodium pentobarbital solution (45 mg/kg). During the experiment supplemental doses were administered as needed. A tracheal tube was inserted to maintain a patent airway. Rats were

wrapped by a water-jacketed pad to maintain the core body temperature which was measured by a thermocouple inserted into the rectum during the experiment. After making a longitudinal slit in the skin along the spine, the spinotrapezius muscle on the right side was partially dissected free from the back of the rat. Neither the nerves nor the feeding vessels were cut. The muscle, which was still attached to and perfused by the rat, was immersed in a tissue bath. The entire surgical procedure required about 30 minutes.

The tissue bath was filled and continuously recirculated from a stock reservoir containing the Krebs solution, which consisted of (in g/l) 6.6 NaCl, 0.35 KCl, 0.28 $MgSO_4$, 0.16 KH_2PO_4, 2.09 dextrose, 2.14 $NaHCO_3$ and 0.28 $CaCl_2$. The osmolality of the solution was also measured at the beginning of each experiment by a vapor pressure osmometer. It was about 280 mOsm/kg·water, near the osmolality of tissue. The solution was maintained at 38 °C, which is close to the muscle *in vivo* temperature. Since the muscle is sensitive to PO_2, PCO_2, pH and the temperature of the bath solution, these values were continuously monitored and adjusted during the experiment to maintain the normal *in vivo* conditions. An Anafaze 8LS controller was used to adjust the bubbling rate of CO_2 and N_2 in the stock reservoir and to keep the PO_2 at 15-30 torr, the PCO_2 at 35-45 torr and the pH at 7.4. Muscle preparations were examined before the measurement protocol. If there was any bleeding or low

blood flow, the experiment would be stopped.

To obtain the vascular architecture of the spinotrapezius muscle, nine male Sprague-Dawley rats (215±19.7 g) were used. A series of 40 to 60 photographs were taken for each muscle using a high magnification stereo microscope (Nikon, 40X), from which a complete montage of the entire muscle was constructed, as shown in Fig. 1.

To measure the blood flow velocity and vessel diameter, eighteen rats (145±8.0 g) were used. The exteriorized spinotrapezius muscle was extended into a flattened sheet with silk sutures over an optical window in the tissue bath. One artery (1A, 2A or 3A) was chosen for study from each rat. Since the *in situ* spinotrapezius muscle is thin and relatively transparent, it can be transilluminated and viewed through a 10X or 20X Nikon water immersion objective. The schematic diagram for the experimental setup is shown in Fig. 2. During the experiment the images were captured with a closed-circuit camera, displayed by the attached monitor and recorded on a video tape for further analyses. The vessel diameter (d; μm) was analyzed using an electronic video caliper (Microcirculation Research). The centerline red cell velocity (V; mm/s) was measured by an optical Doppler velocimeter (Microcirculation Research). Since V is 1.6 times the average blood flow velocity (u) in the vessel (Davis 1987), the volumetric blood flow rate (Q; nl/s) in the individual artery is estimated based on

the centerline red cell velocity and the vessel diameter (d; μm), given as,

$$Q = \frac{\pi(d/2)^2 V}{1.6 \cdot 1000} \tag{2.1}$$

The experimental data were acquired and retrieved with LabVIEW® software running on a Macintosh computer.

2.2.3 Measurement Protocols

Two protocols were used in the experimental studies. In the first protocol, nine rats (215±19.7 g) were used to construct photomontages of the muscle. These rats were a little heavier than those (145±8.0 g) used in the second protocol. This is because the vasculature of larger rats was easier to observe. The anatomical data of these vessels were later used to extrapolate vascular information required for evaluating the enhancement in k_{eff} in vessels up to 195 μm diameter.

In the second protocol, after 20 to 40 minutes stabilization following the surgery, an individual artery was chosen from the muscle for three trials. The first one was to take measurements under the normal condition (baseline). The centerline red cell velocity, the vessel image, and the tissue bath and rectal temperatures were recorded continuously for a two-minute measurement period. In the second trial, norepinephrine (10^{-7} M) was added to achieve the maximum constriction of the microvascular bed. After stabilization, measurements were

made for another two-minute period. The solution was then drained and the drug was washed out by the Krebs solution. The last trial was to make measurements under vasodilation. A maximally dilating dose of sodium nitroprusside ($10^{-4.5}$ M) was used to induce the maximum vasodilation of the microcirculation under study. These three trials covered the full range of vasoregulation induced by the pharmacological vasoactive agents. The resulting potential change of volumetric blood flow rate were used to establish the lower and upper bounds of the blood flow Peclet number and diameter, and thus to predict the enhancement in k_{eff}, accordingly.

2.3 Results

2.3.1 Vascular Architecture of Spinotrapezius

The number of vessel pairs per unit cross-sectional tissue area in generation i, n_i (No./mm^2), and the countercurrent vessel pair length, L_i (mm), were measured from the photomontages. To obtain relationships between these two vascular parameters and the vessel diameter, d (μm), all data, which covered the vessel size from 45 to 165 μm diameter for the 1A to 3A vessel pairs, were plotted in Fig. 3. The regression formulas for n_i and L_i are given by:

$$n_i(No./mm^2) = 5910\,(d(\mu m))^{-2.03} \qquad (2.2A)$$

$$L_i(mm) = 0.0314\,(d(\mu m))^{1.10} \qquad (2.2B)$$

In Fig. 3, the short dashed lines are the regression results given by Eqs. (2.2A,B) for the rat spinotrapezius, whereas the long dashed lines are the regression formulas for n_i and L_i for the rat cremaster muscle obtained previously in (Zhu *et al.* 1995). The trends of the curves for these two types of muscle are similar, except that the results for n_i for the spinotrapezius lie above those for the cremaster for vessels of diameter $d<100$ μm.

The center-to-center spacing between the countercurrent paired vessels, l, and its dimensionless value, l/a, where a is the vessel radius, have an important effect on the efficiency of countercurrent heat exchange. In (Zhu *et al.* 1995) rough estimates were given for the center-to-center spacing between vessels and the same value of l/a, 2.5, was chosen in calculating σ for all vessel generations. In the present study the change in l/a with vessel generation is carefully measured for the first time in the experiment. The results showed that l/a lies within the range of 2.2-3.3 for 1A vessels, 2.3-3.5 for 2A vessels and 2.8-5.0 for 3A vessels.

2.3.2 Centerline Red Cell Velocity, Vessel Diameter and Volumetric Blood Flow Rate

The average vessel diameter (d) and related centerline red cell velocity (V) are given in Fig. 4 for each vessel generation under different vasoregulatory conditions. The detailed values of V and d are presented in Table 1. As discussed earlier in the methods, only one artery was examined in each experiment. Six

arteries for each vessel generation, chosen from a total of eighteen rats, were used in this part of the experimental study. Based on the V and d measurements, the volumetric blood flow rate (Q) can be calculated from Eq. (2.1). Figure 5 shows the average value of Q for the 1A, 2A and 3A vessels under different vasoregulatory conditions. The volumetric blood flow rate of the 1A, 2A and 3A vessels increased 7, 8 and 11 fold, respectively, when conditions were changed from vasoconstriction to vasodilation. As we shall see in the following these changes in Q produced a dramatic increase in k_{eff} mainly due to the 1A vessels.

2.3.3. Enhancement in the Effective Thermal Conductivity

The general expression for the tensor conductivity $(k_{ij})_{eff}$ derived in the Weinbaum and Jiji theory (1985) is given by:

$$(k_{ij})_{eff} = k_t\left(\delta_{ij} + \sum_i \frac{k_b^2 n_i \pi^2 d^2 Pe^2}{16 k_t^2 \sigma} l_i l_j\right) \tag{2.3}$$

where l_i and l_j are the direction cosines of the vessel axis relative to the local tissue temperature gradient, Pe is the blood flow Peclet number, and σ is the conduction shape factor which will be discussed later.

To simplify the expression for k_{eff} in one-dimensional expression, $k_b = k_t$ and $i=j$, and $l_i \cdot l_j = 1$ were used in Eq. (2.3), which resulted in k_{eff} as a function of Pe or Le,

$$k_{eff} = k_t \left(1 + \sum_i \frac{n_i \pi^2 d^2 Pe^2}{16\sigma} \right), \tag{2.4A}$$

$$or \quad k_{eff} = k_t \left(1 + \sum_i n_i \sigma Le_i^2 \right) \tag{2.4B}$$

where $Le_i = \pi d Pe / 4\sigma$ is defined as the characteristic thermal equilibration length for vessel generation i. These equations give the total contribution to k_{eff} from all generations of countercurrent pairs.

The blood flow Peclet number is expressed as:

$$Pe = \rho_b c_b d u / k_b \tag{2.5}$$

where u, the average velocity of the blood flow, is estimated by $u = V/1.6$ (Davis, 1987). In this study, Pe varied from 0.8 to 17.9 as shown in Fig. 6. One observes that the results for all vessels, including the data for vasoconstriction and vasodilation, fall along a single curve which is given by the regression formula

$$Pe = 0.00438 (d(\mu m))^{1.70} \tag{2.6}$$

This result is close to the prediction $Pe = \text{constant} \cdot (d)^2$ obtained from Murray's law (Murray 1926a).

As previously noted, the asymptotic analysis in (Weinbaum and Jiji 1989) reveals that Eqs. (2.4A,B) can be expected to provide reasonable accuracy provided $\varepsilon < 0.2$, since this condition guarantees that the average artery-vein temperature gradient will be close to that of the local tissue. In addition, a

second criterion, $(d/2)\cdot Pe<3$ mm, was established for the two-dimensional tissue preparations in (Zhu *et al.* 1996) as described earlier in the introduction. Figure 7 shows the variations of ε and $(d/2)\cdot Pe$ with respect to the vessel diameter d. ε changes from 0.003 to 0.129 and $(d/2)\cdot Pe$ is less than 1.3 mm, indicating that the theory for k_{eff} should be valid for all the vessels used in this experiment.

The original form of the conduction shape factor used in the Weinbaum-Jiji equation was determined for paired vessels embedded in an infinite medium:

$$\sigma_{in} = \pi/\cosh^{-1}(l/d) \tag{2.7}$$

Since the rat spinotrapezius muscle is a two-dimensional tissue preparation with tapered thickness, a new shape factor needs to be calculated for this particular configuration. In (Zhu and Weinbaum 1995) a mathematical model was developed for evaluating σ for two-dimensional tissue preparations with uniform thickness and width. The geometry is shown in Fig. 8. This basic model was modified in (Zhu *et al.* 1996) to take account of axial conduction in the tissue and the supporting glass slide. The boundary conditions are the continuity of temperature and heat flow at the vessel-tissue boundary, and a free convection boundary condition at both the tissue and glass surfaces. A Green's function was first developed for a line source arbitrarily positioned within the tissue region to simulate the thermal effect of the vessel. The temperature solution for the paired vessels undergoing countercurrent heat exchange was then constructed by

superposing the Green's functions for both vessels. The desired expression for the shape factor was derived from the solution of temperature distributions in the cross-sectional plane. This expression has the following form if the supporting glass slide is neglected and the ratio of blood to tissue conductivity is unity:

$$\sigma_{2D} = \frac{1}{2\overline{G}_{va} - 2\overline{G}_{aa} + 11/(24\pi)} \tag{2.8A}$$

where

$$\overline{G}_{aa} = \frac{1}{2\pi}\int_{-\pi}^{\pi} G(x,y;\ \xi_a,\eta_a)|_{\rho_a=1}\, d\phi_a \tag{2.8B}$$

$$\overline{G}_{va} = \frac{1}{2\pi}\int_{-\pi}^{\pi} G(x,y;\ \xi_v,\eta_v)|_{\rho_a=1}\, d\phi_a \tag{2.8C}$$

and $G(x,y;\ \xi_a,\ \eta_a)$ and $G(x,y;\ \xi_v,\ \eta_v)$ are Green's functions which were derived and given by Eq. (A.11) in Appendix 1 of (Zhu and Weinbaum 1995). These Green's functions, which satisfy Laplace's equation in the tissue region, are functions of the tissue conductivity, k_t, free convection coefficient at the tissue surface, h, and the vessel-tissue configuration.

Representative solutions for σ_{2D} in the rat spinotrapezius muscle (H=6) and a thin mesenteric tissue (H=2) are shown in Fig. 9. σ_{2D} was calculated based on the values of H, D, l/a and Biot number Bi, where $Bi=h\cdot H_t^*/k_t$. $H=H_t^*/a$ and $D=D^*/a$ are dimensionless parameters, where a, H_t^* and D^* are the dimensional

vessel radius, half tissue thickness and half width, respectively. To apply Eq. (2.8A) for σ_{2D} to the spinotrapezius muscle preparation, in which the tissue thickness and width vary, several approximations were made. According to the experimental data, the average vessel radius, muscle thickness and width were assumed to be 50 μm, 600 μm and 8 mm, respectively. Therefore, H=6 (H_t^*=300 μm) and D=80 for the spinotrapezius muscle. For other two-dimensional tissue preparations such as a thin mesenteric tissue, H=2 and D=80. For free convection in air, h_{air} varies between 5 and 25 W/m °C (Incropera and Dewitt 1981) and if k_t=0.5 W/m^2°C, Bi_{air} lies between 0.003 and 0.015. For water, h_{water} is approximately 250 W/m °C (Incropera and Dewitt 1981), Bi_{water} is therefore 0.15. Fig. 9 illustrates how vessel spacing and Biot number influence σ_{2D}. One observes for free convection in air ($0.003<Bi<0.015$), the relationship between σ_{2D} and l/a is insensitive to Bi for both H=6 and H=2. Therefore, an average value of 0.009 is chosen for Bi_{air} in our calculations. When H=6, D=80, and values of l/a=2.2, 2.5 and 3.0 representative of the 1A to 3A vessels in the rat spinotrapezius, the expression (2.8A) for σ_{2D} yields 2.42, 2.18 and 1.99, respectively. For the same vessel spacings, σ_{in} from Eq. (2.7) for an infinite medium is 7.08, 4.53, and 3.26, which is approximately 1.5 to 3 times as large as σ_{2D}. σ_{in} describes perfect countercurrent heat exchange in an infinite medium whereas σ_{2D} describes heat exchange between paired vessels in a tissue layer with

free convection at its surfaces. The smaller values of σ_{2D} are due to the fact that the heat loss to the environment reduces the heat exchange between the countercurrent vessel pairs.

From Eq. (2.4B), the enhancement in k_{eff} is determined by the summation $\sum_i n_i \sigma Le_i^2$. The variation of $n_i \sigma Le_i^2$ with vessel diameter is plotted in Fig. 10. The value of $n_i \sigma Le_i^2$ is insignificant for vessels <100 μm diameter and then increases rapidly achieving a value of 0.68 for vessels of 130 μm diameter. The total increase in k_{eff} is the sum of the contributions from 1A, 2A and 3A vessel generations. To determine the relative contribution of each vessel generation to k_{eff}, the average vessel diameters were first obtained for the 1A to 3A vessels for vasoconstriction or vasodilation from Table 1 or Fig. 4. For vasoconstriction the 1A, 2A and 3A vessel diameters are 54, 43 and 27 μm, respectively. The magnitude of $n_i \sigma Le_i^2$ is negligible for all three vessel generations and there is no enhancement in k_{eff}. In contrast, for vasodilation the 1A, 2A and 3A vessel diameters are 119, 90 and 58 μm. The corresponding magnitudes of $n_i \sigma Le_i^2$ from the regression curve given in Fig. 10 are 0.46, 0.14 and 0.02. The total enhancement in k_{eff}, $\sum_i n_i \sigma Le_i^2 = 0.62$, is due primarily to the 1A vessels as noted previously in (Zhu *et al.* 1995). Detailed data of enhancement in k_{eff} are summarized in Table 2.

2.4 Discussion

In the present study simultaneous measurements of flow and diameter were obtained for countercurrent microvessels from 25 to 130 μm diameter in the *in situ* rat spinotrapezius muscle. In the previous study on the rat cremaster muscle these measurements were limited to vessels <75 μm in diameter where there was little enhancement in k_{eff}. In contrast, a 1.7-fold increase in k_{eff} has been found from the present experimental measurements for microvessels maximally dilated to 130 μm using pharmacological vasoactive agents.

The Weinbaum-Jiji expression for k_{eff} is valid provided $\varepsilon<0.2$. Under this condition, the axial gradient of the mean artery-vein temperature will closely follow that of the mean tissue temperature. This guarantees in a nearly infinite medium a small heat loss between the countercurrent vessel pair and the surrounding tissue. In thin two-dimensional tissue preparations heat exchange occurs not only between the artery and vein, but also between the paired vessels and the external environment. A more rigorous criterion for applying the Weinbaum-Jiji theory in the two-dimensional tissue preparations shown in (Zhu *et al.* 1996) is: $(d/2)\cdot Pe<3$ mm. This condition again insures that the vessel bulk temperature gradients closely follow the tissue temperature gradient. Table 3 presents values for ε and $(d/2)\cdot Pe$ which have been extrapolated using the regression curves in Fig. 7, which shows that when the vessel diameter is less than 195 μm, both the criteria for ε and $(d/2)\cdot Pe$ are satisfied. Therefore, the

Weinbaum-Jiji theory for k_{eff} is valid for vessels as large as 195 μm and Eqs. (2.4A,B) can be used to this limit. The extrapolation of the present experimental measurements for $n_i \sigma L e_i^2$ is presented in Fig. 11. An approximate 5-fold increase in k_{eff} is predicted for 195 μm diameter 1A vessels.

Another important factor in evaluating the enhancement in k_{eff} is the conduction shape factor. The original form of the shape factor, σ_{in}, used in the Weinbaum-Jiji theory was for paired vessels in an infinite medium. In the present study, a newly derived shape factor for two-dimensional tissue preparations, σ_{2D}, which is a function of D, H, l/a, and Bi has been used. Fig. 9 illustrates the dependence of σ_{2D} on these parameters. As shown in Fig. 9, σ_{2D} decreases when l/a increases or H decreases. The reason is that increasing the vessel spacing or decreasing the tissue thickness results in a less efficient heat exchange between the paired vessels and thus leads to a decrease in σ_{2D}. In addition, σ_{2D} increases with increasing Bi. At first glance this increase in σ_{2D} may seem surprising since larger Bi allows more heat to leave the artery as well as the countercurrent vein. However, the degree of the Bi effect can be different on the artery and the vein. When Bi is increased, the lower blood flow velocity in the vein may allow more heat flow into the surrounding which results in a relatively larger artery-vein temperature difference. Therefore, a modest increase in heat exchange between the paired vessels can be produced. It is also found that σ_{2D}

decreases significantly as l/a increases when $l/a<5.0$ but this decrease is much more gradual for $l/a>>1$ with the result that σ_{2D} depends primarily on Bi and H when $l/a>>1$. In general, σ_{2D} is 1/3 to 2/3 of σ_{in} for the range of l/a measured in the experiment. This decrease in conduction shape factor is due to the heat loss to the environment from the tissue layer.

In proceeding from vasoconstriction to vasodilation the volumetric blood flow rate increased 7, 8 and 11 fold for the 1A, 2A and 3A vessels, respectively. In contrast, the increase in the flow rate for the 1A to 3A vessels from baseline to maximum vasodilation in (Zhu *et al.* 1995) was only 2 to 3-fold. One observes similar results in Fig. 5 where a typically 1.5 to 2-fold increase from baseline values is obtained for maximum dilation. This suggests that the trauma of the experiment may cause the vessels to be far from their normal resting state which is probably much closer to the vasoconstricted condition.

The large change in Q from vasoconstriction to vasodilation suggests that a significant enhancement in k_{eff} can be achieved through vasoregulation. For the 1A, 2A and 3A vessels in Fig. 4 there is no significant increase in k_{eff} of the rat spinotrapezius in the vasoconstricted state, but a total 62 percent increase in k_{eff} is predicted for 145 g rats in the vasodilated state. One can estimate the effect of vasoregulation of the spinotrapezius in larger rats where the enhancement in conductivity is much more dramatic. Figure 4 shows that for maximum

vasodilation, the diameter of the 1A, 2A and 3A vessels is approximately twice as that of their vasoconstricted state. Consider a large rat whose vasoconstricted 1A, 2A and 3A vessels were 100, 75 and 50 μm diameter, respectively (These diameters are scaled roughly in the same proportion as the 1A, 2A and 3A vessels of the 145 g rat whose diameters are shown in Fig. 4.). The contribution of $n_i\sigma Le_i^2$ to k_{eff} for this larger rat would be from Fig. 11 about 0.2 for the 1A vessels, 0.06 for the 2A vessels and negligible for the 3A vessels yielding a k_{eff} that is approximately $1.26k_t$. Assume now that these vessels doubled in size for conditions of maximum vasodilation as shown for the 145 g rats in Fig. 4 and the 1A, 2A and 3A vessel diameters increased to 200, 150 and 100 μm, respectively. From Fig. 11 the contribution of $n_i\sigma Le_i^2$ to the dilated 1A, 2A and 3A vessels would be 4.36, 1.26 and 0.22, respectively, yielding a k_{eff} of $6.84k_t$. This simple example shows that vasoregulation can cause a remarkable increase in tissue conductivity, even in a region where there was little or no enhancement in k_{eff} under vasoconstricted conditions. The evaluation of the enhancement in k_{eff} due to vasoregulations in large rats has been summarized in Table 4 and 5. For comparison, Table 5 presents a similar example where the vessel precisely follows Murray's law (Murray 1926a) at bifurcating sites, and the dilated diameter for the 1A vessel reaches to the limit of the validation of the Weinbaum-Jiji theory in the rat spinotrapezius muscle. Similar results have been obtained.

Chapter 3. Scaling Vasculature in Rat Spinotrapezius Muscle

The current chapter studies the scaling of the vascular architecture and blood flow in the rat spinotrapezius muscle. Detailed allometric biological scaling relations were established based on experimental measurements of the tissue weight, vessel diameter, and blood flow rate in the rat spinotrapezius muscle under the normal, vasoconstricted, and vasodilated conditions. Using these relationships, blood flow rates within microvessels of different generations in the spinotrapezius muscle can be extrapolated over a wide range of muscle weights and vessel sizes. This method provides an opportunity to predict blood flow in large microvessels where it is difficult to make direct measurements using optical methods due to the high blood flow rate and the thickness of the tissue and vessel wall. Furthermore, the allometric relationship between the blood flow rate and vessel diameter indicates that the shear stress at the vessel wall is approximately constant which follows the previously proposed minimum work principle (Murray 1926a,b).

3.1 Introduction

Blood flow rate plays an important role in the local transport of oxygen, nutrients, hormones, as well as the exchange of heat and mass in the vascular

system. Theoretical models and experimental measurements of thermal equilibration in blood perfused tissue have shown that the primary countercurrent heat exchange occurs in microvessels up to 200 μm diameter (Lemons *et al.* 1987, Zhu *et al.* 1995). Significant enhancement in the tissue thermal conductivity due to blood perfusion were found in vessels ranging from 100 to 200 μm diameter, as described in last chapter. To study the role of blood flow in thermally significant vessels, it is desired to measure blood flow in vessels within this range.

Different techniques have been used for measuring blood flow in large and small vessels, respectively. For large vessels, flow transducers can be directly placed around or on the vessels to make the measurement. Ultrasonic Doppler (Doucette *et al.* 1992, Haaland 1994, Upton *et al.* 1994), electromagnetic flowmeter (Haaland *et al.* 1994), indicator dilution (Hansell 1992), and thermal clearance methods (Cameron 1970, Nitzan *et al.* 1993) are widely used. In the microcirculatory studies, image tracking (Schmid-Schönbein 1975), dual-slit and dual window methods (Intaglietta *et al.* 1975, Lipowsky and Zweifach 1978, Wayland and Johnson 1967), spatial correlation (Tyml and Sherebrin 1980), prism gratings and arrays (Kiesewetter *et al.* 1982), and laser and optical Doppler techniques (Zhu *et al.* 1995) are commonly used for the measurement of flow in vessels up to about 100 μm diameter. These techniques are based on detection of the signals produced by the individual red cell motions. As vessel size increases

the hematocrit also increases and it becomes more difficult to detect individual red cell movement. For vessels ranging from 100 to 300 μm diameter, neither the methodology for large vessels nor that for small vessels is accurate enough for *in situ* blood flow measurement. However, vessels in this range are believed to play an important role in the blood-tissue thermal equilibration (Lemons *et al.* 1987, Zhu *et al.* 1995). Therefore, extrapolations of the experimental measurements are needed to obtain blood flow rates within these vessels.

Biological scaling analyses are widely used for extrapolations of physiological or anatomical variables as functions of body mass (Adolph 1949, Calder III 1981, 1987, Jungers 1985, McMahon 1973, Schmidt-Nielsen 1984). Scaling analysis aids in the efficient handling, interpretation, and correlation of experimental data by reducing the number of experiments. In comparative physiology, this is the most useful and powerful tool to analyze the anatomical structures and physiological functions in relation to an animal's body size. In cancer risk assessment and clinical medicine, the allometric equations are used to extrapolate the observed experimental results between animal species and human beings. Allometric equations are useful for estimating the magnitude of some variable as a function of an organ or a given body size. A general allometric form of $Y = c_1 \cdot M^{c_2}$ or $\log(Y) = \log(c_1) + c_2 \cdot \log(M)$ is a common empirical expression for such relation, where Y is the variable as a function of body mass M raised to a

power c_2; c_1 is a proportionality constant for the phylogenetic category in a defined set of environmental and physiological conditions. The allometric scaling has become a basic mathematical tool for analyzing the form, structure composition, and function associated with change in size in animals. Many variables have been subject to scaling: organ size (Armstrong 1990, Holt and Rhode 1976, Jungers 1985, Schmidt-Nielsen 1984, Van Der Meulen and Carter 1995), energy metabolism (Feldman and McMahon 1983, Heusner 1982, Kleiber 1947), toxicity study (Ings 1990, Travis 1991, Vocci and Farber 1988), and growth (Siddiqui *et al.* 1992). Although such a power function is an empirical statistical relationship rather than a biologically meaningful interpretation of interspecific differences (Heusner 1987), it can be used as an extrapolation formula for physiological variables in the same tissue of the same animals but of different sizes.

In addition to the scaling relations, the vascular architecture is another interesting topic. It has been widely believed that in the process of evolution the competitive effect of natural selection has left most biological systems in an optimally designed system. The vascular architecture, especially the branching characteristics, is the most important factor to make the vascular network more efficient. The complex branching hierarchy of vessels resembles a globally optimal system that minimizes the cost of the construction and maintenance of

hemodynamic flow. In 1926, Murray first suggested that branch diameters and branch angles at a bifurcation are governed by certain optimal principles which optimize the bifurcation in its blood conducting function (Murray 1926a,b). Murray's original derivation minimized the energy cost of overcoming the viscosity of blood in the vessels and the metabolic cost of maintaining the volume of blood and vessel tissue involved in the flow. A Newtonian laminar flow was intrinsically assumed. Murray's law was also extended to turbulent flow (Roy and Woldenberg 1982, Uylings 1977) as well as to non-Newtonian rheological behavior (Mayrovitz 1987). The more direct derivation of Murray's law by Sherman (1981) suggested that a functional relationship exists between the vessel diameter and the volumetric flow, vessel-wall shear stress, Reynolds number, etc.. In an optimum system, the volumetric flow (Q) and the vessel diameter (d) has the following relationship: $Q=c\cdot d^3$, where c is a constant which results in a constant vessel-wall shear stress and the Reynolds number proportional to the square of the vessel diameter. Research on the optimum principles have led to two aspects which are dependent on each other. One is related to the diameters of the parent and daughter vessels. This is equivalent to considering the relation between volumetric flow and vessel diameter. The other aspect concerns the bifurcation angles in tree structures such as the air paths in the lung and the vasculature. The dependence of branching angle at a bifurcating site on the

relative size of the parent and daughter vessels has been the subject of attention of many authors (Liu and Ritman 1986, Uylings 1977, Zamir 1982, Zamir *et al.* 1984). Experiments have been performed in the microvasculature by Zamir *et al.* (1976, 1984), Mayrovitz and Roy (1983) and others to examine the branching characteristics as well as the validity of Murray's law.

In this study, allometric relationships describing the muscle weight, vessel diameter and blood flow rate in the rat spinotrapezius muscle were derived based on experimental data obtained within measurable range via an optical Doppler velocimeter. Measurements were made in vessels under baseline, vasoconstriction and vasodilation. The volumetric blood flow rate, vessel diameter and bifurcation angle were analyzed in a various levels of perfusion. Also, the experimental results were used to examine the validity of the optimal principles in the muscle. The obtained allometric relationships will allow one to obtain blood flow in large microvessels in the tissue where it is difficult to make direct measurements using optical methods due to the high flow rate and the thickness of the tissue and vessel wall by extrapolating results from small vessels.

3.2 Methods

3.2.1 Experimental Methods

Male Sprague-Dawley rats were used in this study. The rat was weighed

by a digital scale (Sunbeam) at the beginning of each experiment, and then anesthetized with an intraperitoneal injection of sodium pentobarbital solution (40 - 45 mg/kg). Supplemental doses would be administered as needed during the experiment. Microsurgery was subsequently performed to expose the spinotrapezius muscle. This surgery as well as the experimental conditions were similar to those described in Chapter 2.

To obtain the blood flow rate, both the centerline red cell velocity (V; mm/s) and vessel diameter (d; μm) were measured in the experiment. The volumetric blood flow rate (Q; nl/s) in the individual artery was estimated based on the centerline red cell velocity and the vessel diameter according to the formula $Q=\pi(d/2)^2V/1600$ proposed in (Davis 1987).

The 1A, 2A and 3A microvessels were chosen for study in each experiment. The stabilization took 20 to 40 minutes following the surgery. The centerline red blood velocity, the vascular image of each vessel generation, and the bath and rectal temperatures were recorded continuously for a two-minute measurement period in baseline. Then, sodium nitroprusside ($10^{-4.5}$ M) was added to achieve the maximum vasodilation. A two-minute measurement period followed after the stabilization. The drug was washed out before norepinephrine (10^{-7} M) was added to achieve the maximum vasoconstriction under which a similar measuring procedure was repeated. The drug-induced maximum vasoconstriction and

dilation were used to obtain the potential range of volumetric blood flow rate under vasoregulatory conditions. After the blood flow velocity was measured, the spinotrapezius muscle was dissected from the rat. The solution on the muscle was dried by a paper tissue and the muscle was immediately weighed by an analytical balance (Mettler). Statistical analysis was performed by SlideWrite™ software to obtain the best curve fit with the *R* value, the square root of the coefficient of determination, to the experimental data.

3.2.2 Measurement Protocols

In the first experiment, sixteen rats from 70 to 160 g were used for obtaining the relationship between the rat weight and the spinotrapezius muscle weight.

In the second experiment, twelve rats from 69 to 162 g were used for measuring the allometric relations of the blood flow rate. After the microsurgery and the stabilization period, measurements for the blood flow rate were taken for the 1A, 2A and 3A vessels in baseline. Afterwards, measurements in the vasodilation were acquired in ten of these twelve rats. Finally, only six of them were used to continue the measurements in vasoconstriction due to the animal condition in the experiment.

3.3 Results

3.3.1 Allometric Scaling Relations

The weight of spinotrapezius muscle (w) increases with the rat body weight (W). Figure 12 shows the spinotrapezius weight measurements from sixteen rats from which an allometric relationship, $w(\text{mg})=0.0273\cdot(W(\text{g}))^{1.65}$, was obtained. Although the exponent of the equation is 1.65, larger than most exponents (~1) in equations relating quantitative properties (heart weight, brain weight, tidal volume, *etc.*) to the body mass among mammals (Adoph 1949), a good correlation exists between w and W with the R value of 0.97.

Using the muscle weight (w) as an index, Fig. 13 presents the experimental results of the volumetric blood flow rate (Q) for the 1A, 2A and 3A vessels under the vasoconstricted condition (n=6). Results for the three vessel generations in baseline (n=12) and vasodilation (n=10) are given in Fig. 14 and 15, respectively. The regression curves for individual vessel generations at each vasoregulatory condition are drawn through the experimental data. Mathematical expressions for these curves and the corresponding R values are summarized in Table 6.

3.3.2 Optimal Principles in Vascular Circulation

Volumetric Blood Flow Rate. A relationship between blood vessel diameter (d) and its related volumetric blood flow rate (Q) found in this study is shown in Fig. 16. This figure includes all of the measured data for the three vessel

generations in various vasoregulated conditions. Using an optimal power curve (solid line) to fit the experimental data, the empirical relation is given by

$$Q(nl/s) = 0.00141 \cdot (d(\mu m))^{2.48} \qquad (3.1)$$

with the R value of 0.96. The dash line, $Q(\text{nl/s}) = 0.00140 \cdot (d(\mu\text{m}))^3$, has also been plotted in Fig. 16 to give a comparison. This line is the optimal cubic fit to the experimental data which results from the lease-square regression. The "cubic law", which has the expression of $Q = c \cdot d^3$ (c is a constant), implies that the complex branching hierarchy of vessel is approximated to a globally optimal system that minimizes the cost of the construction and maintenance of hemodynamic flow. It is found from the figure that the empirical fitting is close to the cubic fitting, especially in vessels less than 100 μm diameter. Figure 17 is the logarithm plot of volumetric blood flow rate as a function of vessel diameter with the 95% confidence limits for the experimental data.

Including the blood flow measurements obtained in Chapter 2, Table 7 presents the measured allometric relations of the two groups of rat weight range (69-162 g, 145±8.0 g) in baseline and in all three vasoregulatory states. Since there exist no significant differences among vasoconstriction, baseline and vasodilation in each group, one regression curve of flow versus diameter was used to fit data in all three states. The experimental data from the rats weighed of 145±8.0 g in all three states are shown in Fig. 18. A better correlation can be

found in this figure than that shown in Fig. 16 for a larger weight range.

Shear Stress. Based upon the above mentioned relationship between volumetric blood flow rate (Q) and vessel diameter (d) for the rats weighed 145±8.0 g ($Q=0.00128 \cdot d^{2.48}$), we can calculate the vessel wall shear stress in the rat spinotrapezius muscle. The apparent blood viscosity (μ) used by Hyness (1959) is $\mu = \frac{0.03}{(1+12/d)^2}$ (μ; poise, d; μm). In this experiment, μ ranges from 0.0178 to 0.0248 poise. The wall shear stress (τ) can be estimated from $\tau=32\mu Q/\pi d^3$ for laminar flow (Kamiya *et al.* 1984). This application is justified by the Reynolds number ($Re=4\rho_b Q/\pi\mu d$) ranging from 0.293 to 0.307, which is far below the critical value of 2300. Therefore, when vessel diameter changes from 40 to 120 μm, the related wall shear stress changes from 27.07 to 24.83 dyn/cm^2, indicating a much smaller change in shear stress as compared to the change in diameter.

Branching Pattern. Understanding the vascular branching pattern is necessary in developing a vascular optimal system as well as interpreting certain vascular diseases. The study of the arterial branching pattern in the spinotrapezius muscle is conventional since the principal branching from the 1A to 2A, and 2A to 3A is bifurcation (Fig. 1), where the parent vessel divides into two daughter vessels. In every photomontage obtained from the rat muscle as described in Chapter 2, bifurcation sites from the 1A to 2A and the 2A to 3A

were chosen for analyses. The parent artery diameter d_0, the two branch diameters d_1 and d_2 were measured. By definition, d_1 denotes the larger diameter of the two daughters. Also measured were the angles θ and φ which are the respective angles of the daughter vessels (d_1 and d_2) relative to the parent vessel's central axis. The geometric parameters about diameters and angles have been specified in Fig. 19. The relationship between d_2/d_1 and d_2/d_0 has been measured, plotted and compared with the optimal predictions $\frac{d_2}{d_0} = \frac{\alpha}{(1+\alpha^3)^{1/3}}$ and $\frac{d_2}{d_1} = \alpha$ in Fig. 20. The data are reasonably well packed around the theoretical curve indicating a good qualitative agreement. Different optimal criteria combined with Murray's cube law predict the branching angles. For minimum power and lumen, the following relations can be derived: $\cos\theta = \frac{(1+\alpha^3)^{4/3}+1-\alpha^4}{2(1+\alpha^3)^{2/3}}$, and $\cos\varphi = \frac{(1+\alpha^3)^{4/3}+\alpha^4-1}{2\alpha^2(1+\alpha^3)^{2/3}}$. For minimum drag and lumen surface, there exist: $\cos\theta = \frac{(1+\alpha^3)^{2/3}+1-\alpha^2}{2(1+\alpha^3)^{1/3}}$, and $\cos\varphi = \frac{(1+\alpha^3)^{2/3}+\alpha^2-1}{2\alpha(1+\alpha^3)^{1/3}}$. These two optimal criteria provide two different predictions for θ and φ. Figure 21 shows the comparison between the measured θ and the corresponding predictions from the optimal criteria. Also, Fig. 22 presents the results for φ. One notices that the criterion for minimum power and lumen gives a better prediction for both θ and φ, and the measured angles of θ fit better to the predicted values than those of φ.

3.4 Discussion

3.4.1 Allometric Scaling

In this study, the intraspecific allometric blood flow scalings were obtained as functions of muscle weight and vessel diameter, respectively. Measurements were taken in the same species at various stages of maturation. These allometric relationships may reflect the influence of growth. An allometric relationship between the rat and muscle weight ($w(\text{mg})=0.0273\cdot(W(\text{g}))^{1.65}$) was gained in this study. In this relationship, the exponent, 1.65, is much larger than 1. It may be due to the spinotrapezius being nearly two-dimensional rather than a three-dimensional variable (i.e. heart, brain, tidal volume, etc.) vs. the body mass in many allometric scalings (Adolph 1949, Schmidt-Nielsen 1984). On the other hand, the spinotrapezius is a typical skeletal muscle. The previous interspecific investigation in skeleton has shown that the skeleton of a large animal is relatively heavier than that of a small animal. With increasing size, the skeleton increases out of proportion to the body mass i.e. the exponent is larger than 1 in the allometric scaling (Schmidt-Nielsen 1984). This argument is, if not fully confirmed, similar to what has been found in the rat spinotrapezius.

The allometric scaling for blood flow in the rat spinotrapezius has been studied for the first time, which provides an opportunity to observe its relationships with the body weight, muscle weight, and vessel diameter. These relationships can then be used to predict blood flow where it is difficult to

measure. Allometric equations are, however, descriptive rather than biological laws. It is possible that values predicted by allometric equations may differ from real measurements because of the individual variation. Since the vessels of interest in this study, ranging from 100 to 200 μm diameter, are not far beyond the scope of the experimental range (30-130 μm diameter), a reasonable accuracy can be expected in extrapolation using the obtained allometric equation with 95% confidence as shown by Fig. 17.

Table 6 shows that the exponents in the allometric equations increase from the 1A to 3A vessels in all three vasoregulatory states. The blood flow rate in the 3A vessels is almost proportional to its related tissue weight given the exponent is 0.96, 1.06 and 0.95 in vasoconstriction, baseline, and vasodilation, respectively. This phenomenon is expected since the 3A vessels supply the small arterioles prior to the capillary beds which perfuse the local tissue. Considering the energy expenditure in a typical skeletal muscle, blood perfusion can be directly related to its mass and thus the exponent in the allometric scaling between Q and w is very close to 1. The relationship between the blood flow rate and muscle weight is more nonlinear in the 1A and 2A vessels. These vessels are major supplying vessels and less uniformly distributed in the muscle. Examining the vascular geometry of spinotrapezius, it is found that in a large percentage of rats, besides the main blood vessel, there is a small secondary blood vessel along the lateral

border of the muscle, i.e. more than one 1A vessel can supply the rat spinotrapezius. On the other hand, if one compares the exponent values among various vasoregulatory conditions, these values vary little from vasoconstriction to vasodilation for the same vessel generation, but they are quite different from those under baseline. This suggests that the physiological situations might be very similar under maximum vasoconstriction and vasodilation. Here, the so-called baseline state in the experiment really reflects the physiological status of the rat right after the microsurgery but before administering any drug except the anesthetic, in which the degree of surgical trauma can vary in each experiment.

Throughout each experiment the rat was maintained in deep anesthesia and the vasoconstriction and vasodilation were locally induced by pharmaceutical agents. These vascular changes were caused by the direct effect of drugs on the vascular smooth muscle, which is different from that caused by the increased muscle metabolism in exercise or neural or hormonal regulation which involve both central and local factors can result in large changes in Q.

3.4.2 Murray's Law

Murray's law and its derivation provide a model of vascular organization and regulation. The relationships of Q/d^3=constant for vascular flow was developed by minimizing the cost of forcing the fluid (blood) through the pipes (blood vessels) against the fluid viscosity, and the cost of building and

maintaining the system (blood and blood vessels) (Murray 1926a). The exponent 3 which matches with the flow rate in pipe in an ordinary dimensional analysis, is an ideal value derived from the laminar, Newtonian flow. Further, $Q=c\cdot d^3$ also holds for non-Newtonian power-law fluid according to Mayrovitz (1987). The theoretical model derived by Pollanen (1992) showed that the exponent value is 2.33 and 3 for the laminar and turbulent flow, respectively. Also, the latest experiments by Zamir *et al.* (1992) showed that the relation between diameter and flow is governed by a 'square law' rather than the classical cube law in major branches of the aorta. They suggested that the square law may apply to the first few levels of the arterial tree, while the cube law is perhaps suitable for the subsequent to the precapillary levels. However, previous research found that the statistical value of the exponent is approximately 2.6 for the systemic arterial tree (Groat 1948) and 2.7 for the renal, mesenteric and other arterial systems in man (Suwa and Takahashi 1971), while it is 2.48 (W: 69-162 g, vasoconstriction, baseline and vasodilation) from this study. For the rat cremaster and cat mesentery Q and d satisfy the following relationships, respectively: $Q(\text{nl/s})=0.00022\cdot(d(\mu\text{m}))^{2.73}$ and $Q(\text{nl/s})=0.00016\cdot(d(\mu\text{m}))^{2.91}$ (House and Lipowsky 1987, Zweifach and Lipowsky 1977). Comparing the variations of the blood flow rate with respect to vessel diameter for vessels ranging from 30 to 200 μm in the rat spinotrapezius, cremaster, and cat mesentery, similar trends exist

in the rat spinotrapezius and the cat mesentery. However, a relatively low blood flow rate is obtained in the rat cremaster, especially when the vessel diameter is large. This lower flow could be in part due to the fact that the cremaster is the muscle covering of the testes whose the normal *in vivo* temperature is 34°C. This temperature is significantly lower than the rat's normal *in vivo* rectal temperature which is approximately 38 °C. The relatively low blood flow rate may be associated with a lower metabolic rate in the muscle.

If Murray's law holds in a vascular circulatory system, then it requires that shear stress to be kept as a constant in this system. Results from this experiment show that Murray's law is a good approximation in the rat spinotrapezius.

3.4.3 Short- and Long-Term Effects

One specific regression formula ($Q(\text{nl/s})=0.000510\cdot(d(\mu\text{m}))^{2.70}$) with a good correlation could be used to summarize the relationship between vessel diameter and blood flow in vasoconstriction, baseline and vasodilation for the rat weight range of 145±8.0 g (Fig. 18). So did the relationship for a wider rat weight range as shown in Fig. 16, where all data were summarized in one formulation ($Q(\text{nl/s})=0.00141\cdot(d(\mu\text{m}))^{2.48}$) without distinguishing their vasoregulatory conditions. This suggests that no matter under what kind of vasoregulatory condition, the relationship between Q and d does not change much, and it probably follows certain criterion of growth and downstream blood

distribution in muscle vascular system.

Since the data were obtained shortly after the vasoactive drugs were administered when the stable situations were reached, the results from the experiments reflect short-term responses. The time required for some of the endothelial responses to hemodynamically related forces, such as cell shape change, cell cycle entry and cell mechanical stiffness, is normally much longer than the time of our observations being on the order of hours to days. Whether these long-term changes are due to local autoregulatory mechanism to maintain a constant shear stress (Kamiya *et al.* 1984) or a structural reorganization of the vessel wall (Langille and O'Donnell 1986) is still unclear.

Short-term and long-term effects of flow in vessels are both mainly due to the responses of the vascular endothelial cells to the flow. The endothelium is continuously subject to hemodynamic forces, particularly the shear stress. Furchgott and Zawadzki discovered the first endothelium dependent response (Furchgott and Zawadzki 1980). It was found by Holtz *et al.* (1984) that the dilation of epicardial coronary arteries was endothelium-mediated. Similarly, Langille *et al.* (1986) observed that the arterial response to reduced blood flow was abolished when endothelium was removed from the vessel, and endothelium appeared to be essential to the compensatory arterial response to long-term changes in blood flow. Studies revealed that there exist different interactions

between the short-term and long-term effect of blood flow on endothelium. To understand its mechanism, a more comprehensive experiment should be designed to collect the information of flow, shear stress and endothelium simultaneously at each time stage. Also, the experiment should last long enough to allow an observation of the entire process of the flow-induced, endothelium-dependent and time-related vascular regulation. This will help us to interpret the resultant macroscopic changes at the microscopic level and thus to have a better understanding of the physiological mechanism in the microcirculation.

In conclusion, some allometric relationships for the vascular architecture and blood flow in the rat spinotrapezius muscle have been obtained in this part of the study. These empirical relationships are useful for extrapolating blood flow rates over vessel sizes beyond the measurable range. Also, the optimal principles in vascular circulation have been examined. $Q=c\cdot d^n$ has been obtained for various rat weight ranges. n has been found to be 2.48 and 2.70, respectively, and Murray's law is approximately followed.

Chapter 4. Microvascular Thermal Equilibration in Rat Spinotrapezius Muscle

This chapter investigates heat exchange in the thermally significant countercurrent paired vessels of the rat spinotrapezius muscle. Detailed tissue surface temperatures under normal (after the microvascular surgery) and pharmacologically vasodilated states were measured using high resolution infrared thermography. During vasodilation, a measurable temperature difference between the first-order feeding vessel pair and its surrounding tissue was found. The measured tissue temperatures were compared with those predicted by modifying the theoretical model for two-dimensional tissue preparations given by Zhu *et al.* (1996). A close agreement between the theory and experiment was obtained for the surface temperature profiles.

The Weinbaum-Jiji k_{eff} theory for heat exchange between the paired vessels and their surrounding tissue was also examined in this muscle. A close agreement was obtained between the theoretically predicted k_{eff} and the measured value calculated using a fin approximation for the tissue layer. This experimental study examined for the first time the thermal nonequilibration between blood vessels and the surrounding tissue, where the enhancement in k_{eff} due to the incomplete countercurrent heat exchange becomes comparable to the tissue axial conduction.

4.1 Introduction

In Chapter 2, the vascular structure and blood flow rate in an exteriorized rat spinotrapezius muscle have been experimentally measured. The largest first-order feeding artery where blood velocity and vessel diameter measurements were taken was 140 μm diameter. Based on these measurements, the effective thermal conductivity of the muscle, k_{eff}, which accounts for the enhancement of heat transfer due to the thermally significant countercurrent vessels, was estimated using the Weinbaum-Jiji theory. Also, the maximum enhancement in k_{eff}, which would be achieved through vasoregulation, was predicted. This analysis indicated that vasoregulation could have a dramatic effect on k_{eff}. Vessels which were approximately 100 μm diameter in their vasoconstricted state could undergo a 2-fold increase in diameter and a 5-fold enhancement in k_{eff} under conditions of maximum vasodilation (Table 4).

To measure tissue thermal conductivity or temperature profiles, self-heated thermistors and thermocouples have been extensively used in the past (Chen *et al.* 1981, Lemons *et al.* 1987, Patel *et al.* 1987, Valvano *et al.* 1984). However, neither method can be used to provide accurate local measurements of microvascular blood-tissue energy exchange due to their size limitations. Zhu *et al.* (1996) introduced an infrared thermography technique, which was successfully used to obtain the first measurement of axial thermal equilibration of a

countercurrent vessel pair in microcirculation. Measurements were performed in the rat cremaster vessels of 80 to 150 μm diameter, which were pharmacologically dilated. A significant transitional change was observed in thermal images when the Peclet number (*Pe*) increased from 1 to 14. However, the thermal nonequilibration between the blood vessels and the tissue was not obvious even when *Pe* reached 14. This was mainly due to the fact that the blood flow in the paired vessels was still not high enough to show a significant countercurrent convective effect. Their experiments suggested that only when countercurrent heat exchange is comparable to the tissue axial conduction will the thermal nonequilibration between the tissue and blood vessels be easily observable and the enhancement in k_{eff} be significant. The present study was designed to achieve these objectives by measuring the temperature distribution in a two-dimensional tissue preparation, the rat spinotrapezius muscle, where the major feeding vessels (1A) have a Peclet number that exceeds 20.

The rat spinotrapezius muscle is a paired muscle extending along the back of a rat. For the vascular heat transfer study, its thermal state is more characteristic of most skeletal muscle tissue than the rat cremaster whose normal temperature is only 34 °C. The microsurgery performed to exteriorize the spinotrapezius muscle is less traumatic than the cremaster isolation procedure since both the major feeding vessels and nerves can be kept intact during the

surgery. This flat tissue allows one to take infrared images of the muscle surface from which tissue temperature distributions can be measured like the cremaster but over a wider range of blood flow Peclet number. The resolution of the infrared system resolution is 0.025 °C in temperature and 30 to 40 μm in space.

The present experiment was performed on the first-order feeding vessels of the muscle, whose vasodilated diameters were larger than 140 μm but less than 200 μm. Blood flow in these vessels is high enough so that the convection effect of the blood is easily observable. These vessels also lie in the range of vessel diameter less than 200 μm where the Weinbaum-Jiji theory for countercurrent blood-tissue heat exchange is valid as described in Chapter 2. The detailed *in vivo* surface temperature field above individual microvessels as well as the microvascular geometry were measured. With these measurements, the local microvascular geometry and flow were related to the tissue temperature measurements. The enhancement of tissue thermal conductivity predicted by the Weinbaum-Jiji theory was compared with that experimentally measured. A good agreement has provided a direct experimental verification of the theory.

4.2 Methods

4.2.1 Experimental Methods

Ten male Sprague-Dawley rats (266.4±25.9 g) were used in this study.

The rats were anesthetized with an intraperitoneal injection of sodium pentobarbital solution (45 mg/kg) and supplemental doses were administered as needed. The rat was wrapped by a water-jacketed pad to maintain its core body temperature. After the microsurgery was done as described in Chapter 2, the right spinotrapezius muscle was exteriorized and rested on a supporting glass slide covering an optical window in the tissue bath. The muscle, still attached to and perfused by the rat, was immersed in the continuously circulated bathing solution. The schematic diagram for the experimental setup is shown in Fig. 23. The solution, which was similarly controlled as described in Chapter 2, was drawn from a stock reservoir and recirculated through the system.

The tissue preparation was transilluminated on the microscope stage (Zeiss) and viewed through a 10X Nikon water immersion objective. Due to the high blood flow rate and the thick tissue surrounding the major feeding vessels, not all the blood flow velocities could be directly measured using the optical Doppler velocimetry in this experiment. In those cases the previously measured relationship between the vessel diameter and average blood flow velocity, u(mm/s) $=0.650(d(\mu m))^{0.704}$ from the study in Chapter 2, was used to estimate the blood flow. During each experiment, the field of view was displayed on a video monitor and videotaped. The vessel diameter was measured with an electronic video caliper (Microcirculation Research Institute, TX) from the videotape.

The muscle surface temperature distributions were obtained via a high resolution infrared imaging system, the IRRIS-160ST with the CE Image+ software (Cincinnati Electronics Corporation, OH). The system allows an on-screen temperature readout with high resolution of 0.025 °C (@30 °C). Image signals were sent to a VGA connector for viewing as well as to a digital data port of a personal computer for recording. Before the experiment the infrared imaging system was calibrated by a thermocouple. The emmisivity was set at 0.95 for the muscle tissue (Cheesier and Eberhart, 1985).

To obtain the information on tissue vascular geometry, photographs of the isolated muscle were taken by a camera (Nikon PAX) with a Polaroid 545 film holder connected to a stereo microscope (Nikon SMZ-10, Japan) while the tissue was still in the bath. At the end of each experiment, the spinotrapezius was separated from the rat. The solution on the muscle was dried by paper tissue and the muscle was extended over a pre-cleaned slide for measurement of the muscle thickness and the depth of the feeding vessels from muscle surface. These measurements were made under the microscope by calibrating the focal length of the lens against a reference glass slide with known thickness. The precision was 4 to 7 μm.

4.2.1 Experimental Protocols

1) Microsurgery & stabilization

The microsurgery to exteriorize the spinotrapezius muscle typically required half an hour. After the muscle was immersed in the tissue bath, a stabilization period of approximately twenty minutes allowed the preparation to achieve its new steady state.

2) Measurement in the first trial (baseline)

After the stabilization period, video of the first-order feeding artery-vein pair was recorded continuously for a one-minute measurement period. The preparation was then moved under the infrared camera and the solution was drained. The thermal image of the preparation was immediately taken and recorded. The vessel diameter and the tissue surface temperature distribution were later analyzed from the videotape and the infrared image, respectively.

3) Measurement in the second trial (vasodilation)

The preparation was moved back to the tissue bath under the optical microscope. To increase blood flow rate in the feeding paired vessels, a vasodilator (Na nitroprusside $10^{-4.5}$ M) was introduced in the bath. After the drug was added, a ten-minute period was given for the preparation to reach its maximum vasodilated state. Then, the video and the thermal images were recorded as described in 2).

4) Vascular geometry

Upon completion of 1) to 3), the preparation was rinsed with a Krebs

solution for five minutes. Then, it was moved under the stereo microscope where photos of the vascular geometry were taken. Finally, the spinotrapezius was excised and the muscle thickness and the depth of the feeding vessels from the tissue surface were measured.

4.3 Results

4.3.1 Experimental Measurements

Figure 24 presents a typical first-order feeding vessel pair of the spinotrapezius. The artery is closely paired with the vein to form a countercurrent pair. The pair branches into the second order vessels, and so forth. In this case the diameter of the vasodilated artery is 141.7 μm, and of the vein is 184.3 μm.

Infrared thermal images of the first-order vessel pair were taken under normal conditions (baseline) as well as pharmacologically vasodilated conditions (vasodilation) as shown in Fig. 25 and Fig. 26. These images demonstrate a substantial change in thermal profile above the vessel pair from baseline to vasodilation. In each image a rectangular grid was drawn in the same location around the artery-vein pair to analyzed. The vessel pair was located in the center and oriented along the long axis of the rectangular area. The local x and z axes were defined with respect to this box, where z axis was set in the center of the

rectangular area along the vessel pair direction while the x axis was perpendicular to the vessels. The thermal disturbance produced by the first-order vessel pair is clearly evident in Fig. 26 for vasodilation, but is not distinguishable from the background temperature gradient for baseline. This effect was reproduced in all other nine experiments.

Figure 27 shows the surface temperature profiles normal to the axial direction of the first-order feeding vessel pair at three different axial locations under the baseline condition. The x, z locations correspond to the x-z coordinates given in Fig. 24. Locations of the paired vessels are represented by the two circles. Figure 28 shows the corresponding temperature profiles for vasodilation. One observes that the tissue surface temperature decays in the axial direction for both baseline and vasodilation. However, there is a distinct difference between the two flow states. In baseline, the vessel influence is small and the temperature profiles show only a moderate departure from linearity along the x direction at any given z location. In contrast, for vasodilation, the thermal disturbance caused by the blood vessels results in an elevated plateau in the temperature profile in the x direction, which is positioned over the vessel pair.

4.3.2 Theoretical Approximation

A three-dimensional heat transfer model was developed based on the schematic drawing given in Fig. 29. by Zhu *et al.* (1996). In this model,

countercurrent paired vessels were embedded in a two-dimensional tissue layer with free convection at both the tissue surface and the bottom of the glass slide. In (Zhu *et al.* 1996) an adiabatic condition was applied at $x=\pm D^*$, the tissue edge of a periodic array of blood vessels in the symmetric cremaster tissue preparation. For rat spinotrapezius, one side is connected to the body and the other is exteriorized in the tissue bath and the tissue temperature decreased in the x direction as shown in Fig. 27. Therefore, the existing mathematical model needed to be modified for its application in the present study.

To simplify the problem, we assume the temperature profile in vasodilation at each z location can be approximated by the superposition of two effects: a linear background tissue temperature in the x direction caused by the fact that one side of the muscle was connected to the body, and the thermal disturbance due to the incomplete countercurrent heat exchange of the paired vessels. The linear background in the x direction was obtained from the regression of the temperature profile at different z locations in baseline, since the vessel effect is not significant as shown in Fig. 27. The vessel effect is very similar to that addressed in (Zhu *et al.* 1996) expect for the inclusion of the artery-vein size difference and their asymmetric positioning relative to the tissue midplane in the present study. The theoretical temperature prediction has therefore been constructed by adding the perturbation due to the blood vessels to the linear

background temperature gradient.

Several geometrical and physical parameters are needed to apply the theoretical model. These include the convection coefficient h, the tissue-glass conductivity ratio, the vessel-tissue geometry and the thickness of the supporting glass slide. The measured major feeding artery diameter, d, was 141.7 μm and the tissue thickness, H_t^*, was 1030 μm. The center of the vessel was asymmetrically located 210 μm beneath the upper free surface and this thickness was assigned as H_l^*. Thus, the dimensionless tissue thickness above the centers of the paired vessels was $H_l=H_l^*/a=3.0$, where a is the major feeding artery radius. The dimensionless artery-vein spacing was $l/a=3.1$. The half width of the box was selected as $D^*=1420$ μm, since at this distance the thermal disturbance produced by the vessel pair had become negligibly small, and its dimensionless value is $D=D^*/a=20$. The thickness of the supporting glass plate beneath the tissue, H_g^*, was 1000 μm. To account for the additional thermal resistance in the vertical, the y direction, the glass was converted into an equivalent tissue layer of thickness $H_g^* \cdot k_t/k_g$, which was 360 μm. Thus, the countercurrent vessels were embedded in an equivalent tissue layer of thickness 1390 μm, which had a total dimensionless thickness, $H=H_t^*/a+(H_g^* \cdot k_t/k_g)/a$, of 19.6.

The free convective coefficient of the experimental environment, h, is an important parameter in theoretically modeling and evaluating the tissue thermal

conductivity. The value of h was measured by a microfilm for different experimental room temperatures, T_∞. A correlation between h and T_∞ can be found in Fig. 30. A regression curve, $h(\mathrm{W/m^2\,^\circ C}) = 1.59 \cdot 10^7 \cdot (T_\infty(^\circ\mathrm{C}))^{-4.66}$, which was represented by a dash line in the figure, provided a best fitting for these data (R=0.84, R: square root of the coefficient of determination). Using this relationship, h can be estimated for different experimental room temperatures. For the specific experiment presented in Fig. 24 to Fig. 28, h=3.9 W/m^2 °C was obtained at the room temperature T_∞=26.3 °C.

Figure 31 compares the theoretical predictions and the experimental data for the surface tissue temperature at three different axial locations under vasodilation. One observes a close agreement between the two at all three z locations.

4.3.3 The Effective Thermal Conductivity

Blood flow plays an important role in countercurrent heat exchange. In Fig. 24, the diameter of the first-order artery was increased from 115.0 μm under the baseline condition to 141.7 μm under the vasodilated condition, and it resulted in a significant increase in vessel blood flow. This dramatically affected the pattern of the thermal images.

Weinbaum and Jiji (1985) predicted that the primary mechanism for blood-tissue energy exchange in microcirculation is the incomplete countercurrent

exchange in thermally significant microvessels. The current study clearly reveals the thermal nonequilibration between these microvessels and the surrounding tissue. The one-dimensional Weinbaum-Jiji expression which accounts for the enhancement in the tissue effective thermal conductivity, k_{eff}, due to countercurrent heat exchange is:

$$k_{eff}=k_t(1+\sum_i \frac{n_i\pi^2(2a)^2Pe^2}{16\sigma}) \qquad (4.1)$$

where n_i is the number of vessel pairs per unit cross-sectional tissue area for generation i, Pe is the blood flow Peclet number ($Pe=\rho_b c_b du/k_b$) and σ is a conduction shape factor. The summation over i accounts for the contribution to the enhancement in the thermal conductivity due to all vessel generations. In the current experiment, only the first-order vessels had a measurable contribution to k_{eff}. This is because only vessels larger than 100 μm diameter can produce a significant enhancement in k_{eff} as suggested by the analysis in Chapter 2. Thus, the estimation for k_{eff} can be simplified to

$$k_{eff}=k_t(1+\frac{n_1\pi^2d^2Pe^2}{16\sigma}) \qquad (4.2)$$

Based on the measured vessel size both n_1 and Pe were calculated according to the following formulas obtained from the measurements in the rat spinotrapezius in Chapter 2:

$$n_1(No./mm^2) = 5910(d(\mu m))^{-2.03} \tag{4.3}$$

$$Pe = 0.00438(d(\mu m))^{1.70} \tag{4.4}$$

The expression for the two-dimensional tissue conduction shape factor, σ, has the following form if the supporting glass slide is converted into an equivalent effective tissue thickness and the ratio of blood to tissue conductivity is unity:

$$\sigma = \frac{1}{\begin{matrix} 2\overline{G}_{aa} - 2\overline{G}_{va} + 11/(24\pi) \\ 2G_{va} - 2G_{aa} + 11/(24\pi) \end{matrix}} \tag{4.5A}$$

where

$$\overline{G}_{aa} = \frac{1}{2\pi}\int_{-\pi}^{\pi} G(x,y:\ \xi_a,\eta_a)|_{\rho_a=1}\, d\phi_a \tag{4.5B}$$

$$\overline{G}_{va} = \frac{1}{2\pi}\int_{-\pi}^{\pi} G(x,y:\ \xi_v,\eta_v)|_{\rho_a=1}\, d\phi_a \tag{4.5C}$$

and $G(x,y: \xi_a, \eta_a)$ and $G(x,y: \xi_v, \eta_v)$ are Green's functions which were derived in Appendix 1 of (Zhu and Weinbaum, 1995). These Green's functions, which satisfy Laplace's equation in the tissue region, are functions of the tissue conductivity, k_t, free convection coefficient at the tissue surface, h, and the vessel-tissue configuration. Evaluating all the parameters in Eq. (4.2), one can calculate the k_{eff} values for the ten rats used in our experiment, which were summarized in Table 8.

To derive the tissue thermal conductivity in vasodilation, the muscle tissue was approximated by a fin. From the infrared image strips above the major feeding vessels in vasodilation and baseline, one obtains the temperature difference between these two states, $\Delta T(x, z)$, which is the temperature perturbation caused by the paired vessels. The fact that $\Delta T(x, z)$ was nearly a constant at any given z location allowed one to eliminate the temperature variation along the x direction. According to the Weinbaum-Jiji theory, the perturbation in the z direction is due to the increase in the effective tissue thermal conductivity along the vessel direction. In all ten cases studied, the Biot number $Bi=h\cdot(H^*/2)/k_t$, is less than 0.015 for $k_t=0.5$ W/m °C when there is no blood flow in tissue. This indicates the temperature variation across the muscle thickness is negligible. Thus, the exteriorized muscle layer can be well approximated by a one-dimensional fin with a constant base temperature $T_{exp}(0)$, and tip temperature $T_{exp}(L^*)$. The temperature distribution along the fin $T_{ave}(z)$ can then be calculated from the following equation (Incropera and Dewitt 1981):

$$T_{ave}(z) = T_\infty + (T_{\exp}(0) - T_\infty)\cdot \frac{\frac{T_{\exp}(L^*) - T_\infty}{T_{\exp}(0) - T_\infty}\cdot \sinh\left[\sqrt{\frac{2h}{kH^*}}\cdot z\right] + \sinh\left[\sqrt{\frac{2h}{kH^*}}\cdot (L^* - z)\right]}{\sinh\left[\sqrt{\frac{2h}{kH^*}}\cdot L^*\right]} \quad (4.6)$$

$T_{ave}(z)$ was compared with the experimental measurements and the least-squares residual method was used to find the value of k which minimized the difference

between them. Using one experimental case as an example, T_∞, $T_{cap}(0)$ and $T_{cap}(L^*)$ were 26.30, 35.47 and 34.28 °C, respectively. In order to avoid the thermal effect of branching from the first-order vessels to the second-order vessels, the fin length, L^*=1.40 mm, was chosen which was 40% of the length of the box in Fig. 24. As mentioned earlier, the equivalent tissue thickness, H^*, was 1.39 mm and the convective coefficient, h, was 3.9 W/m^2°C. Fig. 32 presents $T_{cap}(z)$ and its best fit $T_{ave}(z)$ from Eq. (4.6) when k is equal to 0.66 W/m °C. This value of k agrees reasonably well with the predicted value of k_{eff}, 0.65 W/m °C obtained from the Weinbaum-Jiji theory (Case 3 in Table 8). Following the same procedure, k has been estimated for all ten cases and the results are presented in Table 8. A paired t-test reveals k_{eff} to be significantly greater than k (p<0.004) though the average difference between k_{eff} and k is less than 10%.

4.4 Discussion

The thermal disturbance caused by the major feeding vessels has been clearly shown in the exteriorized rat spinotrapezius muscle using high resolution infrared thermography. Although the individual thermal effect caused by the artery and vein could not be distinguished, the combined effect produced by the vasodilated artery-vein pair is clearly visible. The dramatic change in thermal image from baseline to vasodilated conditions demonstrates that vasomotor

adjustments significantly affect the blood-tissue thermal equilibration, and that blood flow has a profound effect on the heat transfer in microcirculation.

In the current study, infrared images were also taken in pharmacologically vasoconstricted states (10^{-7} M norepinephrine). No observable difference in image was found between the vasoconstriction and baseline state. This implies that the blood flow increase from vasoconstriction to baseline does not produce a measurable effect on heat transfer, which is consistent with the results from our previous research in Chapter 2 that the enhancement in k_{eff} is insignificant for vessels less than 100 μm diameter. In the present study, the average vessel diameter increased approximately from 60.7 μm to 94.8 μm from vasoconstriction to baseline. Thus, the enhancement in k_{eff} was insignificant. However, in proceeding from baseline to vasodilation the vessel diameter increases from 94.8 μm to 121.4 μm on average, and the corresponding increase of the enhancement in k_{eff} became significant enough to be measured by the infrared imaging system.

When the muscle was approximated as a fin to estimate the tissue thermal conductivity, several assumptions were made. First, it was assumed that the muscle strip of interest had a zero-net heat exchange on two sides. This was due to the fact that the experimentally measured temperatures at $x=\pm D^*$ could be satisfactorily described as the superposition of the adiabatic condition and a linear temperature gradient. It was also assumed that the muscle strip had the same

convective condition at the top and bottom surfaces. Even though there was no measurement of the temperature distribution at the bottom surface, the Biot number of the muscle was found to be less than 0.015, indicating that the temperature variation in the direction of the muscle thickness is be negligible.

In the present study, the measured k included the combined effect of the tissue and the glass slide. In the calculation of k_{eff}, the glass slide effect was considered. As mentioned previously the equivalent tissue thickness including the glass is significantly larger than the measured tissue thickness. To find the effect of the equivalent tissue thickness on k_{eff}, the predictions for the enhancement in k_{eff} are presented in Fig. 33 both with and without the glass slide. The enhancement in k_{eff}, $n_l\pi^2 d^2 Pe^2/16\sigma$ (or $n_l\sigma Le^2$), is obtained from Eq. (4.2). The solid line accounts for the equivalent glass thickness and the dashed line does not. The calculation is based on the specific vascular geometry given by Fig. 24, where the artery is 141.7 μm diameter, the paired vein is 30% larger than the artery and dimensionless tissue thickness above the centers of the paired vessels is 3.0. Figure 33 shows that the enhancement in k_{eff} is significantly decreased due to the presence of the glass slide. When the effect of the supporting glass slide is considered in all ten cases, one finds that the equivalent tissue layer is 36% thicker than the measured tissue thickness on average. This results in a substantial increase in the conduction shape factor, and thus the enhancement in

k_{eff} is decreased according to Eq. (4.2). Physically, one can see that under otherwise similar conditions, the increase of the tissue thickness will cause a greater heat exchange between the paired vessels. Thus, the enhancement in k_{eff} can be expected to decrease because the vessels will behave more like a perfect countercurrent heat exchanger.

To separate the tissue thermal effect from that of the glass, an expression for pure enhancement in tissue conductivity can be derived from a global energy balance of a composite fin composed of the tissue and glass (see Appendix). Because the temperature is nearly uniform in both tissue and glass at a given z due to the small value of *Bi*, one finds that

$$k^* = \frac{2hL^*(\overline{T}-T_\infty)}{(\frac{dT}{dz}|_{z=L^*}-\frac{dT}{dz}|_{z=0})H_t^*} - k_g\frac{H_g^*}{H_t^*} \tag{4.7}$$

where $\overline{T}$ is the average surface tissue temperature, and $\frac{dT}{dz}|_{z=0}$ and $\frac{dT}{dz}|_{z=L^*}$ are tissue temperature gradients at the entrance and the exit of the tissue strip. These temperature gradients are measured in the experiment. In case 3, the above calculated k^* in vasodilation turns out to be 0.92 W/m °C. The enhancement in tissue thermal conductivity, therefore, is 84% (k^*/k_t-1=0.92/0.5-1). In contrast, the effective tissue thermal conductivity predicted from Eq. (4.2), $k_{eff,t}$, is 0.87 W/m °C, when the glass slide is neglected. Its corresponding

enhancement is 74% ($k_{eff,t}/k_t$-1=0.87/0.5-1). For the major feeding vessel pair in our experiment, the Weinbaum-Jiji theory for the effective thermal conductivity has been shown to reasonably describe the enhancement in thermal conductivity due to countercurrent blood flow.

Though the size of the countercurrent vessel pair used in the present study is similar to that in (Zhu *et al.* 1996) (~150 μm in diameter), the blood flow rate is significantly higher and thus the blood flow Peclet number, 20.3 in the current study, exceeds the maximum value of 14 in (Zhu *et al.* 1996). Two possible causes for the lower blood flow in their research are: (i) the rat cremaster has a lower normal temperature (~34 °C) than most skeletal muscles (~37 °C); (ii) some vessels were traumatized when the rat cremaster was dissected from the testicle. As a result of the relatively higher blood flow in the rat spinotrapezius, the thermal nonequilibration between the tissue and blood vessel is significantly greater in the current study. The temperature difference between the vessels and their surrounding tissue was in the range of 0.06 °C to 0.12 °C.

One surprising finding shown in Fig. 33 is that the predicted enhancement in k_{eff} is significantly smaller than that predicted in our previous study in Chapter 2, where a nearly 5-fold enhancement was predicted for a 200 μm vessel pair. This reduction in k_{eff} is due to (i) a smaller vessel spacing l/a=2.7 (compared to l/a=3.1 in the present case) was used to predict the enhancement in k_{eff} in Chapter

2; and (ii) neither the supporting glass slide nor the diameter difference between the artery and vein were considered in Chapter 2.

Finally, predictions of the surface temperature profile from our three dimensional model were found to be in a good agreement with the experimental results in the muscle tissue. Further improvements can be made in theoretical modeling by developing Green's function solutions for the muscle using actual boundary conditions at $x=\pm D^*$ for $T_t(-D^*)=T_1$, $T_t(D^*)=T_2$, instead of the superposition approximation used in the present study. Vessel branching can also affect the temperature distribution. This should be incorporated in future theoretical modeling studies.

Chapter 5. Conclusions

The present research has led to a better understanding of the importance of countercurrent blood flow in blood-tissue heat exchange at the microvascular level. It has been experimentally demonstrated that vasoregulation and vascular structure can significantly affect blood-tissue heat transfer. The thermal disturbance due to the blood vessels in the surrounding tissue has been observed for the first time in the microcirculation for conditions in which there is a significant increase in k_{eff}. Furthermore, the important role that countercurrent heat exchange plays in microvascular heat transfer has been quantitatively studied. The Weinbaum-Jiji k_{eff} theory has been shown to reasonably predict the average enhancement of tissue thermal conductivity due to blood flow in countercurrent vessels up to approximately 200 μm in diameter, which is the upper limit of validity of the Weinbaum-Jiji theory in microvasculature.

The detailed microvascular structure of the rat spinotrapezius, especially its countercurrent vessel structure, was investigated in Chapter 2. The paired vessel center-to-center spacing, which is important in estimating the efficiency of countercurrent heat exchange, was accurately measured for the first time. The dimensionless spacing, given by the ratio of the center-to-center spacing to the vessel radius (l/a), lies within the range of 2.2-3.3 for the first-order (1A)

countercurrent vessels, 2.3-3.5 for the second-order (2A) vessels and 2.8-5.0 for the third-order (3A) vessels. In Chapter 2, measurements were also made for the changes in vascular diameter and blood flow in pharmacologically induced vasoconstricted and vasodilated states. These measurements have been combined with the Weinbaum-Jiji theory to predict the enhancement in k_{eff} due to local blood perfusion, and to establish the limits of the validity of the Weinbaum-Jiji theory. Furthermore, the conduction shape factor for two-dimensional tissue preparations has been applied for the first time to predict k_{eff}. Using vasoactive drugs, we have shown that the volumetric blood flow rate was increased 7, 8 and 11 fold from vasoconstriction to vasodilation for the 1A, 2A and 3A vessels, respectively. According to the Weinbaum-Jiji theory, k_{eff} is proportional to the second power of the flow rate. Thus, the large change in blood flow from vasoconstriction to vasodilation suggests that a significant enhancement in k_{eff} can be achieved through vasoregulation. A 5-fold increase in k_{eff} was predicted for the maximally dilated 195 μm diameter vessels in the rat spinotrapezius. Results have indicated that the Weinbaum-Jiji expression for k_{eff} is valid in the spinotrapezius muscle for various vasoregulated conditions as long as the largest blood vessels are less than 200 μm in diameter.

The empirical scaling relations for the rat spinotrapezius were described in Chapter 3. These relations reveal the change in blood flow with respective to

vessel size under various vasoregulated conditions. The primary objective of this part of study was to provide a reliable method to predict blood flow in countercurrent vessels where it is difficult to obtain accurate velocity measurements. Experiments were performed on a number of rats of greatly different weights, and the concept of intraspecies scaling was applied in processing the measurements. Scaling relations (Table 6) have been established between the vascular blood flow and the spinotrapezius muscle weight. It is evident that the resulting exponents of these allometric scaling relations are mostly less than 1, and that the measured volumetric blood flow rate does not increase in proportion to the organ size. Also, it has been found that the exponents for the same vessel generation are similar in vasoconstriction and vasodilaton, which differ only slightly from that in baseline. It implies that the physiological flow mechanisms might be very similar for conditions of maximum vasoconstriction and vasodilation. These scaling relations are useful to estimate the magnitude of the blood flow rate in the rat spinotrapezius if the body, tissue or vessel size, which is not too far beyond our experiment range, is given.

In Chapter 4, an experimental approach was developed to obtain noninvasive direct measurements of the thermal disturbance produced by the countercurrent microvessels in the muscle tissue. A high-resolution infrared thermographic technique was used to measure the detailed *in vivo* muscle surface

temperature field. Vasoactive pharmacological agents were employed to increase the local blood flow Peclet number up to 20.3 in the major feeding artery. Measurable temperature disturbances due to the countercurrent blood flow were found only above the first-order feeding vessel pair in its vasdodilated state. They first occurred when the blood flow Peclet number was approximately 14 and the feeding artery was 115 μm diameter. Such disturbances became more observable when the countercurrent pair was vasodilated and the local Peclet number increased to 20.3 and the artery diameter to 141.7μm. The increase in blood flow, due to the increase of vessel diameter and decrease in flow resistance in the downstream vessels, enables much warmer blood to be carried through the tissue preparation. On the other hand, the flow rate increase also produces a higher inlet temperature at the proximal boundary. The dependence of blood-tissue heat exchange on the local blood flow rate has been clearly observed in this study. The infrared thermographic technique has been demonstrated as a useful tool in microcirculatory heat transfer analysis for its high spatial temperature resolution on a length scale of the diameter of the thermally significant microvessels. Using this technique, the blood-tissue heat transfer and the thermal equilibration process in the microcirculation has been localized, and related to the local blood perfusion rate.

The analytical study described in Chapter 4 predicted both the axial and

the cross-sectional temperature distributions with respect to the vessel pair. The close agreement between the analytical and experimental results in the vasodilated state confirms that the analysis accurately accounts for the effect of countercurrent convection. It also indicates the importance of including axial conduction in the tissue, the supporting glass slide, as well as the linear tissue temperature gradient in the direction perpendicular to the vessel axial direction.

The effective thermal conductivity of the tissue given in Chapter 4 was measured experimentally using a fin approximation and predicted theoretically by the Weinbaum-Jiji expression for k_{eff}. The two average values were in a good agreement indicating that the Weinbaum-Jiji theory is valid for the conditions of this experiment. One can, therefore, conclude that in our experiments, where the vessel diameter is smaller than 200 μm, the Weinbaum-Jiji k_{eff} theory successfully accounts for the thermal effect of blood flow in the countercurrently paired vessels and provides a good estimation of the axial decay of the tissue temperature field along the direction of the vessel pair.

As a major result achieved in this study the convective effect of blood flow in microvessels up to 200 μm diameter has been clearly demonstrated. Further research needs to be directed to study the convective effect of blood flow in thermally significant vessels ranging from 200 to 1000 μm diameter where it is lack of both theoretical and experimental studies. The theoretical study of the

heat transfer in vessels ranging from 200 to 1000 μm diameter needs to describe heat transfer between the tissue and the supply artery and vein (SAV) vessels. According to Myrhage and Eriksson (1984), SAV vessels of the skeletal muscle lie between 300 and 1000 μm in diameter and are, thus, just in the desired size range. Due to their location and vascular characteristics, the SAV vessels can be treated as a countercurrent vessel pair embedded in a tissue cylinder. However, this model needs to consider the followings: First, axial conduction will occur in the tissue region. Second, the cross-sectional area of the tissue cylinder, the vessel radius and the blood flow velocity can change in the axial direction. Third, there can be an axial temperature variation on the tissue cylinder surface due to geometrical orientation. By solving the boundary value problem for the tissue cylinder with the SAV vessel pair, one can quantitatively evaluate the heat transfer between blood and tissue for vessels between 200 to 1000 μm in diameter. In addition, by knowing the temperature profiles for the SAV vessel pair, T_{ab0} in the newly derived blood perfusion term $\omega\rho_b c_b \Delta T(T_{ab0}-T_t)$ (Weinbaum *et al.* 1997), will be identified.

Future experimental studies for the heat transfer in vessels ranging from 200 to 1000 μm are required to provide detailed information on vascular structure, blood flow rate and local temperature profiles of these vessels. At first, although comprehensive anatomical studies have been performed on the

arrangement of the vascular beds in different types of skeletal muscles (Myrhage and Eriksson, 1984), for many organs it remains unclear how thermally significant vessels ranging from 200 to 1000 μm diameter are oriented in the vessel tissue cylinders. Techniques and measurements need to be developed and employed to study the vascular structures. Secondly, blood flow rate measurements are essential for predicting convective heat transfer. However, the optical Doppler method for measuring velocity is no longer applicable for the vessels between 200 to 1000 μm diameter due to the large flow rate. Alternative techniques including magnetic resonance angiography and ultrasonic Doppler techniques are to be explored. These techniques, thus far, have only been applied to very large vessels. Thirdly, the local *in vivo* tissue or blood temperature measurement is always a challenge in bioheat transfer. In the present study the amplitude of the temperature difference between blood and tissue has been measured in thermally significant microvessels less than 200 μm diameter using the infrared imaging technique. Lagendijk and Mooibroek (1986) have used thermocouples to study the local heat transfer in very large blood vessels in an isolated organ. However, no one has ever measured the local axial thermal equilibration in the vessels that are between 200 and 1000 μm diameter. Vessels in this range are usually too large to be treated as a continuum thermal source and too small to be considered as vessels with constant temperature. The possibility of making temperature

measurements along the outside wall of the vessels by thermocouples, microsensors, or atomic force microscopy can be investigated. Once the axial temperature measurements along these vessels are performed, the thermal interaction between these partially equilibrated blood vessels and their surrounding tissue could then be analyzed.

Finally, the blood-tissue heat exchange in various thermal environments is also a topic of interest for many researchers. These studies will provide the quantitative basis for predicting the effect of local thermal environment on tissue heat transfer for therapeutic applications such as hyperthermia and diathermy in cancer treatment as well as understanding the normal physiological response of the body to heat stress.

Appendix

The derivation for $k_{eff,t}$ in Eq. (4.7)

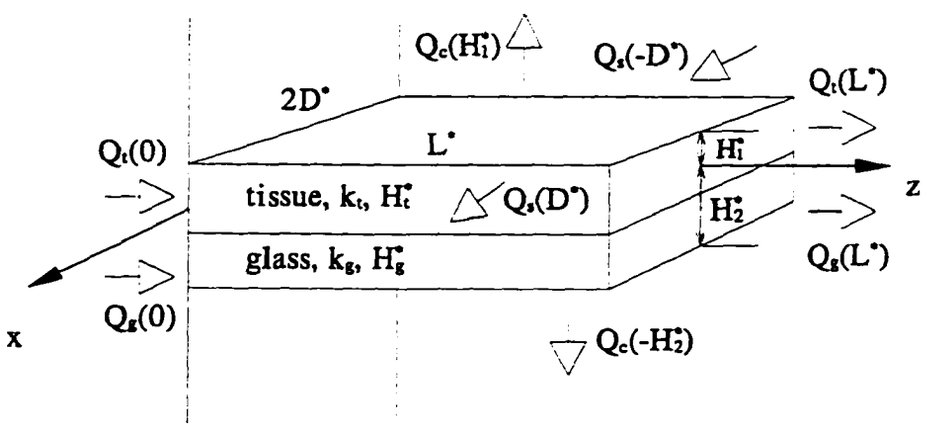

Conservation of heat requires the following:

$$Q_t(0)+Q_g(0)+Q_s(-D^*)=Q_c(H_1^*)+Q_c(-H_2^*)+Q_s(D^*)+Q_t(L^*)+Q_g(L^*) \qquad \text{(A.1)}$$

Q in the current appendix represents the heat flux. Two assumptions have been made. There is zero-net heat exchange on two sides of the muscle strip and the temperature is uniform across the glass-tissue thickness.

$$\begin{aligned} Q_s(-D^*)&=Q_s(D^*) \\ Q_c(H_1^*)&=Q_c(-H_2^*) \end{aligned} \qquad \text{(A.2)}$$

Apply these assumptions, Eq. (A.1) reduces to

$$Q_t(0)+Q_g(0)=2Q_c(H_1^*)+Q_t(L^*)+Q_g(L^*) \qquad \text{(A.3)}$$

$Q_t(0)$, $Q_g(0)$, $Q_c(H_1^*)$, $Q_t(L^*)$ and $Q_g(L^*)$ can be expressed as

$$Q_t(0) = -k_t \frac{dT}{dz}|_{z=0} \cdot 2D^{\cdot} \cdot H_t^{\cdot}$$

$$Q_g(0) = -k_g \frac{dT}{dz}|_{z=0} \cdot 2D^{\cdot} \cdot H_g^{\cdot}$$

$$Q_c(H_1^{\cdot}) = \int_0^{L^{\cdot}} h \cdot (T - T_\infty) \cdot 2D^{\cdot} \cdot dz = h(\overline{T} - T_\infty) \cdot 2D^{\cdot} \cdot L^{\cdot} \qquad \text{(A.4)}$$

$$Q_t(L^{\cdot}) = -k_t \frac{dT}{dz}|_{z=L^{\cdot}} \cdot 2D^{\cdot} \cdot H_t^{\cdot}$$

$$Q_g(L^{\cdot}) = -k_g \frac{dT}{dz}|_{z=L^{\cdot}} \cdot 2D^{\cdot} \cdot H_g^{\cdot}$$

Substituting Eq. (A.4) into Eq. (A.3), we obtain

$$-k_t \frac{dT}{dz}|_{z=0} \cdot 2D^{\cdot} \cdot H_t^{\cdot} - k_g \frac{dT}{dz}|_{z=0} \cdot 2D^{\cdot} \cdot H_g^{\cdot} =$$
$$2 \cdot h \cdot (\overline{T} - T_\infty) \cdot 2D^{\cdot} \cdot L^{\cdot} - k_t \frac{dT}{dz}|_{z=L^{\cdot}} \cdot 2D^{\cdot} \cdot H_t^{\cdot} - k_g \frac{dT}{dz}|_{z=L^{\cdot}} \cdot 2D^{\cdot} \cdot H_g \qquad \text{(A.5)}$$

Solving Eq. (A.5) for k_t, one obtains

$$k_{eff.t} = k_t = \frac{2hL^{\cdot}(\overline{T} - T_\infty)}{(\frac{dT}{dz}|_{z=L^{\cdot}} - \frac{dT}{dz}|_{z=0}) H_t} - k_g \frac{H_g^{\cdot}}{H_t^{\cdot}} \qquad \text{(A.6)}$$

Table 1. Average values of vessel diameter and centerline red cell velocity in vasoconstricted, baseline and vasodilated conditions.

Vessel Generation	Vasoregulatory Condition	V (mm/sec)	d (μm)
1A	VC	20.25±2.78	54.16±6.13
	B	24.95±0.89	99.55±13.82
	VD	29.17±2.15	119.23±11.66
2A	VC	14.94±3.11	42.88±5.05
	B	20.92±3.73	74.90±9.25
	VD	25.56±4.61	90.01±9.46
3A	VC	9.13±2.13	27.00±2.69
	B	16.42±2.33	42.53±3.33
	VD	21.29±4.43	58.40±8.33

VC: vasoconstriction (10^{-7} M Norepinephrine), B: baseline, VD: vasodilation ($10^{-4.5}$ M Na Nitroprusside)

Table 2. Evaluation of k_{eff}/k_t from the experimental measurements.

Vessel Generation	Vasoconstriction		Vasodilation	
	diameter (μm)	$n_i \sigma Le_i^2$	diameter (μm)	$n_i \sigma Le_i^2$
1A	54	--	119	0.46
2A	43	--	90	0.14
3A	27	--	58	0.02
$\sum_i n_i \sigma Le_i^2$	negligible		0.62	
k_{eff}/k_t	$1+\sum_i n_i \sigma Le_i^2 \approx 1$		$1+\sum_i n_i \sigma Le_i^2 \approx 1.62$	

Table 3. ε and $(d/2)\cdot Pe$ for vessel diameters from 75 to 195 μm

d (μm)	75	95	115	135	155	175	195
ε	0.04	0.06	0.08	0.10	0.13	0.16	0.19
$(d/2)\cdot Pe$ (mm)	0.24	0.45	0.75	1.15	1.67	2.32	3.11

Table 4. Evaluation of k_{eff}/k_t for large vessels which are scaled roughly as the same portion of the 1A, 2A and 3A in Table 2.

Vessel Generation	Vasoconstriction		Vasodilation	
	diameter (μm)	$n_i \sigma Le_i^2$	diameter (μm)	$n_i \sigma Le_i^2$
1A	100	0.20	200	4.36
2A	75	0.06	150	1.26
3A	50	--	100	0.22
$\sum_i n_i \sigma Le_i^2$	0.26		5.84	
k_{eff}/k_t	$1+\sum_i n_i \sigma Le_i^2 \approx 1.26$		$1+\sum_i n_i \sigma Le_i^2 \approx 6.84$	

Table 5. Evaluation of k_{eff}/k_t for large vessels which precisely follows the Murray's law and the diameter of the dilated 1A reaches to the limit of the validation of Weinbaum-Jiji theory in the rat spinotrapezius.

Vessel Generation	Vasoconstriction		Vasodilation	
	diameter (μm)	$n_i \sigma Le_i^2$	diameter (μm)	$n_i \sigma Le_i^2$
1A	97.5	0.19	195	3.91
2A	77.4	0.07	154.8	1.44
3A	61.4	0.03	122.8	0.53
$\sum_i n_i \sigma Le_i^2$	0.29		5.88	
k_{eff}/k_t	$1+\sum_i n_i \sigma Le_i^2 \approx 1.29$		$1+\sum_i n_i \sigma Le_i^2 \approx 6.88$	

Table 6. Regression equations for each vessel generation under defferent vasoregulatory conditions.

Vessel Generation	Vasoconstriction (10^{-7} M Norepinephrine) (n = 6)	Baseline (n = 12)	Vasodilation ($10^{-4.5}$ M Na Nitroprusside) (n = 10)
1A	$Q=4.45 \cdot w^{0.68}$ $R=0.99$	$Q=3.39 \cdot w^{0.86}$ $R=0.97$	$Q=11.5 \cdot w^{0.66}$ $R=0.87$
2A	$Q=1.92 \cdot w^{0.73}$ $R=0.96$	$Q=2.22 \cdot w^{0.82}$ R=0.92	$Q=4.62 \cdot w^{0.73}$ $R=0.89$
3A	$Q=0.380 \cdot w^{0.96}$ $R=0.88$	$Q=0.423 \cdot w^{1.06}$ $R=0.89$	$Q=0.922 \cdot w^{0.97}$ $R=0.90$
Q (nl/s): blood flow rate, w (mg): muscle weight, R: square root of the coefficient of determination			

Table 7. Volumetric blood flow rate under various vasoregulatory conditions and different rat weight ranges.

Rat Weight Range	Vascular Condition	
	Baseline	Vasoregulatory States
145±8.0 (g)	$Q=0.00128 \cdot d^{2.48}$ $R=0.98$	$Q=0.000510 \cdot d^{2.70}$ $R=0.98$
69-162 (g)	$Q=0.000533 \cdot d^{2.66}$ $R=0.85$	$Q=0.00141 \cdot d^{2.48}$ $R=0.96$
Q (nl/s): blood flow rate, d (μm): vessel diameter, R: square root of the coefficient of determination, Vasoregulatory States: vasoconstriction, baseline and vasodilation		

Table 8. The effective thermal conductivity by the Weinbaum-Jiji theory (k_{eff}) and by the fin approximation (k).

Case No.	1	2	3	4	5	6	7	8	9	10
k_{eff} (W/m °C)	0.71	0.72	0.65	0.66	0.67	0.60	0.72	0.76	0.70	0.75
k (W/m °C)	0.66	0.67	0.66	0.60	0.62	0.56	0.66	0.76	0.65	0.77
Δ (%) $\lvert(k-k_{eff})/k_{eff}\rvert$	7.04	6.94	1.54	9.09	7.46	6.67	8.33	0.00	7.14	2.66

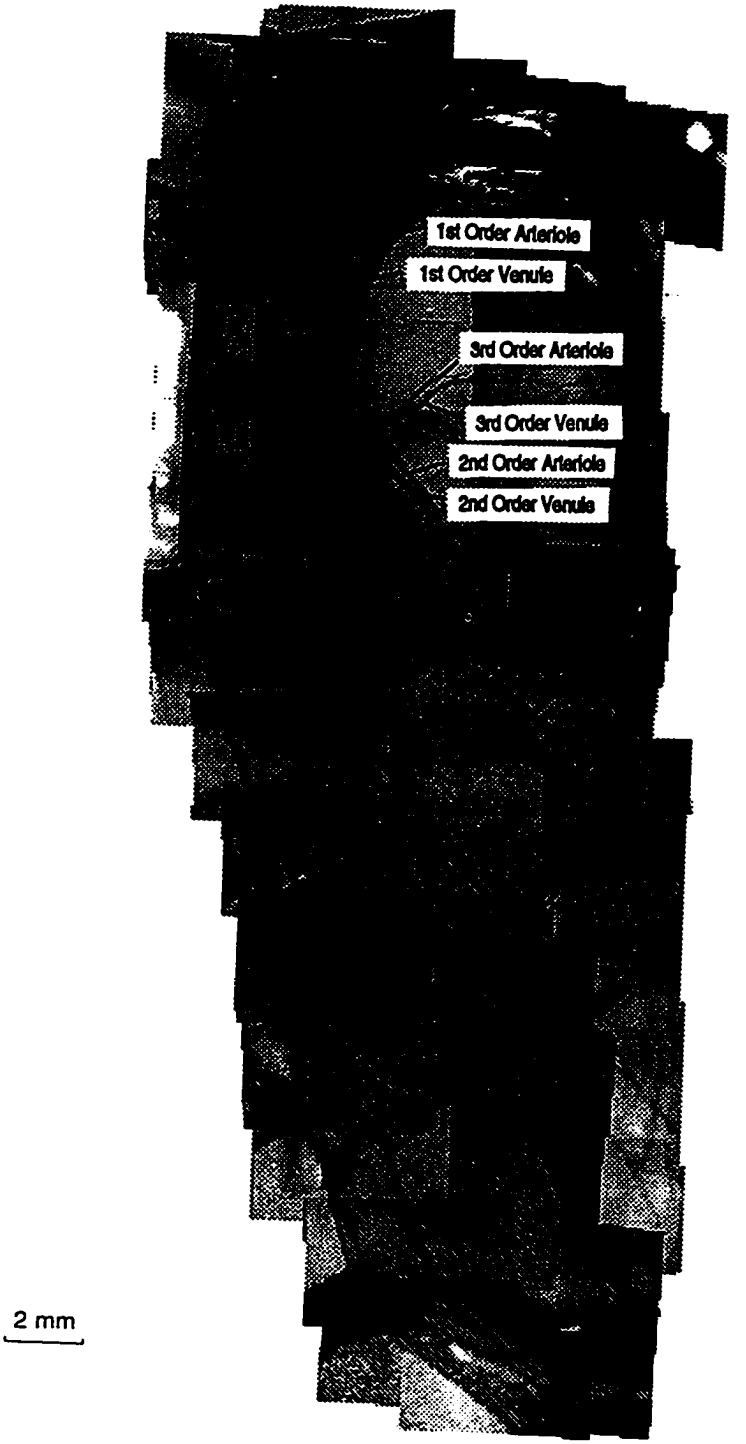

Figure 1. Photomontage of the rat spinotrapezius preparation.

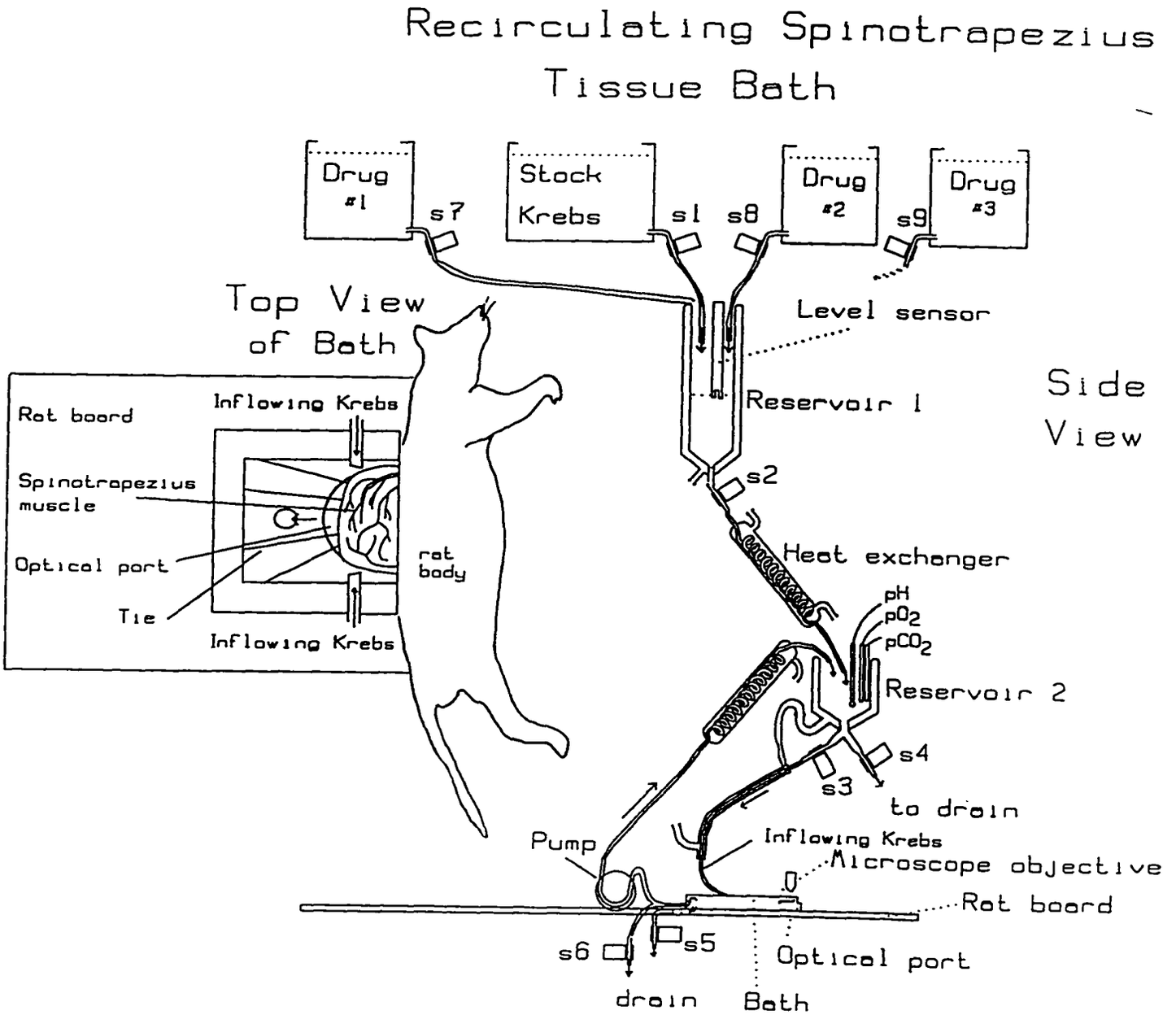

Figure 2. Schematic of the experimental setup used to study the spinotrapezius muscle.

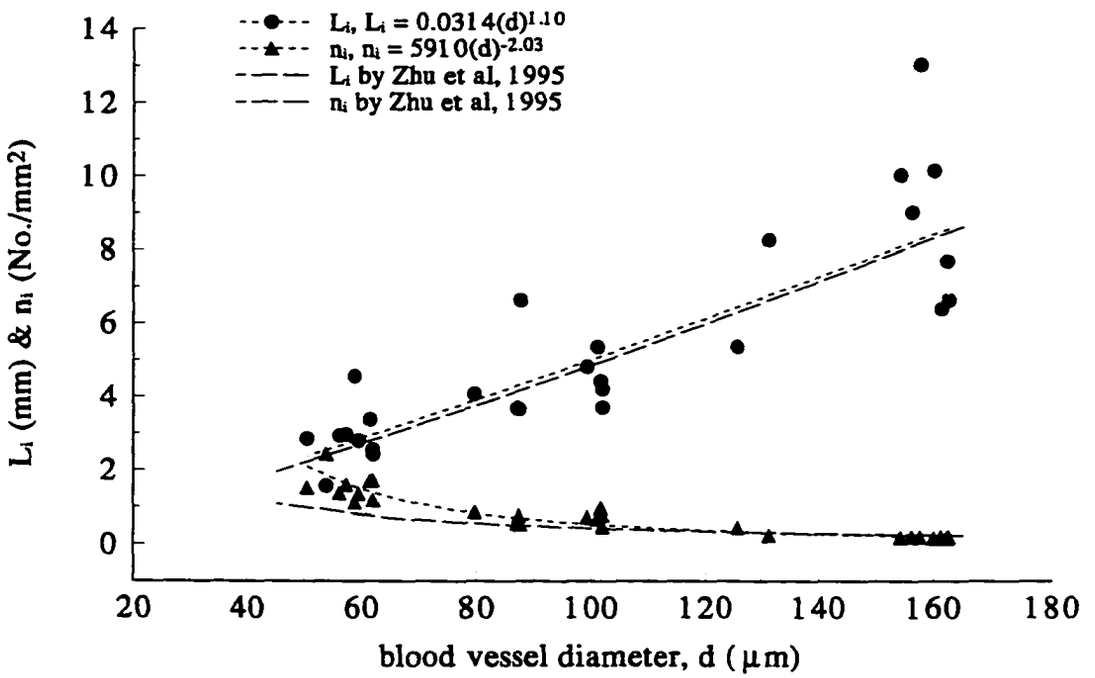

Figure 3. Measurements of vessel length L_i (mm) and vessel pair number density n_i (No./mm^2) from the photomontages of nine rat spinotrapezius muscle preparations and comparison between measurements of the rat spinotrapezius and cremaster muscle.

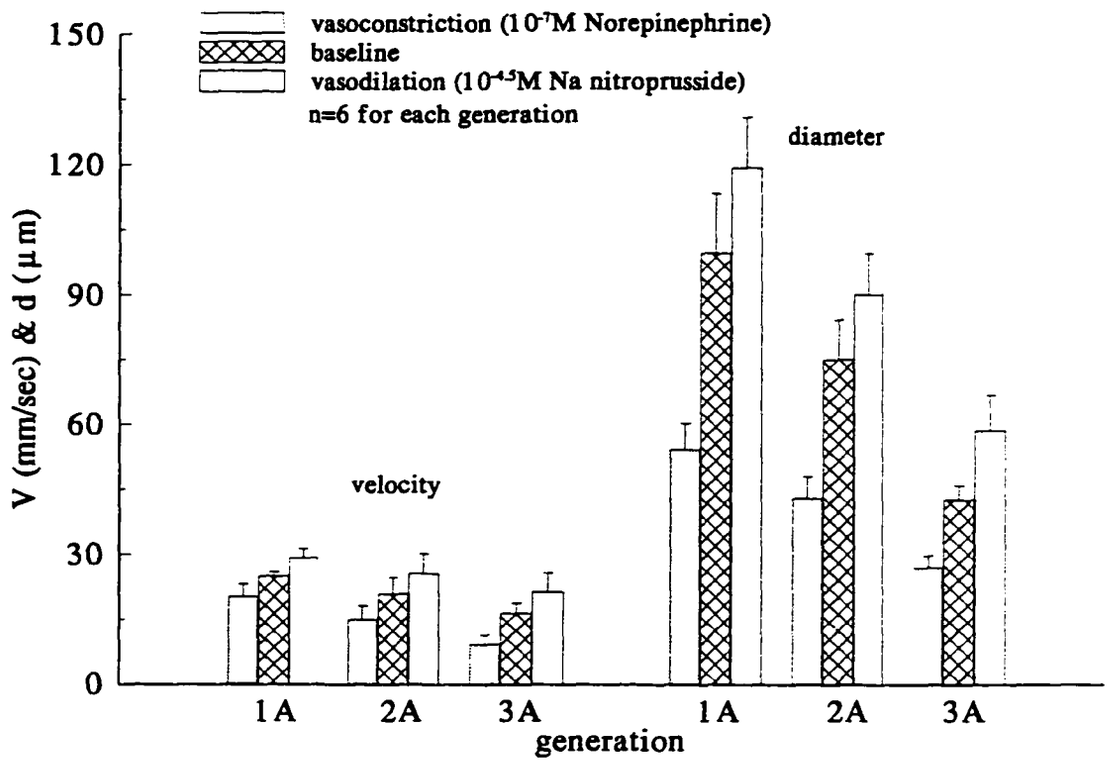

Figure 4. Average values of the 1A, 2A and 3A vessel diameters and the corresponding centerline red cell velocities at vasoconstriction, baseline and vasodilation.

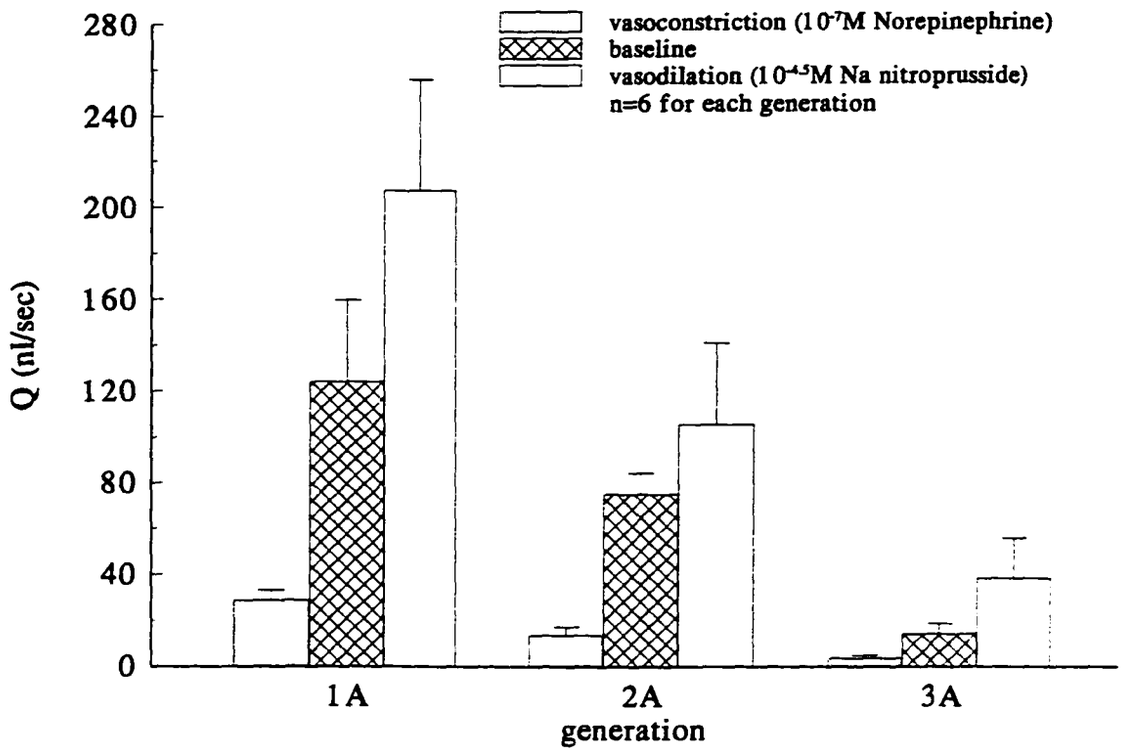

Figure 5. Average volumetric blood flow rates in the 1A, 2A and 3A vessels at vasoconstriction, baseline and vasodilation.

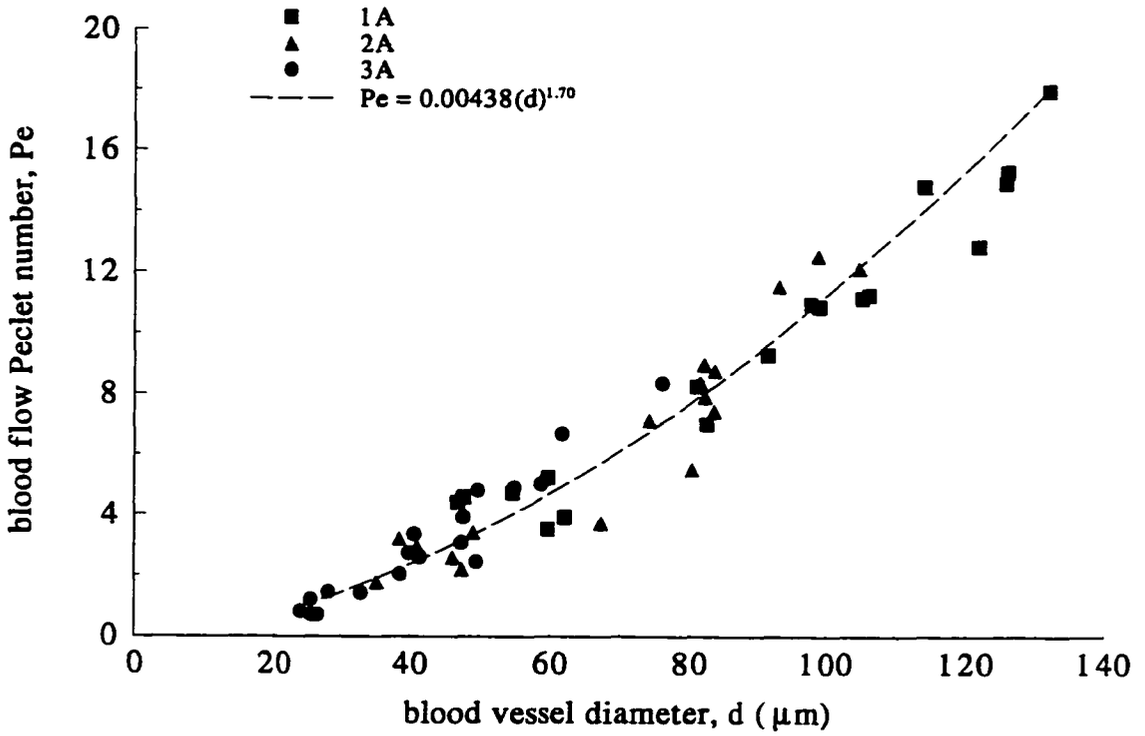

Figure 6. Variation of the blood flow Peclet number with the vessel diameter.

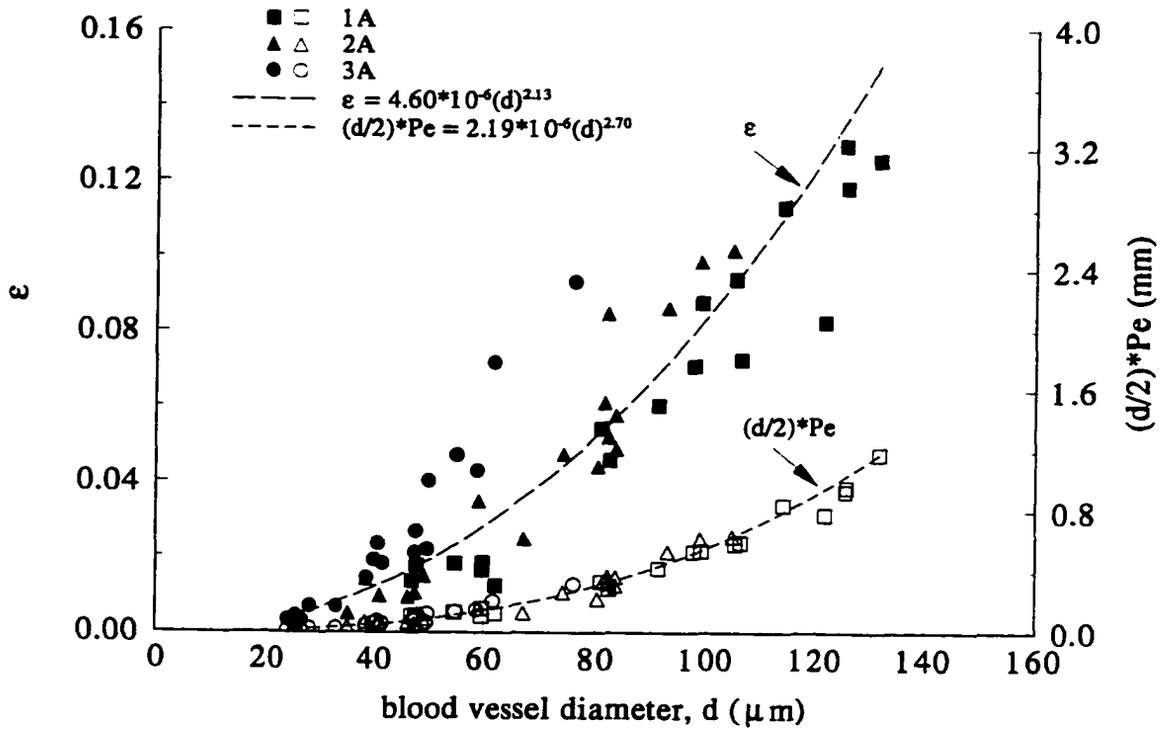

Figure 7. Variation of ε and $(d/2)\cdot Pe$ with the vessel diameter.

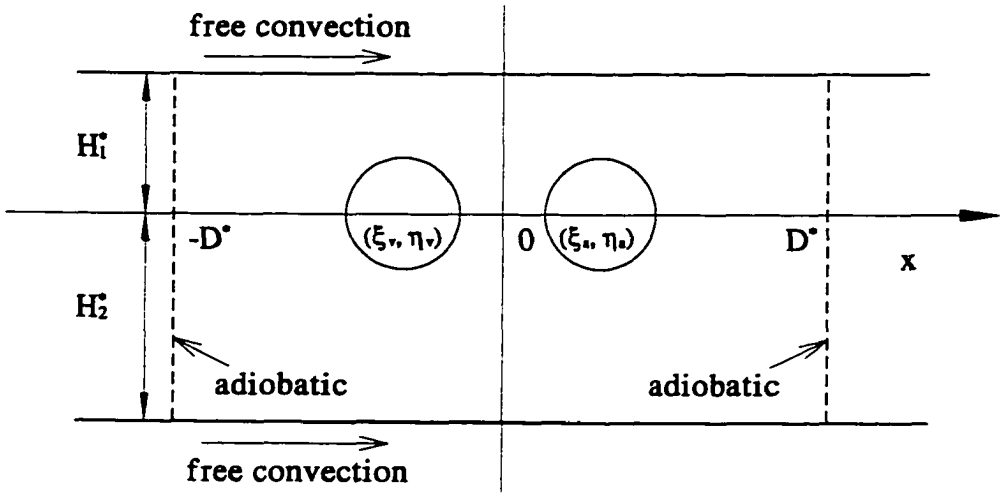

Figure 8. Schematic of the cross-section plane of the rat spinotrapezius.

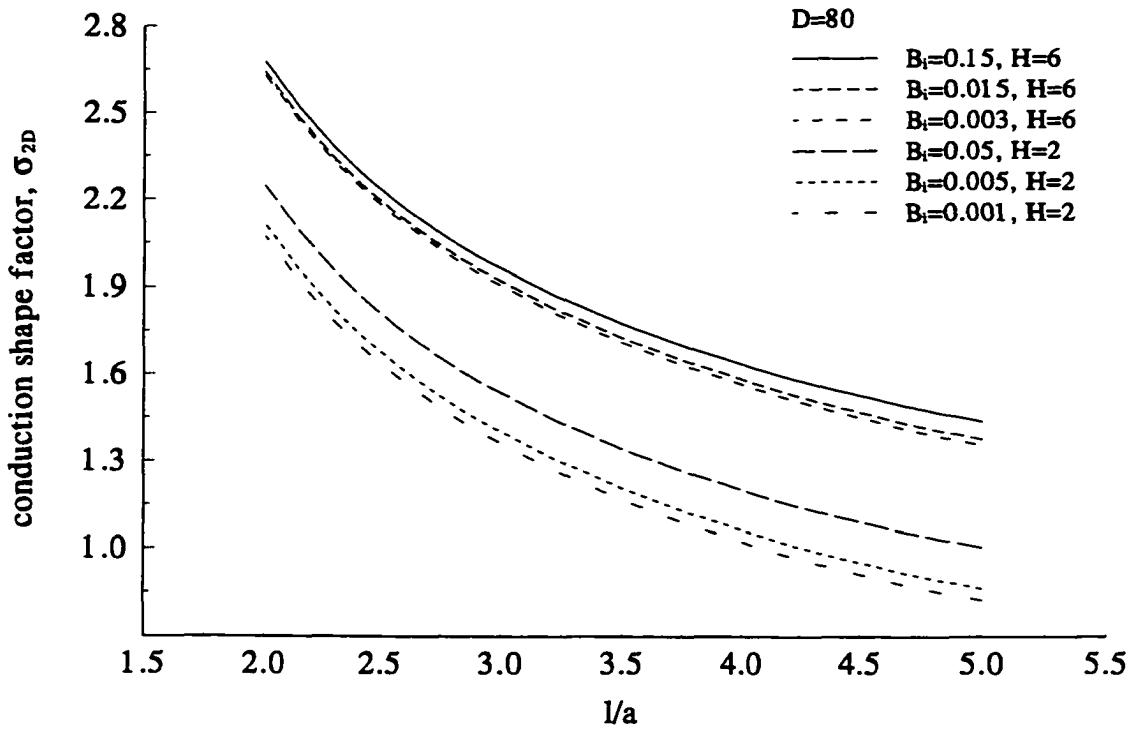

Figure 9. Variation of the newly derived conduction shape factor with the free convection and the vessel spacing (*l/a*).

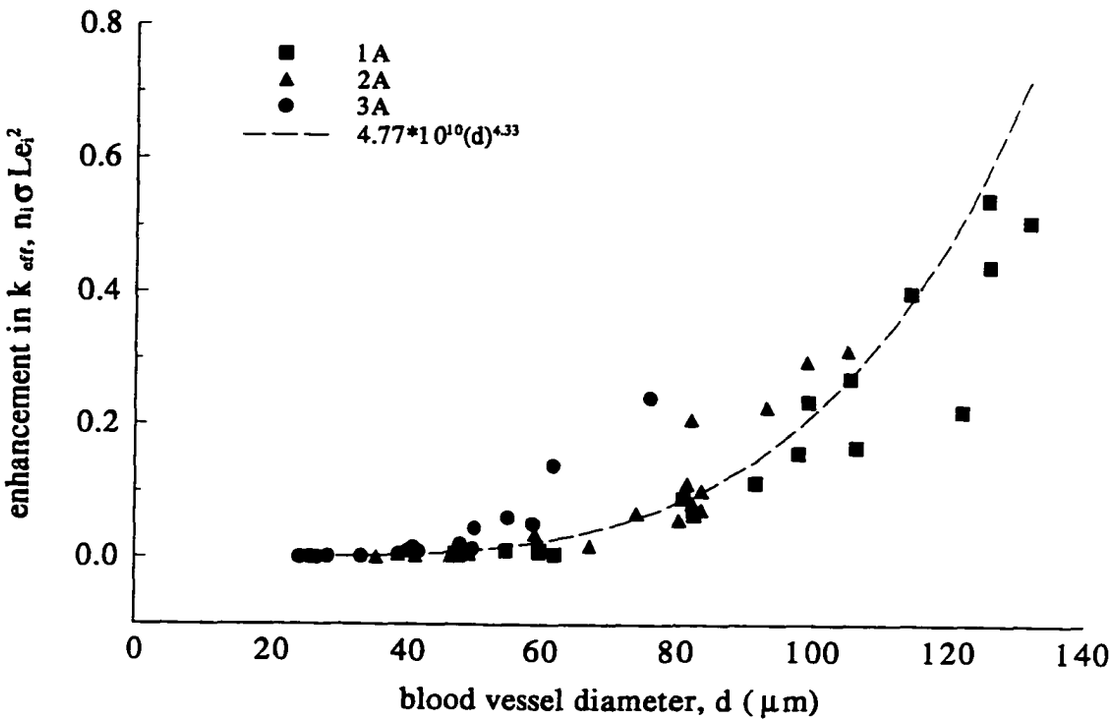

Figure 10. Variation of $n_i \sigma L e_i^2$ with the vessel diameter.

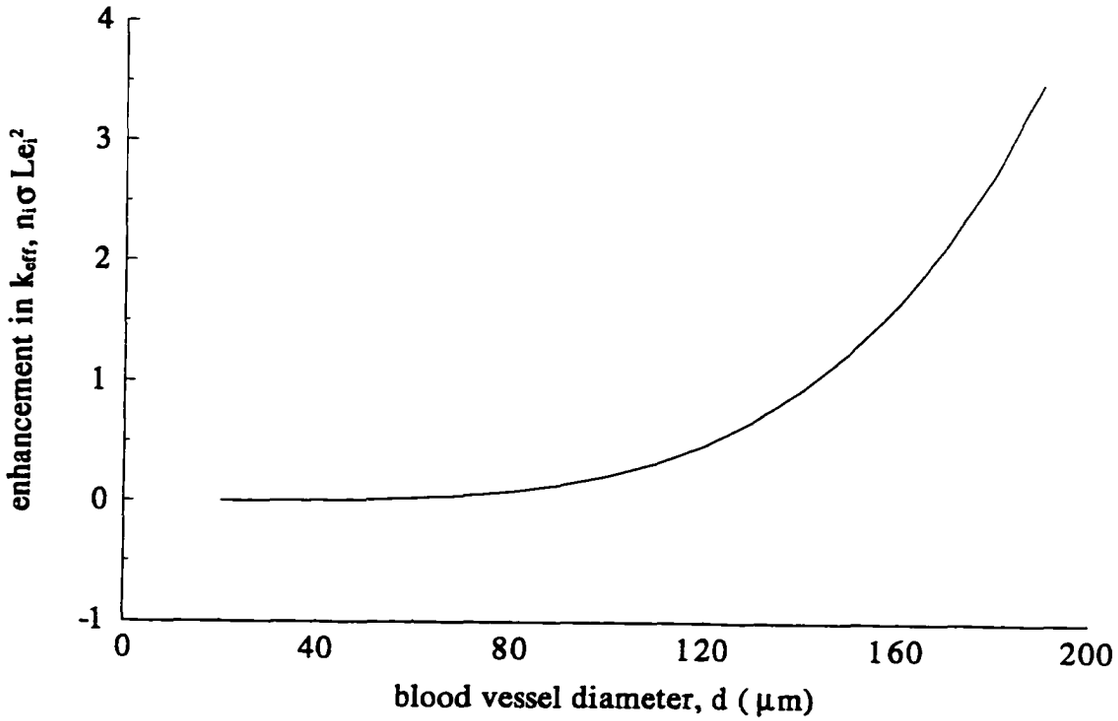

Figure 11. Extrapolation of $n_i\sigma Le_i^2$ for vessels up to 195 μm diameter.

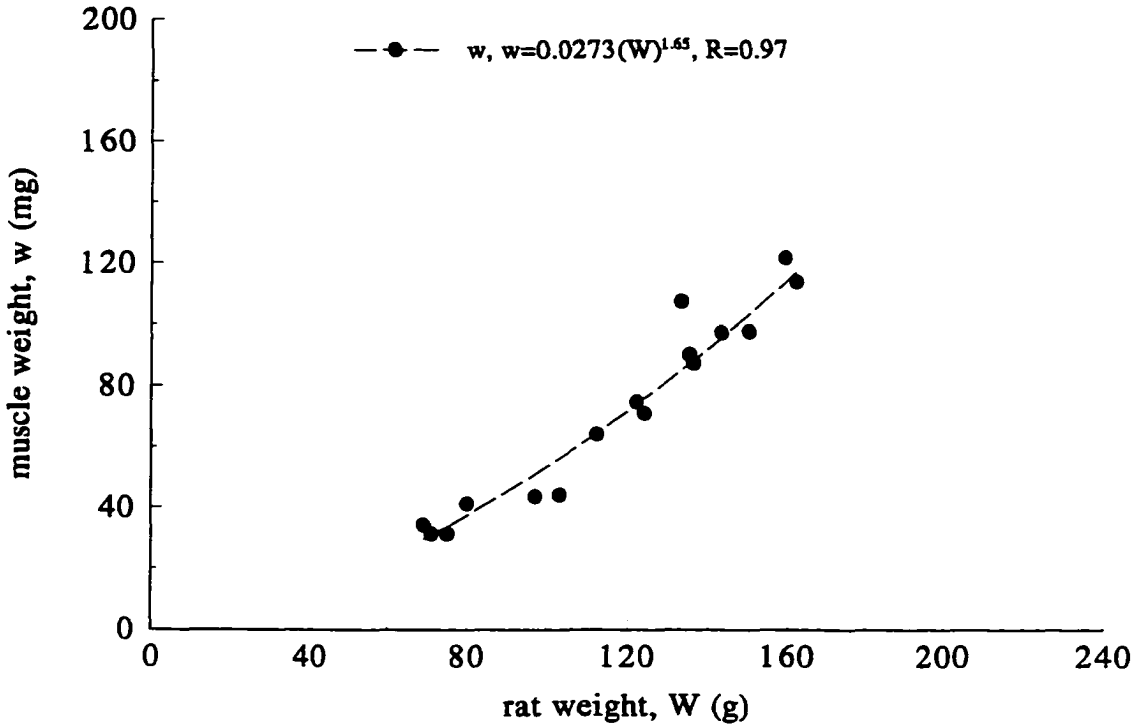

Figure 12. Allometric relationship between the spinotrapezius muscle and the rat weight.

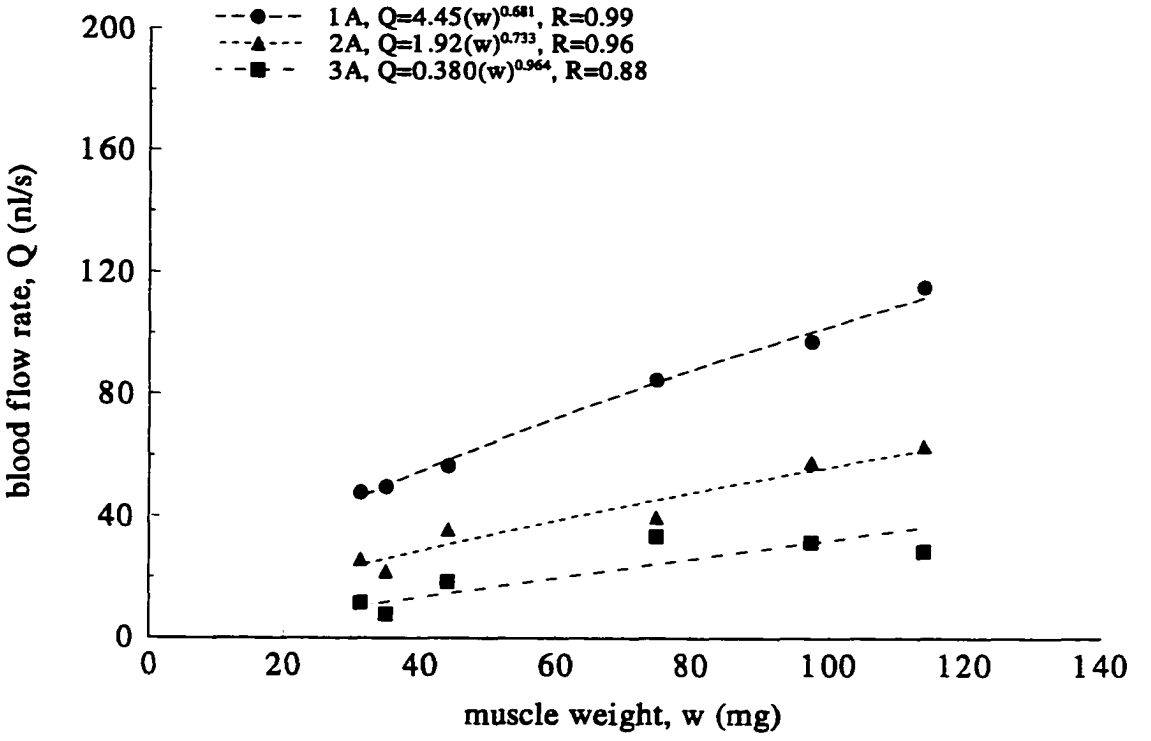

Figure 13. Allometric relationship between the volumetric blood flow rate in the 1A, 2A and 3A vessels and the muscle weight under vasoconstriction.

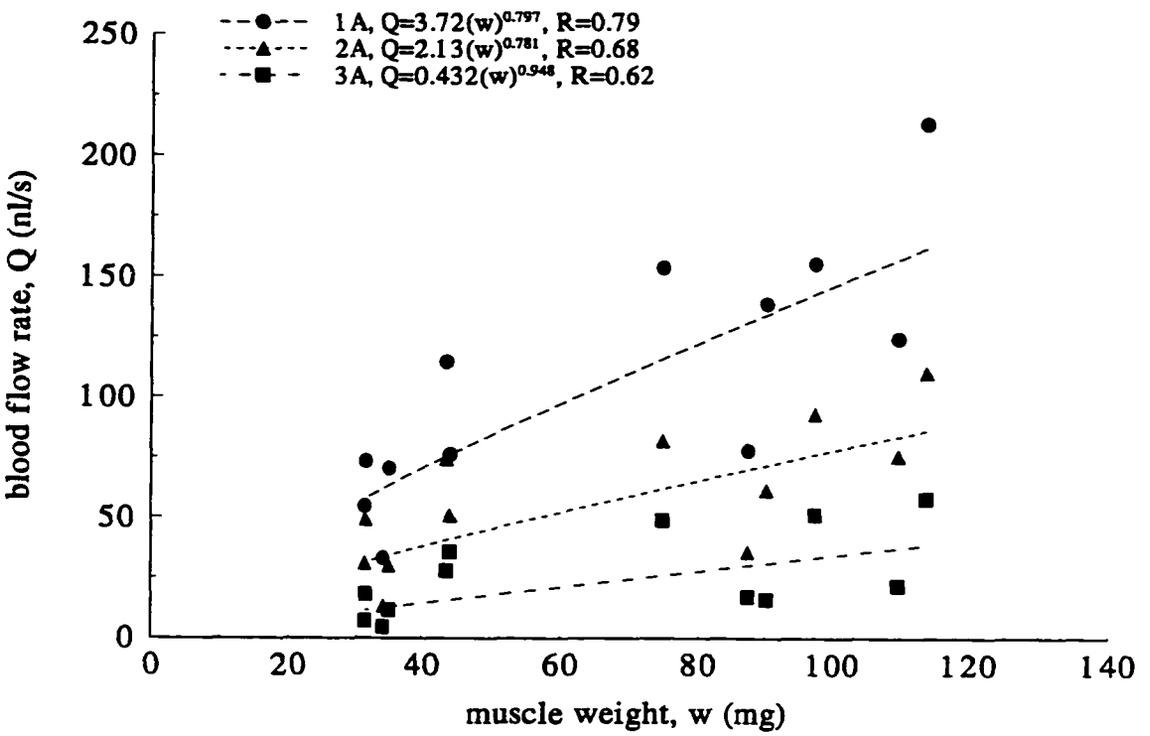

Figure 14. Allometric relationship between the volumetric blood flow rate in the 1A, 2A and 3A vessels and the muscle weight under baseline.

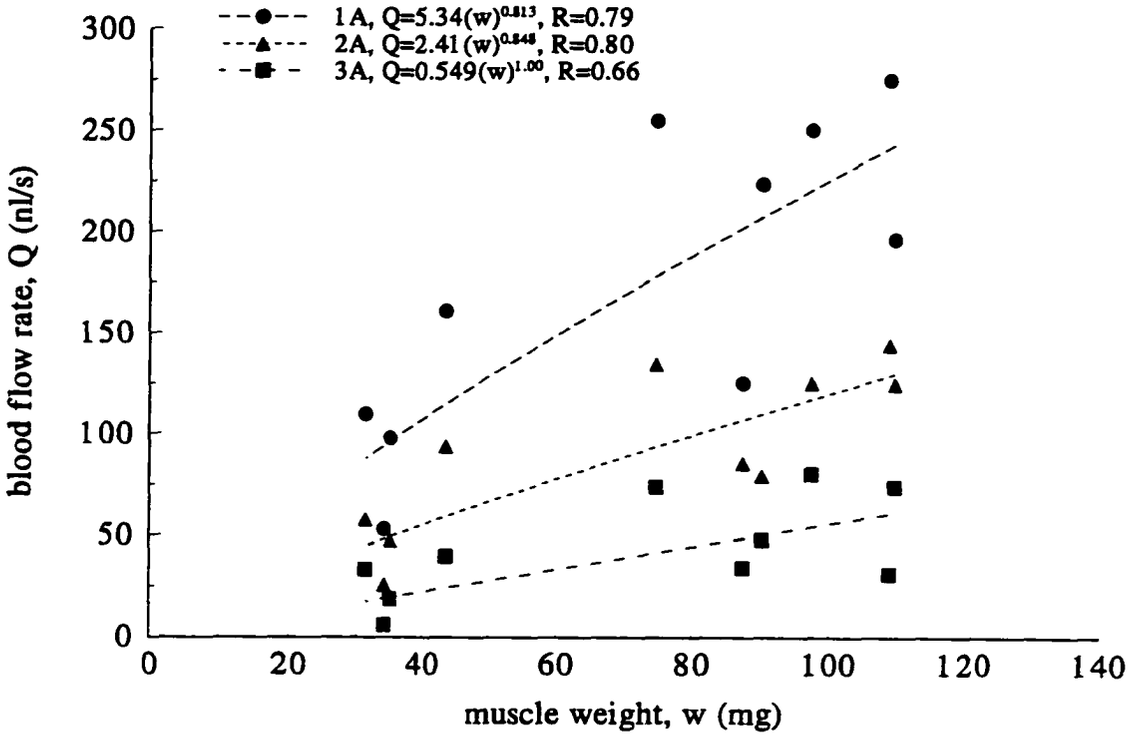

Figure 15. Allometric relationship between the volumetric blood flow rate in the 1A, 2A and 3A vessels and the muscle weight under vasodilation.

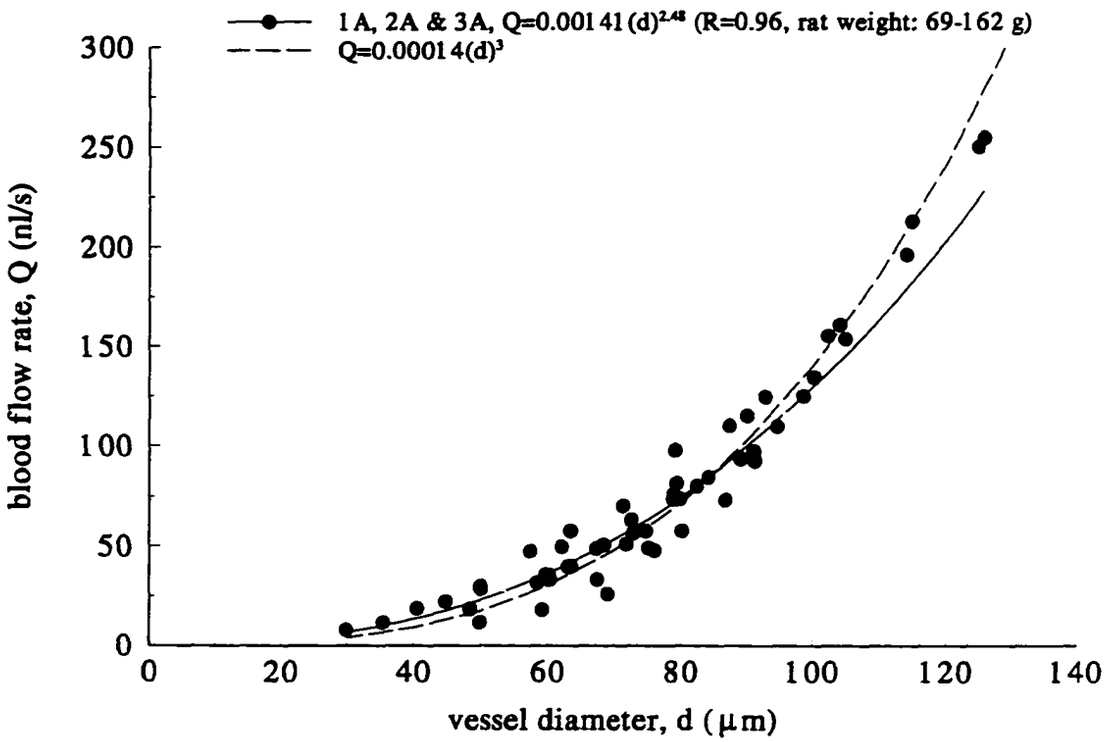

Figure 16. Comparison of the allometric relationship between the volumetric blood flow rate in the 1A, 2A and 3A vessels and the vessel diameter with the optimal cubic fitting curve (rat weight: 69-162 g).

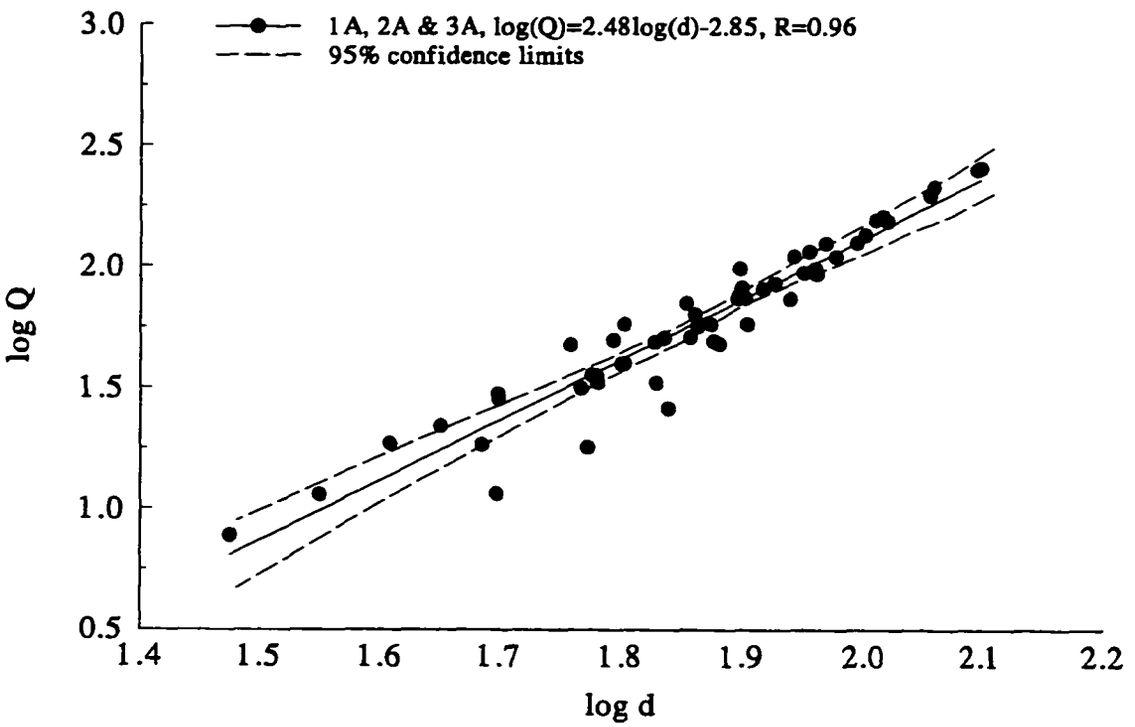

Figure 17. Allometric relationship between the volumetric blood flow rate in 1A, 2A and 3A vessels and the vessel diameter with the 95% confidence limits.

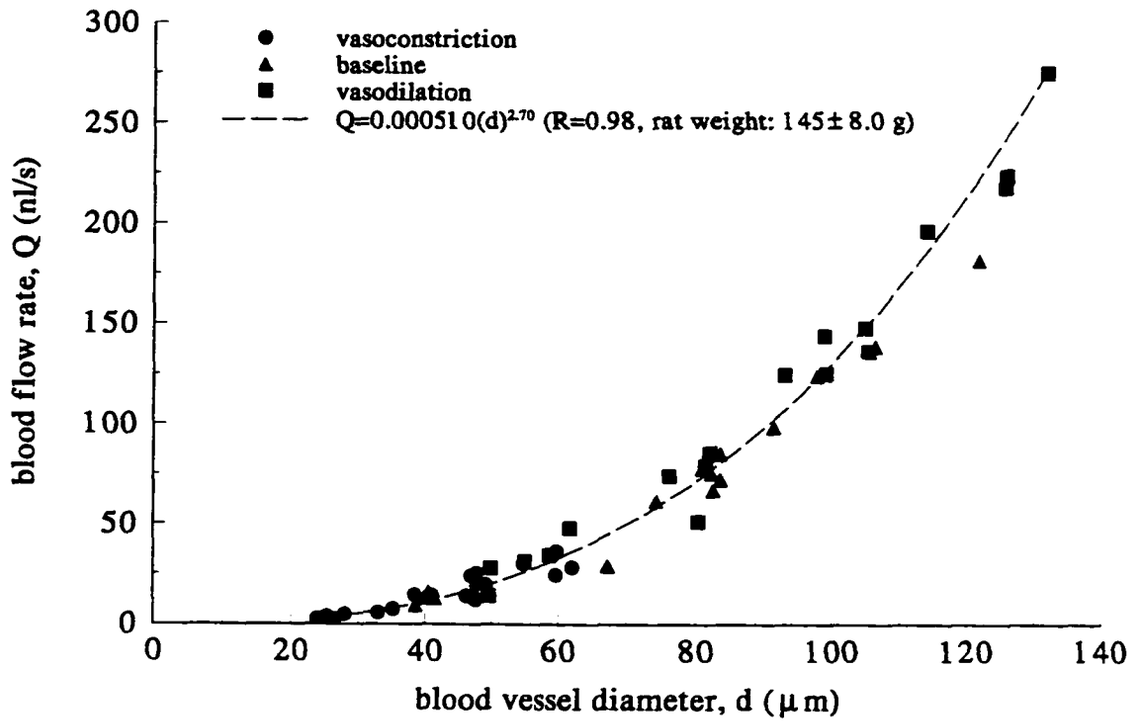

Figure 18. Allometric relationship between the volumetric blood flow rate in the 1A, 2A and 3A vessels and the vessel diameter (rat weight: 145± 8.0 g).

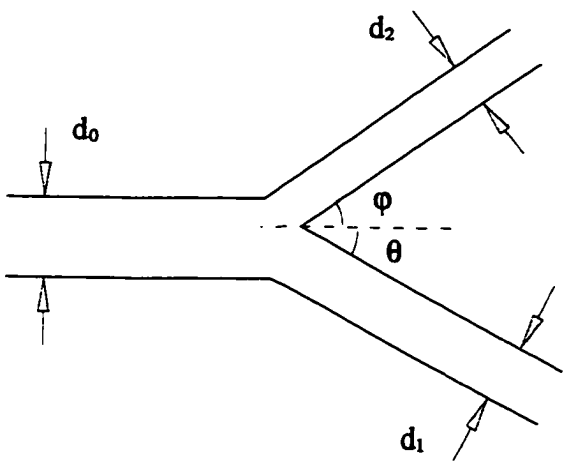

Figure 19. Schematic bifurcation of a blood vessel and its geometric parameters.

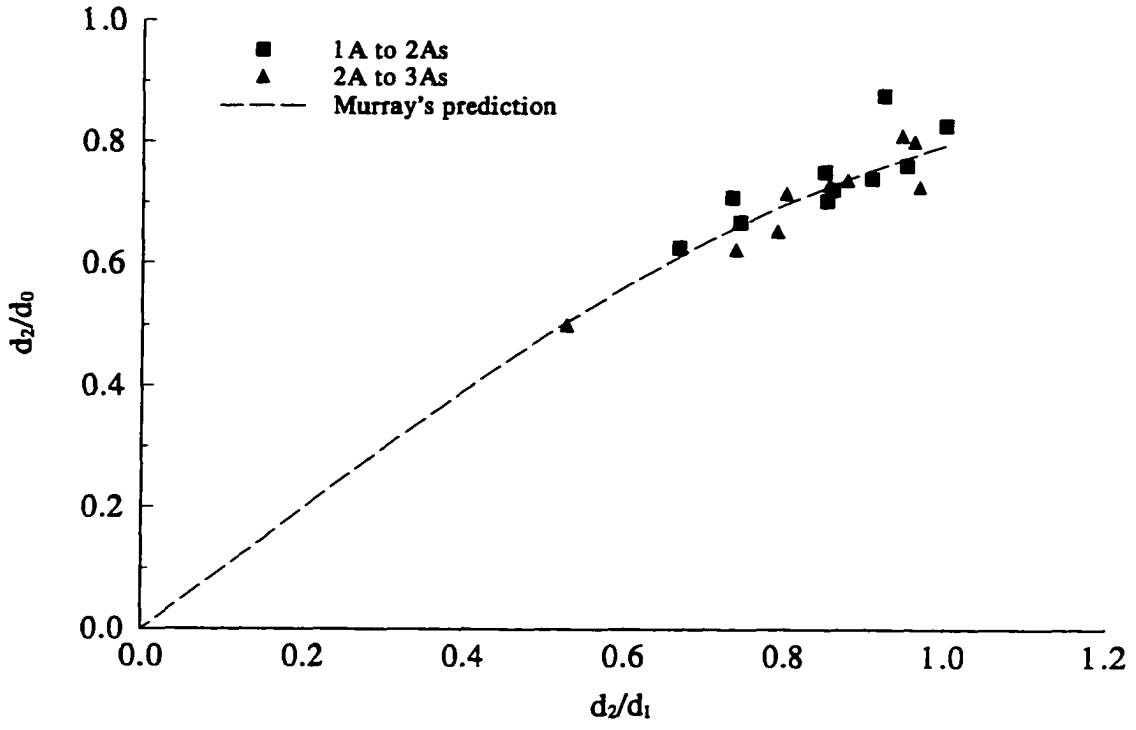

Figure 20. The diameter ratio of the smaller branch to the parent measured at bifurcation sites and those predicted by Murray's law.

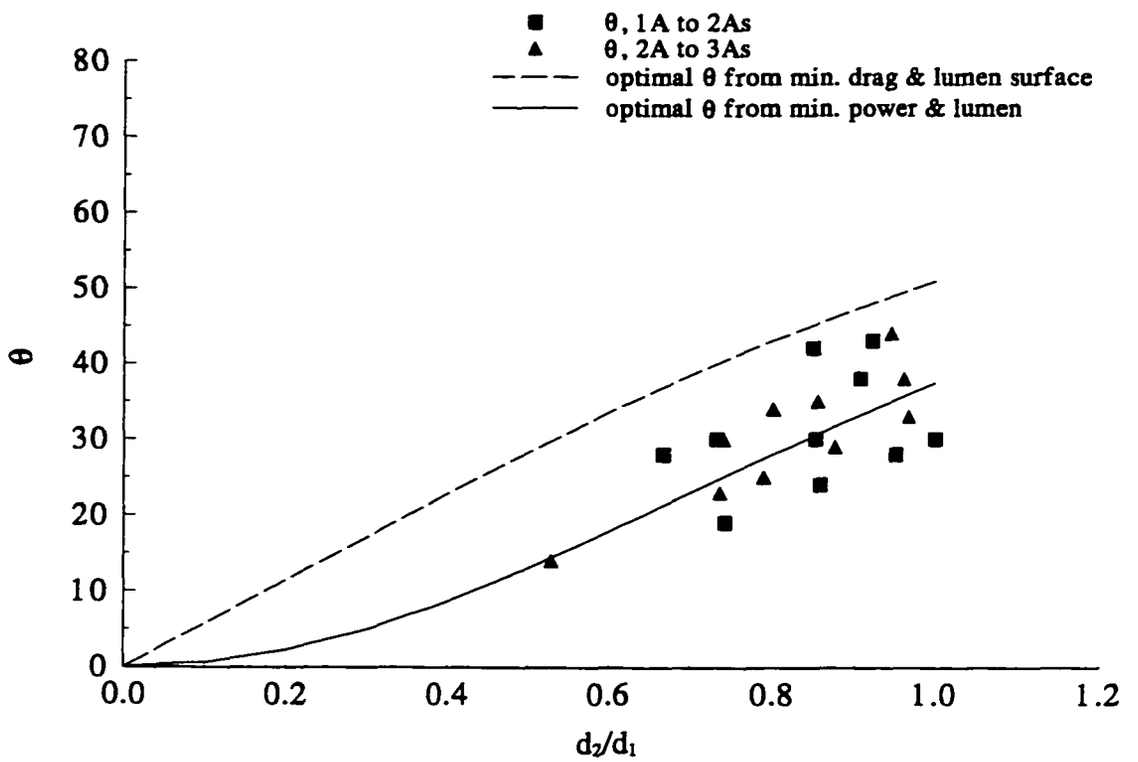

Figure 21. Comparisons between measured branch angles θ and their related optimal region by theoretical predictions.

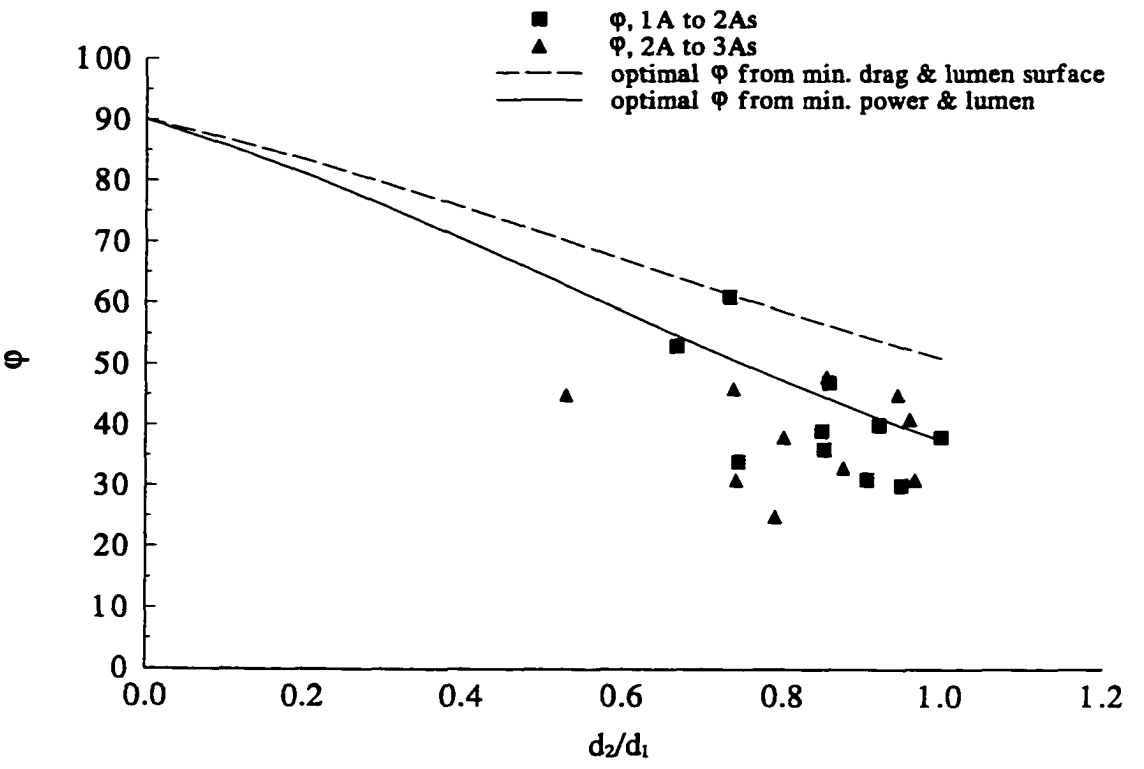

Figure 22. Comparisons between measured branch angles φ and their related optimal region by theoretical predictions.

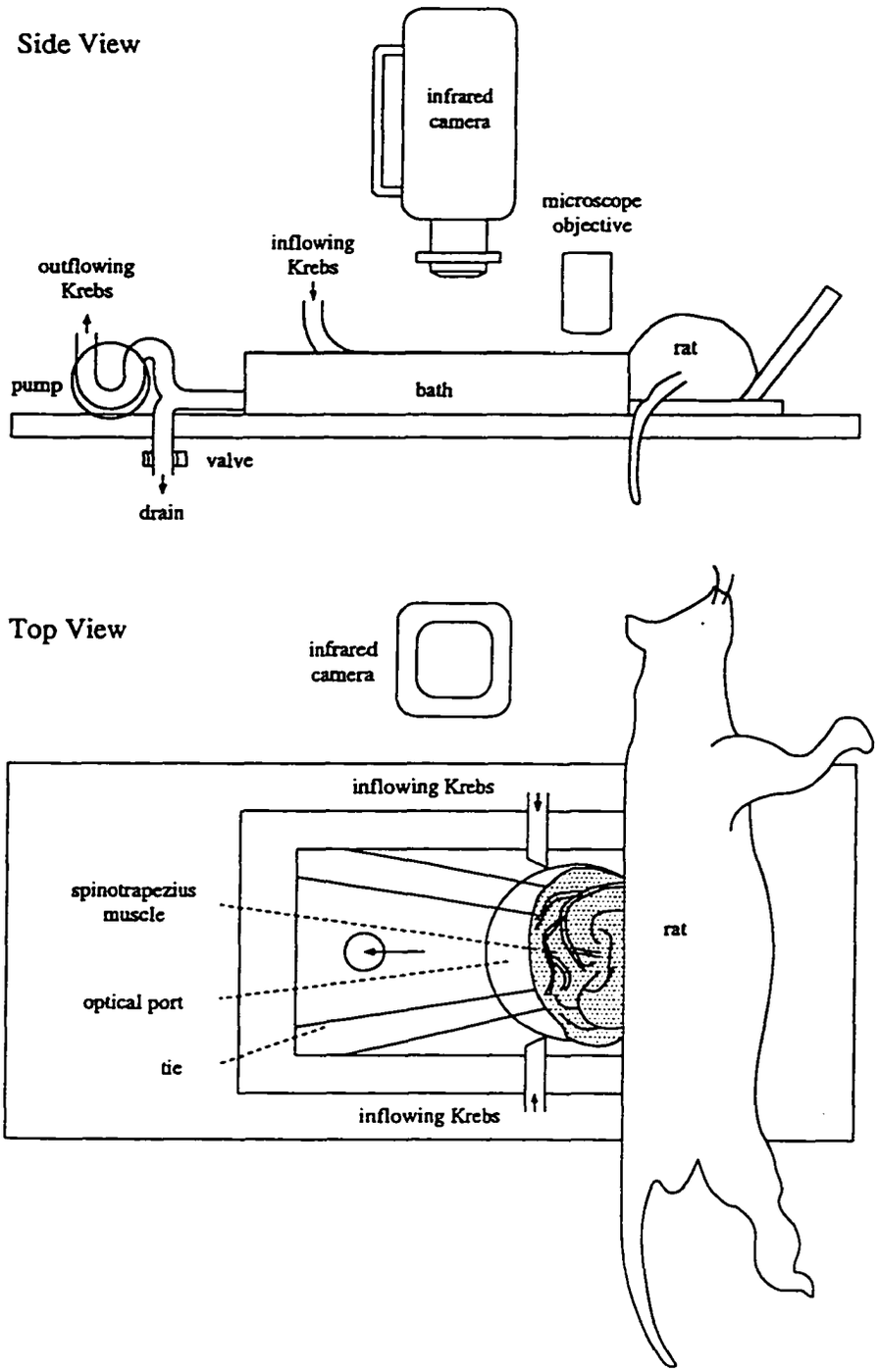

Figure 23. Schematic of experimental setup.

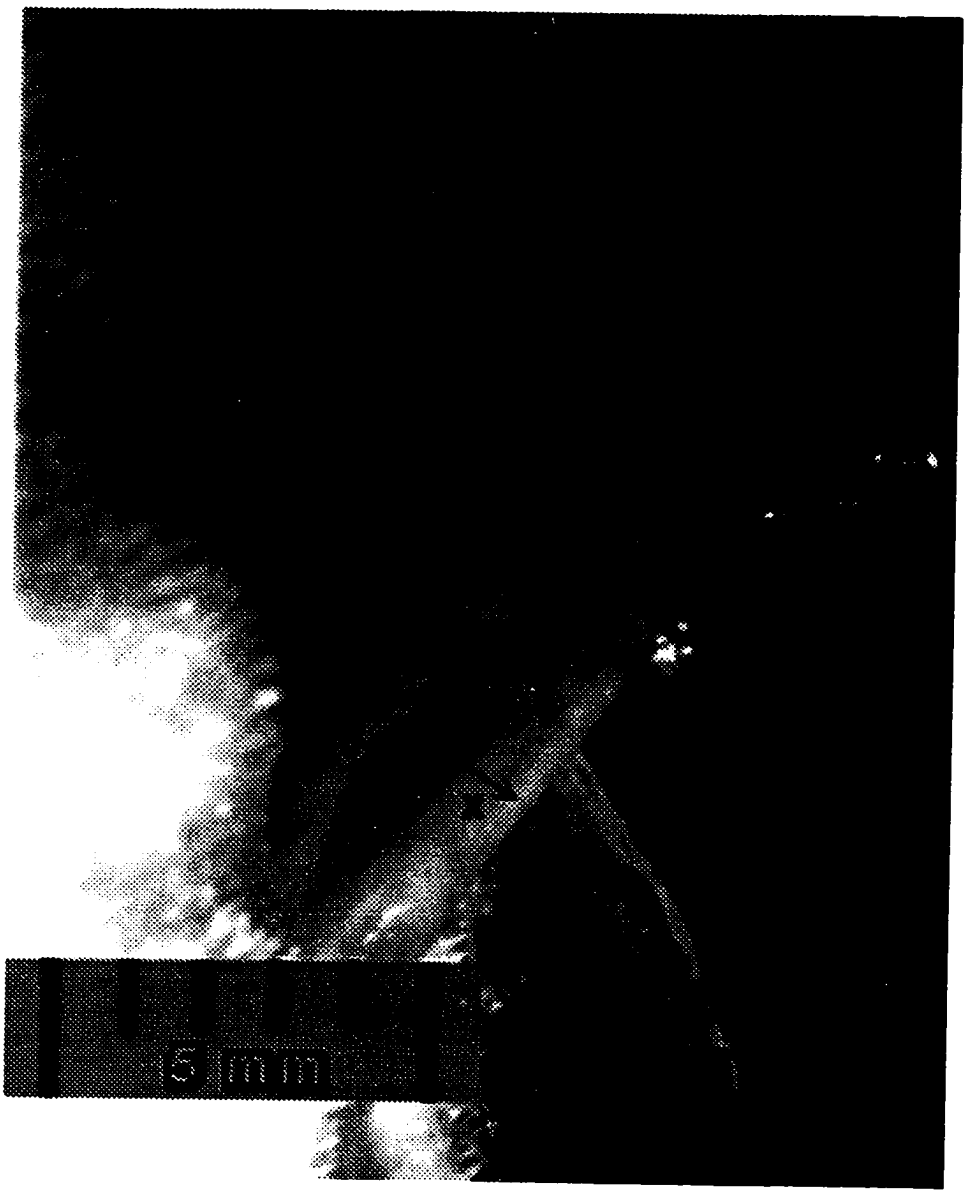

Figure 24. Vascular photo of the first-order vessel pair and its surrounding tissue.

Figure 25. Thermal image of the first-order vessel pair and the surrounding tissue in baseline.

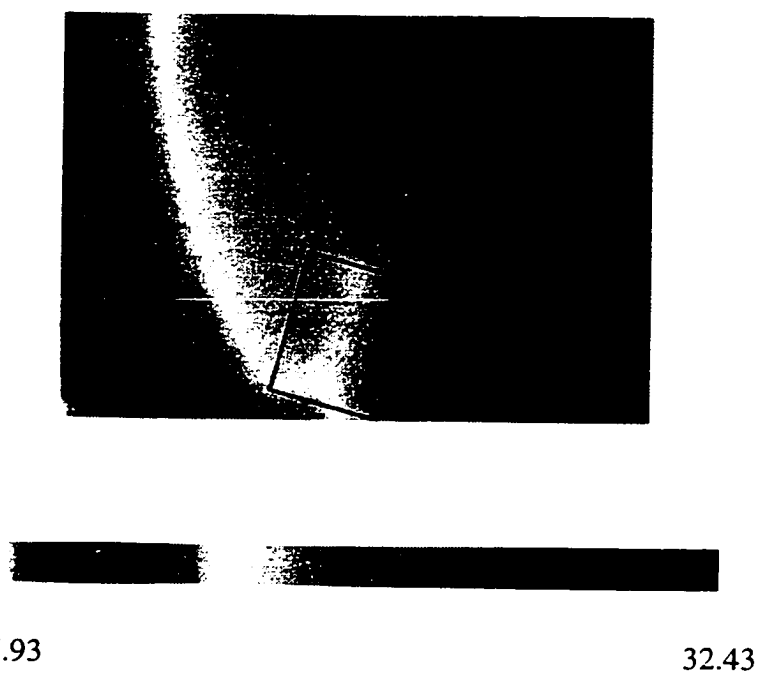

Figure 26. Thermal image of the first-order vessel pair and the surrounding tissue in vasodilation.

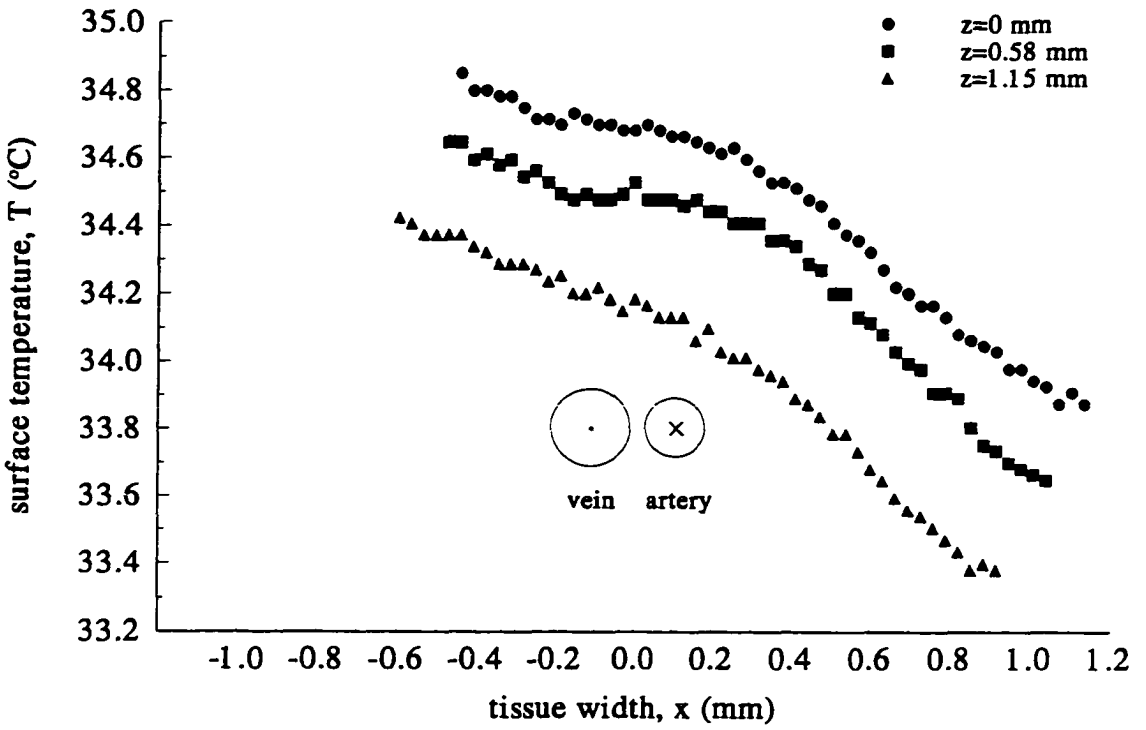

Figure 27. Experimental surface tissue temperature profiles at three different axial locations in baseline.

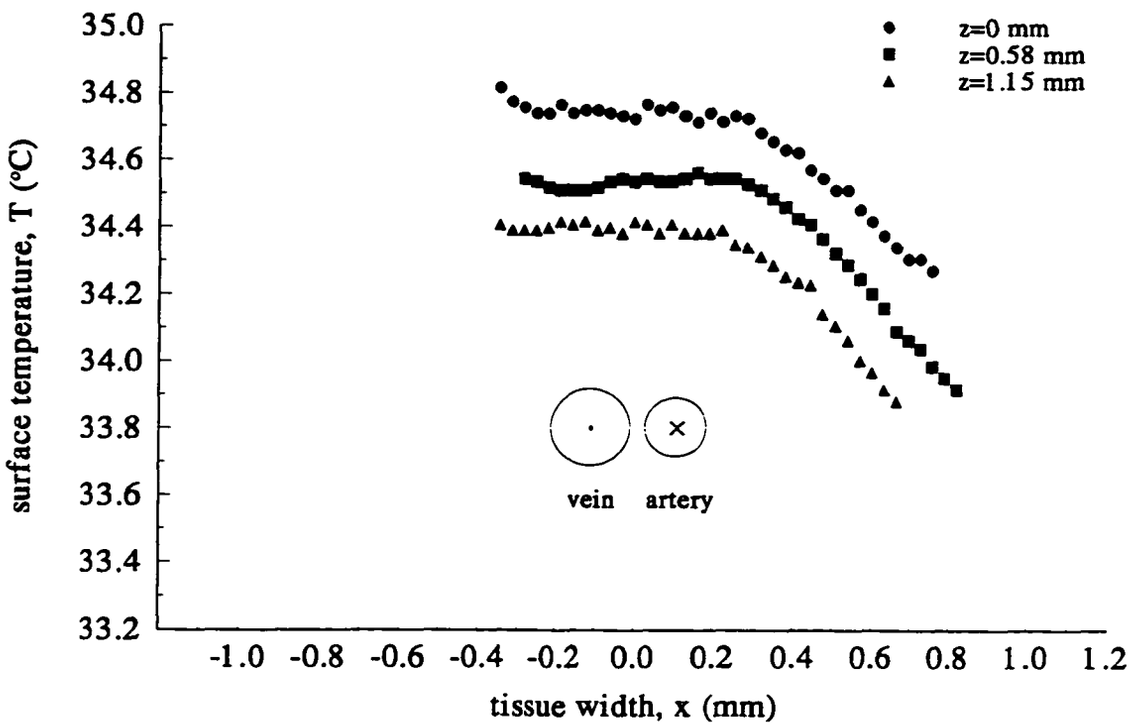

Figure 28. Experimental surface tissue temperature profiles at three different axial locations in vasodilation.

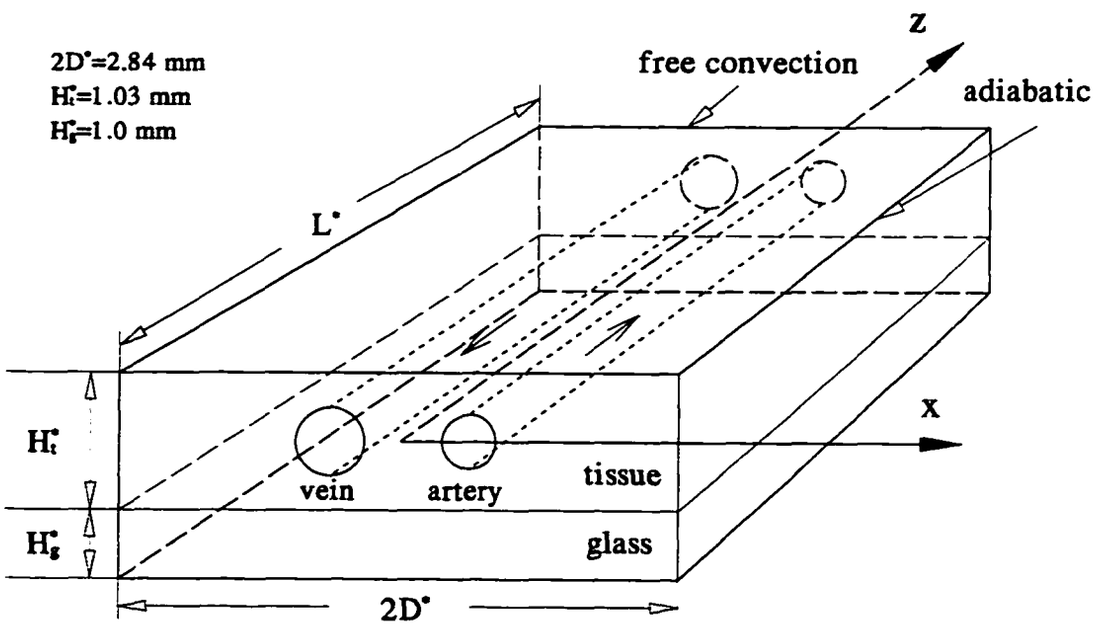

Figure 29. Schematic of tissue-vascular geometry for the theoretical model.

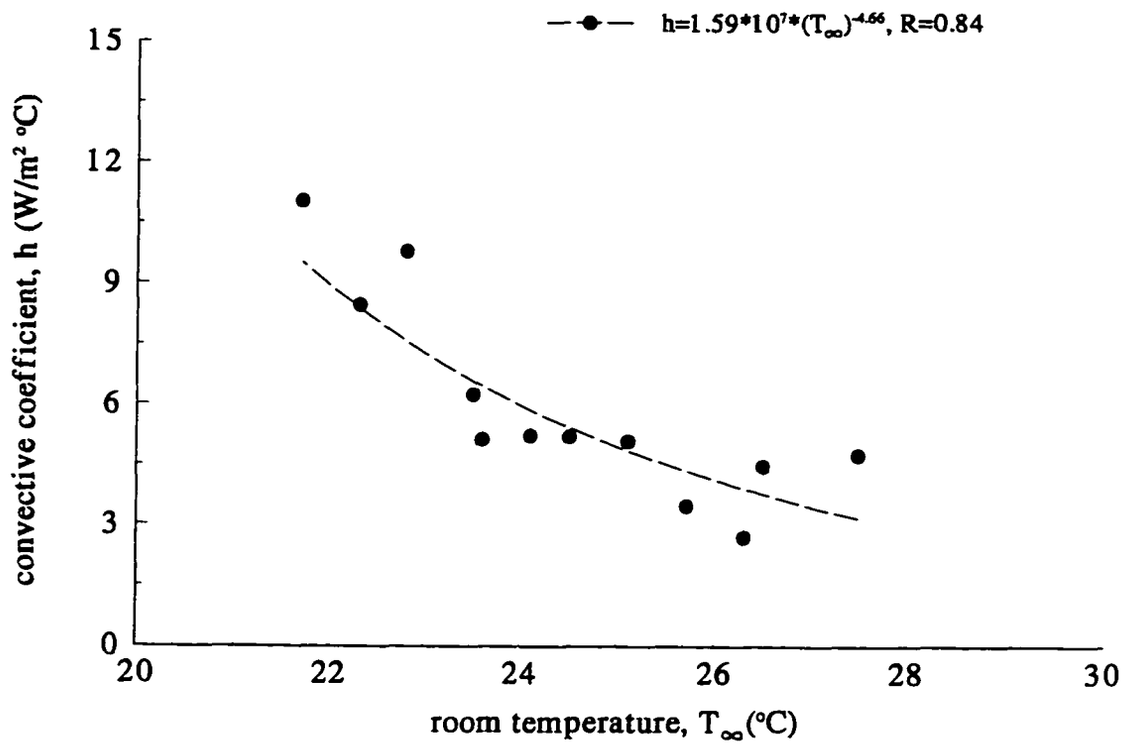

Figure 30. Relationship between the free convective coefficient (h) and the room temperature (T_∞).

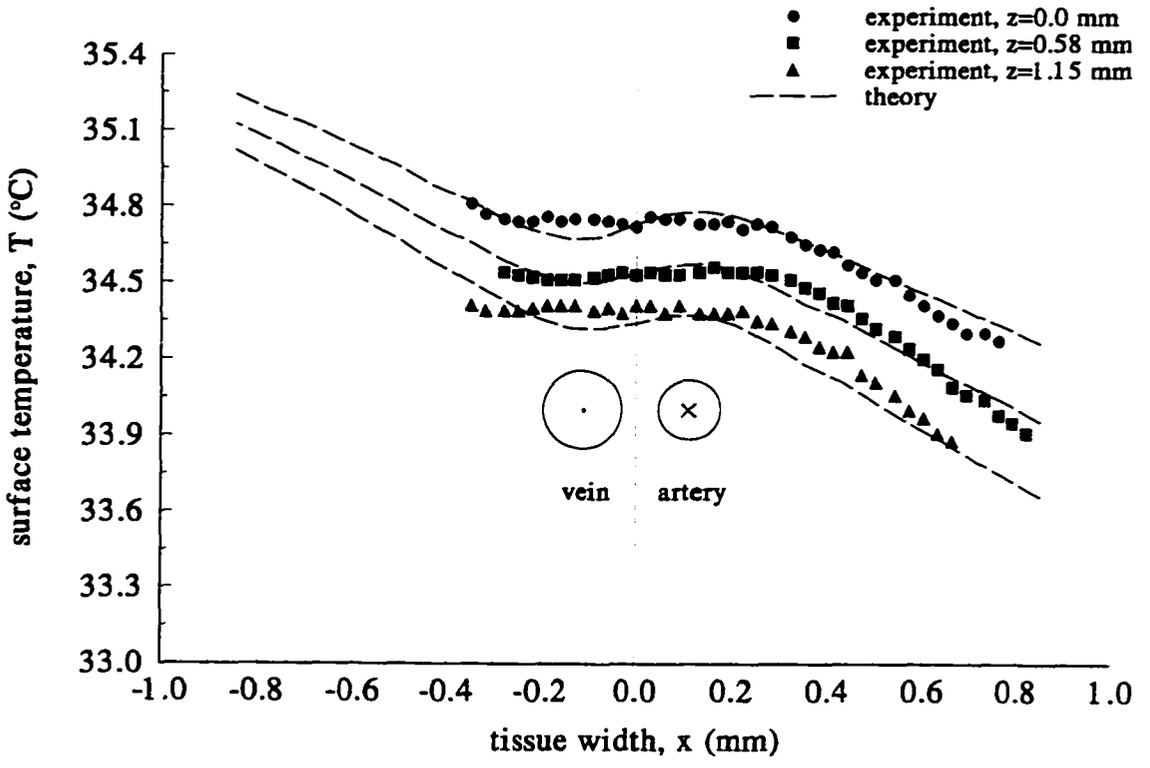

Figure 31. Comparison between the experimentally measured and theoretically predicted surface temperatures.

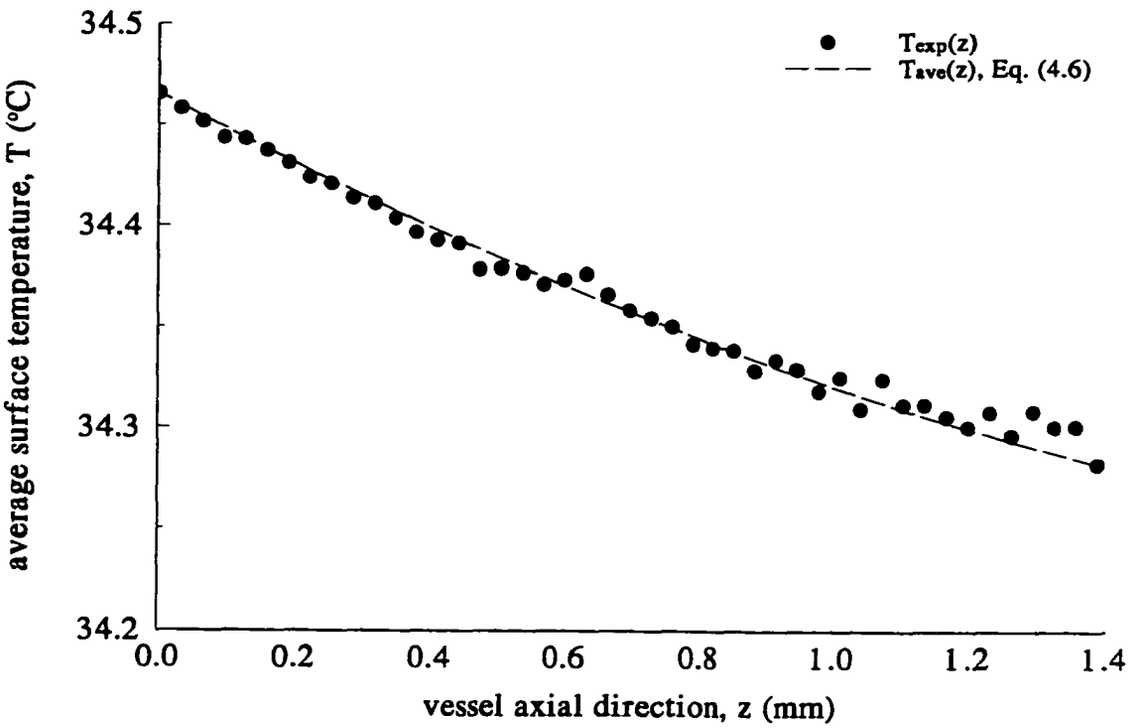

Figure 32. Averaged experimental measurements for $T_{exp}(z)$ and theoretically predicted temperatures $T_{ave}(z)$ (from Eq. (4.6)) along vessel axial direction (k=0.66 W/m°C).

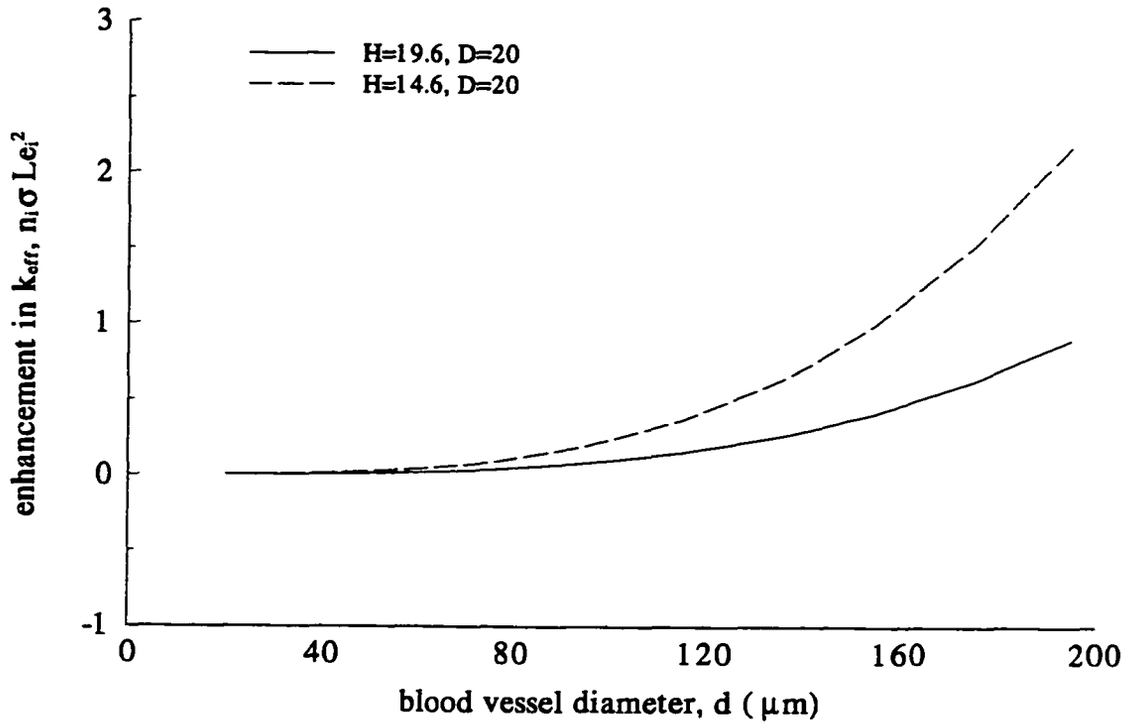

Figure 33. The effect of the equivalent tissue thickness on the enhancement in k_{eff}.

Bibliography

Adolph, E. F. Quantitative relations in the physiological constitution of mammals. *Science*, 109:579-585, 1949.

Anderson, G. T., and J. W. Valvano. A small artery heat transfer model for self-heated thermistor measurements for perfusion in the kidney cortex. *ASME J. Biomech. Eng.*, 116:71-78, 1994.

Armstrong, E. Brains, bodies and metabolism. *Brain Behav. Evol.*, 36:166-176, 1990.

Baish, J. W., P. S. Ayyaswamy, and K. R. Foster. Heat transport mechanisms in vascular tissues: a model comparison. *ASME J. Biomech. Eng.*, 108:324-331, 1986.

Bazett, H. C., I. Love, M. Newton, I. Eisenberg, R. Day, and R. Forest. Temperature changes in blood flowing in the arteries and veins in man. *J. Appl. Physiol.*, 1:3-9, 1948.

Calder III, W. A. Scaling of physiological processes in homeothermic animals. *Ann. Rev. Physiol.*, 43:301-322, 1981.

Calder III, W. A. Scaling energetics of homeothermic vertebrates: an operational allometry. *Ann. Rev. Physiol.*, 49:107-120, 1987.

Cameron, B. D. Determination of regional cerebral cortical blood flow using a heat clearance technique. *Phys. Med. Biol.*, 15(4):715-722, 1970.

Charny, C. K., S. Weinbaum, and R. L. Levin. An evaluation of the Weinbaum-Jiji bioheat equation for normal and hyperthermic conditions. *ASME J. Biomech. Eng.*, 112:80-87, 1990.

Chato, J. C.. Heat transfer to blood vessels. *ASME J. Biomech. Eng.*, 102:110-118, 1980.

Chen, M. M., and K. R. Holmes. Microvascular contributions in tissue heat transfer. *Ann. N. Y. Acad. Sci.*, 335:137-150, 1980.

Chen, M. M., K. R. Holmes, and V. Rupinskas. Pulse-decay method for measuring the thermal conductivity of living tissues. *J. Biomech. Eng.*, 103:253-260, 1981.

Clark, E. R. Arterio-venous anastomoses. *Physiol. Rev.*, 18:229-247, 1938.

Crezee, J., and J. J. W. Lagendijk. Experimental verification of bioheat transfer theories: measurement of temperature profiles around large artificial vessels in perfused tissue. *Phys. Med. Biol.*, 35:905-923, 1990.

Crezee, J., J. Mooibroek, C. K. Bos, and J. J. W. Lagendijk. Interstitial heating: Experiments in artificially perfused bovine tongues. *Phys. Med. Biol.*, 36:823-833, 1991.

Davis, M. J. Determination of volumetric flow in capillary tubes using an optical Doppler velocimeter. *Microvasc. Res.*, 34:223-230, 1987.

Doucette, J. W., P. D. Corl, H. M. Payne, A. E. Flynn, and M. Goto. Validation of a Doppler guide wire for intravascular measurement of coronary artery flow velocity. *Circulation*, 85(5):1899-1911, 1992.

Englson, E. T., T. C. Skalak, and G. W. Schmid-Schönbein. The microvasculature in skeletal muscle I. Arteriolar network in rat spinotrapezius muscle. *Microvasc. Res.*, 30:29-44, 1985.

Feldman, H. A., and T. A. McMahon. The 3/4 mass exponent for energy metabolism is not a statistical artifact. *Respir. Physiol.*, 52:149-163, 1983.

Furchgott, R. F., and J. V. Zawadzki. The obligatory role of endothelial cells in the relaxation of arterial smooth muscle by acetylcholine. *Nature*, 288(5789):373-376, 1980.

Gray, S. D. Rat spinotrapezius muscle preparation for microscopic observation of the terminal vascular bed. *Microvasc. Res.*, 5:395-400, 1973.

Groat, R. A. Relationship of volumetric flow to arterial diameter. *Federation Proc.*, 7:45, 1948.

Günther, B. Allometric ratios, invariant numbers and the theory of biological similarities. *Pflügers Arch.*, 331:283-293, 1972.

Haaland, K., B. Karlsson, E. Skovlund, and M. Thoresen. Simultaneous measurements of cerebral circulation with electromagnetic flowmetry and Doppler ultrasound velocity in the newborn pig. *Pediatric Res.*, 36:601-606, 1994.

Hansell, P. Evaluation of methods for estimating renal medullary blood flow. *Renal Physiology & Biochemistry*, 15:217-230, 1992.

Haynes, R. H. The rheology of blood. Thesis. University of Western Ontalio, 1959.

Heusner, A. A. Energy metabolism and body size. I. Is the 0.75 mass exponent of Kleiber's equation a statistical artifact? *Respir. Physiol.*, 48:1-12, 1982.

Heusner, A. A. Biological similitude: statistical and functional relationships in comparative physiology. *Am. J. Physiol.*, 246:R839-R845, 1984.

Heusner, A. A. What does the power function reveal about structure and function in animals of different size? *Ann. Rev. Physiol.*, 49:121-134, 1987.

Holmes, K. R. Biological structure and heat transfer. Report from the Allerton Workshop on the future of biothermal engineering, 14-37, 1997.

Holt, J. P., and E. A. Rhode. Similarity of renal glomerular hemodynamics in mammals. *Am. Heart J.*, 92(4):465-472, 1976.

Holtz, J., U. Forstermann, U. Pohl, M. Giesler, and E. Bassenge. Flow-dependent, endothelium-mediated dilation of epicardial coronary arteries in conscious dogs: effects of cyclooxyenase inhibition. *J. Cardiovasc. Pharmacol.*, 6:1161-1167, 1984.

House, S. D., and H. H. Lipowsky. Microvascular hematocrit and red cell flux in rat cremaster muscle. *Am. J. Physiol.*, 252:H211-H222, 1987.

Incropera, F. P., and D. V. Dewitt. Fundamentals of heat transfer. New York: John Wiley & Son Wiley, 101-110, 1981.

Ings, R. M. J. Interspecies scaling and comparisons in drug development and toxicokinetics. *Xenobiotica*, 20(11):1201-1231, 1990.

Intaglietta, M., N. R. Silverman, and W. R. Tompkins. Capillary flow velocity measurements *in vivo* and *in situ* by television methods. *Mircovasc. Res.*, 10:165-179, 1975.

Jungers, W. L. Size and scaling in primate biology. New York: Plenum Press. 1985.

Kamiya, A., R. Bukhari, and T. Togawa. Adaptive regulation of wall shear stress optimizing vascular tree function. *Bull. math. Biophys.*, 46(1):127-137, 1984.

Keller K. H. and L. Seiler. An analysis of peripheral heat transfer in man. *J. Appl. Physiol.*, 30:779-786, 1971.

Kiesewetter, H., H. Radtke, N. Korber, and G. W. Schmid-Schönbein. Experimental calibration of a two-stage prism-grating system for measuring cell velocity. *Mircovasc. Res.*, 23:56-66, 1982.

Kleiber, M. Body size and metabolic rate. *Physiol. Rev.*, 27:511-541, 1947.

Klinger H. G. Heat transfer in perfused biological tissue. I. General theory. *Bull. Math. Biol.*, 36:403-415, 1974.

Klinger H. G. Heat transfer in perfused biological tissue. II. The macroscopic temperature distribution. *Bull. Math. Biol.*, 38:183-198, 1976.

Koops, W. J., and M. Grossman. Multiphasic allometry. *Growth, Development & Aging*, 57:183-192, 1993.

Lagendijk, J. J., and J. Mooibroek. Hyperthermia treatment planning. *Recent Research in Cancer Research*, 101:119-131, 1986.

Langille, B. L., and F. O'Donnell. Reductions in arterial diameter produced by chronic decreases in blood flow are endothelium-dependent. *Science*, 231:405-407, 1986.

Lemons, D. E., S. Chien, L. I. Crawshaw, S. Weinbaum, and L. M. Jiji. The significance of vessel size and type in vascular heat transfer. *Am. J. Physiol.*, 253:R128-R135, 1987.

Lipowsky H. H., and B. W. Zweifach. Application of the 'two-slit' photometric technique to the measurement of microvascular volumetric flow rates. *Mircovasc. Res.*, 15:93-101, 1978.

Liu, Y. H., and E. L. Ritman. Branching pattern of pulmonary arterial tree in anesthetized dogs. *ASME J. Biomech. Eng.*, 108:289-293, 1986.

Mayrovitz, H. N. An optimal flow-radius equation for microvessel non-

Newtonian blood flow. *Microvasc. Res.*, 34:380-384, 1987.

Mayrovitz, H. N., and J. Roy. Microvascular blood flow: evidence indicating a cubic dependence on arteriolar diameter. *Am. J. Physiol.*, 245:H1031-H1038, 1983.

McMahon, T. Size and shape in biology. *Science*, 179:1201-1204, 1973.

Mitchell, J. W., and G. R. Myers. An analytical model of the counter-current heat exchange phenomena. *Biophys. J.*, 8:897-911, 1968.

Murray, C. D. The physiological principle of minimum work. I. The vascular system and the cost of blood volume. *Proc. Nat. Acad. Sci. U. S. A.*, 12:207-214, 1926a.

Murray, C. D. The physiological principle of minimum work applied to the angle of branching of arteries. *J. Gen. Physiol.*, 9:835-841, 1926b.

Myrhage, R. and E. Eriksson. Arrangement of the vascular bed in different types of skeletal muscles. *Prog. Appl. Microcirc.*, 5:1-14, 1984.

Nitzan, M., Y. Mahler, and N. Lifshitz. Faster procedure for deriving regional blood flow by the noninvasive transient thermal clearance method. *Annals of Biomed. Eng.*, 21:259-262, 1993.

Patel, P. A., J. W. Valvano, J. A. Pearce, S. A. Prahl, and C. R. Denham. A self-heated thermistor technique to measure effective thermal properties from the tissue surface. *ASME J. Biomech. Eng.*, 109:330-335, 1987.

Pennes, H. H. Analysis of tissue and arterial blood temperatures in resting forearm. *J. Appl. Physiol.*, 1:93-122, 1948.

Pilbeam D., and S. J. Gould. Size and scaling in human evolution. *Science*, 186:892-901, 1974.

Pollanen, M. S. Dimensional optimation at different levels of the arterial hierarchy. *J. Theor. Biol.*, 159:267-270, 1992.

Roemer, R. B., E. G. Moros, and K. Hynynen. A comparison of bioheat transfer and effective conductivity equation predictions to experimental hyperthermia

data. *Adv. Bioeng., ASME WAM*, 11-15, 1989.

Roy, A. G., and W. J. Woldenberg. A generalization of the optimal models of arterial branching. *Bull. Math. Biol.*, 44(3):346-360, 1982.

Schmidt-Nielsen, K. Scaling in biology: the consequences of size. *J. Exp. Zool.*, 194:287-308, 1975.

Schmidt-Nielsen, K. Scaling: Why is animal size so important? Cambridge: Cambridge University Press. 1984.

Schmid-Schönbein, G. W., and B. W. Zweifach. RBC velocity profiles in arterioles and venules of the rabbit omentum. *Mircovasc. Res.*, 10:153-164, 1975.

Scholander, P. F., and J. Krog. Countercurrent heat exchange and vascular bundles in sloths. *J. appl. Physiol.*, 10:405-411, 1957.

Sherman, T. F. On connecting large to small: the meaning of Murray's law. *J. Gen. Physiol.*, 78:431-453, 1981.

Shitzer, A. and R. C. Eberhart, Ed. Heat Transfer in Medicine and Biology, Vol.1, Plenum Press, New York, 1985.

Siddiqui, R. A., S. N. McCutcheon, H. T. Blair, D. D. S. Mackenzie, P. C. H. Morel, B. H. Breier, and P. D. Gluckman. Growth allometry of organs, muscles and bones in mice from lines divergently selected on the basis of plasma insulin-like growth factor-I. *Growth, Development & Aging*, 56:53-60, 1992.

Song, W. J., S. Weinbaum, and L. M. Jiji. A theoretical model for peripheral tissue heat transfer using the bioheat equation of Weinbaum and Jiji. *ASME J. Biomech. Eng.*, 109:72-78, 1987.

Song, W. J., S. Weinbaum, L. M. Jiji, and D. E. Lemons. A combined macro and microvascular model for whole limb heat transfer. *ASME J. Biomech. Eng.*, 110:259-268, 1988.

Suwa, N., and T. Takahashi. Morphological and morphometrical analysis of circulation in hypertension and ischemic kidney. *Munchen, Urban and Schwarzenberg*, 10-39, 1971.

Travis, C. C. Interspecies extrapolation in risk analysis. *Ann. Ist. Super. Ssnita*, 27(4):581-594, 1991.

Tyml, K., and M. H. Sherebrin. A method for on-line measurements of red cell velocity in microvessels using computerized frame-by-frame analysis of television images. *Mircovasc. Res.*, 20:1-8, 1980.

Upton, R., C. Grant, and G. Ludbrook. An ultrasonic Doppler venous outflow method for the continuous measurement of cerebral blood flow in conscious sheep. *J. Cerebral Blood Flow & Meta*, 14(4):680-688, 1994.

Uylings, H. B. M. Optimization of diameters and bifurcation angles in lung and vascular tree structures. *Bull. Math. Biol.*, 39:509-520, 1977.

Valvano, J. W., J. T. Allen, and H. F. Bowman. The simultaneous measurement of thermal conductivity, thermal diffusivity and perfusion in small volume of tissue. *ASME J. Biomech. Eng.*, 106:192-197, 1984.

Valvano, J. W., S. Nho, and G. T. Anderson. Analysis of the Weinbaum-Jiji model of blood flow in the canine kidney cortex for self-heated thermistors. *ASME J. Biomech. Eng.*, 116:201-207, 1994.

Van Der Meulen, M. C., and D. R. Carter. Developmental mechanics determine long bone allometry. *J. Theor. Biol.*, 172:323-327, 1995.

Vocci, F., and Farber T. Extrapolation of animal toxicity data to man. *Regulatory toxicology and Pharmacology*, 8:389-398, 1988.

Wayland, H., and P. C. Johnson. Erythrocyte velocity measurement in microvessels by a two-slit photometric method. *J. Appl. Physiol.*, 22:333-337, 1967.

Weinbaum, S., and L. M. Jiji. A two phase theory for the influence of circulation on the heat transfer in surface tissue. *Adv. Bioeng., ASME WAM*, 179-182, 1979.

Weinbaum, S., and L. M. Jiji. A new simplified bioheat equation for the effect of blood flow on average tissue temperature. *ASME J. Biomech. Eng.*, 107:131-139, 1985.

Weinbaum, S., and L. M. Jiji. Discussion of papers by Wissler and Baish et al.

concerning the Weinbaum-Jiji Bioheat equation. *ASME J. Biomech. Eng.*, 109: 234-237, 1987.

Weinbaum, S., and L. M. Jiji. The matching of thermal fields surrounding countercurrent microvessels and the closure approximation in the Weinbaum-Jiji bioheat equation. *ASME J. Biomech. Eng.*, 111:271-275, 1989.

Weinbaum, S., and L. M. Jiji, D. E. Lemons. Theory and experiment for the effect of vascular microstructure on surface heat transfer, part I. *ASME J. Biomech. Eng.*, 106:321-330, 1984.

Weinbaum, S., L. X. Xu, L. Zhu, and A. Ekpene. A new nundamental bioheat equation for muscle tissue: Part I: Blood perfusion term. ASME *J. Biomech. Eng.*, 119:278-288, 1997.

West, G. B., J. H. Brown, and B. J. Enquist. A general model for the origin of allometric scaling laws in biology. *Science*, 276:122-126, 1997.

Wissler, E. H. Comments on the new bioheat equation proposed by Weinbaum and Jiji. *ASME J. Biomech. Eng.*, 109:226-233, 1987.

Wissler, E. H. Comments on Weinbaum and Jiji's discussion of their proposed bioheat equation. *ASME J. Biomech. Eng.*, 109:355-356, 1987.

Wu, Y., S. Weinbaum, and L. M. Jiji. A new analytic technique for 3-D heat transfer from a cylinder with two or more axially interacting eccentrically embedded vessels with application to countercurrent blood flow. *Int. J. Heat Mass Transfer*, 36:1073-1083, 1993.

Wulff, W. The energy conservation equation for living tissues. *IEEE Trans. Biomed. Eng.*, BME-21:494-495, 1974.

Xu, L. X., M. M . Chen, K. R. Holmes, and H. Arkin. The theoretical evaluation of the Pennes, the Chen-Holmes, Weinbaum-Jiji bioheat transfer models in the kidney cortex. *ASME HTD.*, 189:15-21, 1991.

Zamir, M. Local geometry of arterial branching. *Bull. Math. Biol.*, 44:597-602, 1982.

Zamir, M. Optimality principles in arterial branching. *J. Theor. Biol.* 62:227-251,

1976.

Zamir, M., S. Phipps, B. L. Langille, and T. H. Wonnacott. Branching characteristics of coronary arteries in rats. *Can. J. Physiol. Pharmacol.*, 62:1452-1459, 1984.

Zamir, M., P. Sinclair, and T. H. Wonnacott. Relation between diameter and flow in major branches of the arch of the aorta. *J. Biomech.*, 25:1303-1310, 1992.

Zhu, L., D. E. Lemons, and S. Weinbaum. A new approach for predicting the enhancement in the effective conductivity of perfused muscle tissue due to hyperthermia. *Ann. Biomed. Eng.*, 23:1-12, 1995.

Zhu, L., D. E. Lemons, and S. Weinbaum. Thermal equilibration in rat cremaster muscle. *Ann. Biomed. Eng.*, 24:109-123, 1996.

Zhu, L., and S. Weinbaum. A model for heat transfer from embedded blood vessels in two-dimensional tissue preparations. *ASME J. Biomech. Eng.*, 117:64-73, 1995.

Zhu, M., S. Weinbaum, and D. E. Lemons. A three-dimensional variable geometry countercurrent model for whole limb heat transfer. *ASME J. Biomech. Eng.*, 114:366-376, 1992.

Zweifach, B. W., and H. H. Lipowsky. Quantitative studies of microcirculatory structure and function and rabbit omentum. *Circulation Res.*, 41(3):380-390, 1977.

IMAGE EVALUATION TEST TARGET (QA-3)

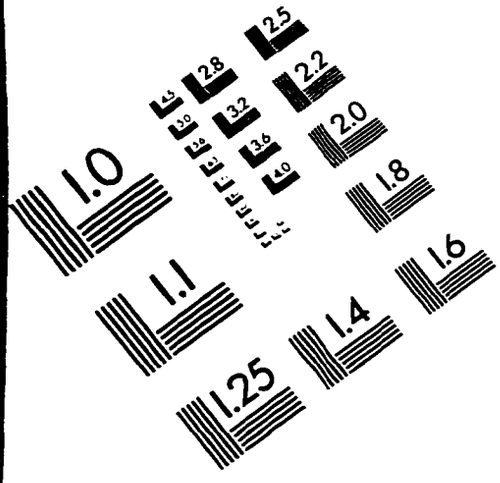

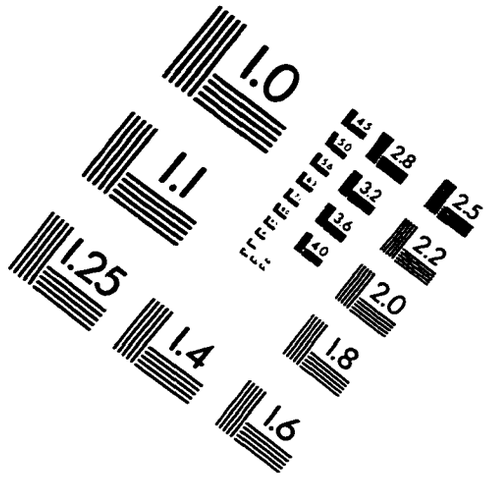

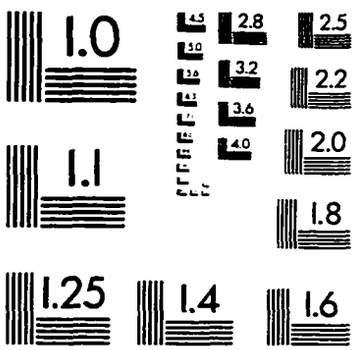

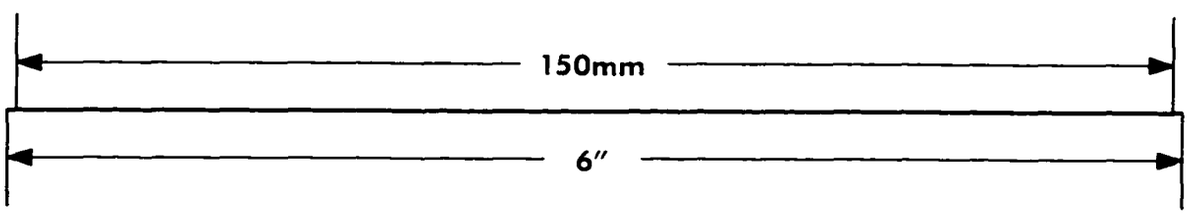

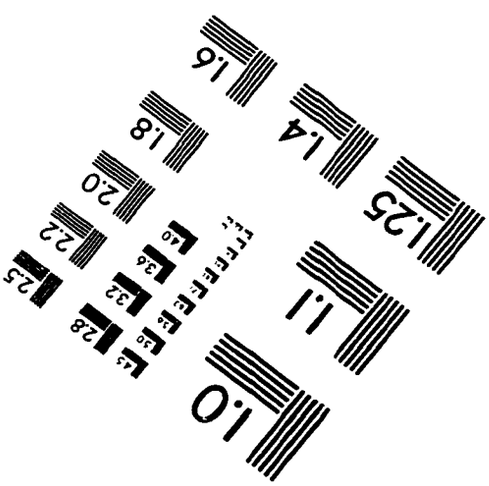

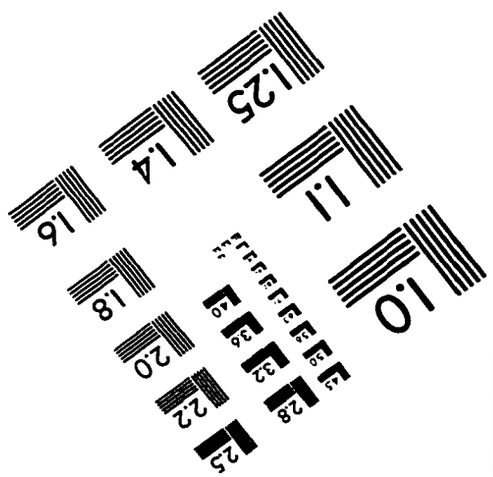

APPLIED IMAGE, Inc
1653 East Main Street
Rochester, NY 14609 USA
Phone: 716/482-0300
Fax: 716/288-5989